Spring 5-6-2021

Prestressed Concrete Slabs with Bonded and Unbonded Tendons

Jasmin Abdelhalim
jasminosama@aucegypt.edu

The American University in Cairo

School of Sciences and Engineering

PRESTRESSED CONCRETE SLABS WITH BONDED AND UNBONDED TENDONS

A Thesis Submitted to

The Department of Construction Engineering

in partial fulfilment of the requirements for the degree of

Master of Science in Construction Engineering

By

Jasmin Abdelhalim

Under the supervision of

Dr. Ezzeldin Yazeed Sayed-Ahmed

Professor

Department of Construction Engineering

The American University in Cairo

DEDICATION

Specially dedicated to my beloved grandfather who passed away last year. Thank you for your endless love, thank you for every single advice and thank you for pushing me to take this opportunity.

Also, this thesis is dedicated to my father in law who passed away a month ago and I wish he was there witnessing me fulfilling one of my dreams. You will always remain in our hearts.

Special thanks to my mum and dad for everything they have done to me, I wouldn't have been here without your forever support and guidance. Thanks to my sisters Rana Abdelhalim and Dalia Abdelhalim, to my dear uncle Dr Amr Samir and to my beloved future husband Ahmed Kandil for your great sacrifices and encouragements.

My deepest heartfelt appreciation and sincere gratitude to all the people who made this journey possible and bearable after God's grace and guidance.

ACKNOWLEDGEMENTS

I would like to thank Prof. Ezzeldin Sayed-Ahmed Yazeed for giving me the opportunity to do this master thesis under his supervision and who is always passionate to transfer all his knowledge by all possible means.

I would also like to acknowledge STRANDS Company, Egypt and GTI Company, USA for the materials funding and research support.

Special thanks to Prof. Osama El-Nesr for encouraging me to take this opportunity and for his supportive advices through my academic journey.

Also, special thanks to the AUC's research grant that without which I could not have done this research.

ABSTRACT

Post-tensioning concrete technology increases the resistance of flexural concrete members. This technology allows for the production of slenderer sections, and sequentially less usage of material preserving the sustainability concept in construction engineering. Post-tensioning process can be done using bonded or unbonded steel tendons. The unbonded tendons are thought to have better resistance to corrosion for structures exposed to severe environmental conditions. The unbonded tendon's steel strands are painted with grease and covered with plastic sheathing to prevent the moisture from reaching the steel strands thus they can provide high corrosion resistance. According to the ACI 318-19 and other codes of practice, the stress in the unbonded tendon at the ultimate limit state is limited to less than or equal to the tendon's yield stress. On the other hand, the bonded tendon's stress at this state is determined to be more than or equal to the tendon's yield stress. This limitation for the unbonded tendons restrained the widespread usage of the unbonded system. Through this research, six-simply supported one-way slabs; two with bonded tendons, two with unbonded tendons and two with unbonded tendons and non-prestressing steel reinforcement are tested in flexure to failure. The post-tension slabs are of 4.0-meters in span and the flexural tests are carried in the AUC structural engineering laboratory in a four-point loading scheme. The ultimate stress of the unbonded tendons are measured at the failure stage. The results of both systems are compared against each other and against the provisions of the ACI 318-19. The unbonded post-tension slabs with non-prestressing steel reinforcement showed higher failure loads than the bonded and unbonded slabs without reinforcement. The ACI 318-19 provisions were critically reviewed versus the results of the experimental investigation. The review reveals that the limitation of the unbonded tendon's ultimate stress is not accurate and can be reviewed.

Contents

List of figures

List of tables

Notations

A_c: area of concrete cross section

A_{ct}: area between the flexural tension face and the centroid of the gross section

A_{ps}: the area of the prestressing tendons

$A_{v,min:}$ minimum shear reinforcement

A: gross area of the cross section

$P_{J:}$ Jacking force

$P_{i:}$ Initial force after short-term losses

$P_{e:}$ Effective force after long-term losses

P_{load}: Point load calculated

P_{Exp}: machine's load

e: eccentricity of the tendon from the centroid of the section

y: distance from the centroid of the shape till the surface the stress is calculated at

M_{ow}: moment due to the own weight only of the slab

M_{total}: moment due to the own weight of the slab plus the moment due to the two point loads from the machine.

I: the moment of inertia of the gross cross section.

L: span of the slab

$\mathcal{E}_{pe}$: strain due to the effective prestress

$\mathcal{E}_{dc}$: the strain due to decompression

$\mathcal{E}_{cs}$: the strain proportional to the distance from the neutral axis

$\mathcal{E}_{y:}$ Steel yielding strain

$\varepsilon_{cu:}$ concrete top fiber strain at the ultimate stage

E_{ps}: prestressing steel modulus of elasticity

E_c: concrete modulus of elasticity.

c: depth of the neutral axis for the ultimate stress of the section

d_p: the length from the top of concrete till the centroid of the prestressing tendons

$\mathfrak{f}_{ps}$: the tendons stress at ultimate

f_{pe}: effective prestress

f'_c: concrete cylindrical compressive strength

f'_{ci}: concrete initial cylindrical compressive strength

f_{cu}: concrete cube compressive strength

f_{cui}: concrete initial cube compressive strength

$f_{s:}$ non-prestresssing steel reinforcement stress

$f_{y:}$ non-prestressing steel reinforcement yielding stress

$f_{py:}$ tendons Yield Stress

$f_{pu:}$ tendons ultimate strength

α_1= 0.85 c according to the ACI

β_1: concrete compression block reduction factor $d_{p:}$ effective depth

ρ_{ps}: ratio of prestressing steel reinforcement (A_{ps} to bd_p)

$V_{u:}$ ultimate shear force due to external loads only

$M_{u:}$ ultimate moment due to external loads only

$V_{c:}$ nominal shear strength provided by concrete.

λ: bond reduction coefficient

$c_{pe:}$ neutral axis depth at the effective stress

$q_{e:}$ prestressing steel index

1 Introduction

1.1 Introduction

The Egyptian government adopts a new developmental plan by constructing major projects in different locations all over the country. From these projects; The Alamein City, The New Administrative Capital and The Grand Egyptian Museum. The Alamein City as an example is designed to have a number of towers facing the sea with special architectural aspects. Architectural and constructional considerations directed the design of the flooring slabs of the New Alamein

Towers to be made up of pre-stressed concrete. Pre-stressed concrete structures produce high strength and resistance compared to the traditional concrete structures. In addition, multiple other advantages are provided by the usage of pre-stressed concrete such as the faster construction rates, saving of material and preservation of the sustainability concept in the construction area.

The New Alamein Towers slabs are made of pre-stressed concrete using bonded tendons as shown in Figure 1-1. The ACI 318-19 and other codes of practice provisions provide higher nominal strength for the bonded tendons than the unbonded tendons. The difference between both types of tendons, is that the bonded tendons are fixed inside a duct and this duct is filled with grout, creating a bond between the concrete and the tendon. While, the unbonded tendons are made of steel strands that are coated with grease and wrapped in plastic sheathing, providing protection for the steel strands against corrosion but unbonded to the concrete surrounding it. Bonded tendons are mostly used by Egyptian designers and contractors due to the code of practice limitations on the ultimate strength of the unbonded tendons. For example, the ACI 318-19 states that the bonded tendon's ultimate stress exceeds the strand's yield stress, while on the other hand the same code limits the unbonded tendon's ultimate stress to a maximum value equals to the tendon's yield stress.

The limitation specified by most of the codes of practice on unbonded tendon's ultimate stress is mainly due to the absence of the bond between the streel strands and the concrete because of the plastic cover and the grease. So, the strain compatibility between the steel and the concrete cannot be applied for the determination of the ultimate stress in case of using unbonded tendons. According to researches carried before, it was concluded that the limitation on the unbonded strands ultimate stress is safer to be limited to a maximum value equals to the strand's yield stress.

Another reason for the wide usage of the bonded system over the unbonded system is the ACI 318-19 requirement for the usage of non-prestressing steel reinforcement upon using the unbonded system only.

Figure 1-1 New Alamain towers post-tension bonded slab under construction

1.2 Problem statement

In the post-tension applications, can the unbonded tendons withstand an increase in their ultimate stress design values beyond the yield stress? Also, and due to the ease of constructing the unbonded tendons system, can this system be widely used in the post-tension applications in the same way as the bonded tendons system in Egypt?

1.3 Objectives

The objectives of this thesis is to:

- Compare the behavior of the bonded and the unbonded tendons system for post-tension slabs
- Verify the ACI 318-19 code equation's applicability and accuracy in calculating the unbonded tendon’s stress at the ultimate limit state.
- Experimentally investigate the effect of non-prestressing steel reinforcement on the ultimate limit state behavior of post-tension slab with unbonded tendons

1.4 Research methodology

An experimental program is designed to test six post-tension concrete slabs in flexure via four-point loading system. The objective is to find answers for the questions raised earlier. Two slabs of the six specimens are prestressed using bonded tendons while another two slabs are prestressed by unbonded ones. The four specimens are designed and constructed according to the ACI 318-19 code's provisions. Another two slabs are prestressed by unbonded system with no non-prestressing steel reinforcement as stated by the code in order to be able to compare the behavior of the bonded system to that of the unbonded one without the effect of the non-prestressing steel. Also, with the aim of examining the effect of the usage of the non-prestressing steel on the unbonded system behavior. The six slab specimens' dimensions are 4.3 m x 1.0 m x 0.16 m, made up of normal weight concrete of compressive strength 30 MPa. All the slabs have three no. 12.7-millimeter mono-strands tendons in which each tendon is made of seven wires strands with an 1860 MPa ultimate stress and 98.7 mm^2 cross-sectional area. The four unbonded slabs tendons have a grease layer and are coated with plastic sheathing. Zero void encapsulated anchors are used for the unbonded slabs, while iron anchors are used for the bonded slabs. For the bonded system, the tendons are located inside a 25mm diameter duct. The grout is injected into the ducts after the tendons' stressing. The non-prestressing steel reinforcement used for the two unbonded slab specimens are calculated according to the ACI 318-19 provisions; no.10mm @ 200mm are provided in both the longitudinal and transverse direction. The tendons have a double harped profile with a mid-span eccentricity of 40mm from the concrete section center of gravity, and zero eccentricity at the slab ends. The cables' stresses are measured using strain gauges located on the strands at the centroid sections and end sections. Strain gauges are also located on the concrete top surface at the mid-span to measure the deformation of the concrete surface under the applied stresses. LVDTs are situated in the concrete bottom surface at the mid-span to measure the specimen deflection.

Ready-mix concrete is transported to the lab from a supplier and cast at the lab's location. The bonded and unbonded tendons, ducts, anchors, and wedges are provided by GTI (USA) and Strands (Egypt). The strands' stressing after the concrete reaching its desired compressive strength is done using hydraulic jacks. This stressing process is done by a stressing certified team from Strands (Egypt). Six concrete cubes are molded while casting the concrete and tested after seven

days and 28 days in a standard compressive strength test. Detailed preliminary calculations are carried before testing to determine the theoretical failure load value for each system. These calculated values are compared later to the experimental failure loads recorded during testing.

1.5 Thesis content

The first chapter reviews the motivation behind this thesis research, stating the objectives and the methodology followed. Then, the second chapter presents the different types of prestressing, the pre-tension system and the post-tension system. The chapter also compares the various aspects of post-tension concrete slabs using bonded and unbonded system. Chapter two presents some applications of the prestressing concrete in addition to the specific applications for the pre-tension and the post-tension concrete. The chapter review relevant researches carried out to assess the different factors that affect the ultimate stress of the unbonded tendons. Chapter three presents a detailed explanation for the design steps followed for producing tested slab specimens. The design of both bonded and unbonded slab specimens followed the provisions of the ACI 318-19. Chapter four presents the details of the experimental program carried in the AUC structural engineering laboratory to test the six slabs in flexure test. Chapter five contains the results of the experimental program and presents a discussion of the research findings. Chapter six includes a brief summary of the research work and presents its main conclusions. The chapter also lists some recommendations for future investigation in the same area.

2 Literature Review and Background

2.1 Introduction

Prestressing concrete is a relatively new technology that provides concrete members with higher flexural and tensile strength than traditional concrete. Sequentially, prestressing of concrete produces slenderer cross-sections with higher capacity for the same directed loads. The prestressing technology employs a less amount of materials usage and a significant reduction in the structure's embodied energy (Süleymanoğlu et al. 2018). Prestressing of concrete members provides several advantages over ordinary concrete. Prestressed concrete slabs afford a fast floor construction cycle, more durable concrete and fewer materials usage that sequentially leads to a cost-effective structure. In addition, the usage of high-strength steel for the prestressed slabs tendons can reduce the amount of ordinary non-prestressed reinforcement usage (Abdelrahman, 2017). One of the main advantages for prestressed concrete is deflection and cracks control (Kang et al. 2015).

Concrete is mainly strong in resisting the compressive stresses while it is weak in resisting tensile stresses. Concretes tensile strength is almost 10% of the concrete compressive strength. For the traditional non-prestressed concrete members, concrete is considered cracked during all stages of loading. The tensile stresses are mainly resisted by non-prestressed steel reinforcement. For the compressive flexural stresses, the concrete is only designed to withstand these compressive stresses with almost less than half the cross-section. The rest of the concrete of the cross section is contemplated to connect the steel reinforcement to the concrete compressive zone (Post-Tensioning Institute Manual, 2006).

Prestressed concrete members are highly efficient in resisting tensile stresses. Prestressing of concrete involves the elongation of the high-strength steel tendons using hydraulic jacks. Then, the tendons are cut from between the buttresses and the concrete's surface, creating compression forces and bending moment on the zone subjected to tensile stresses at the stage of external loading. The prestressing technology produces concrete members with high efficiency for stress resistance, as it allows for the increase in the imposed loads at the service stage that would cause the first crack due to flexural stresses. And due to the imposed compression forces on the concrete member due to prestressing, the crack and deflection are controlled. Prestressed concrete members

can be either pre-tension or post-tension. Post-tension members can either be made of bonded or unbonded systems (Post-Tensioning Institute Manual, 2006). Figure 2-1 illustrates the different systems of prestressed concrete members.

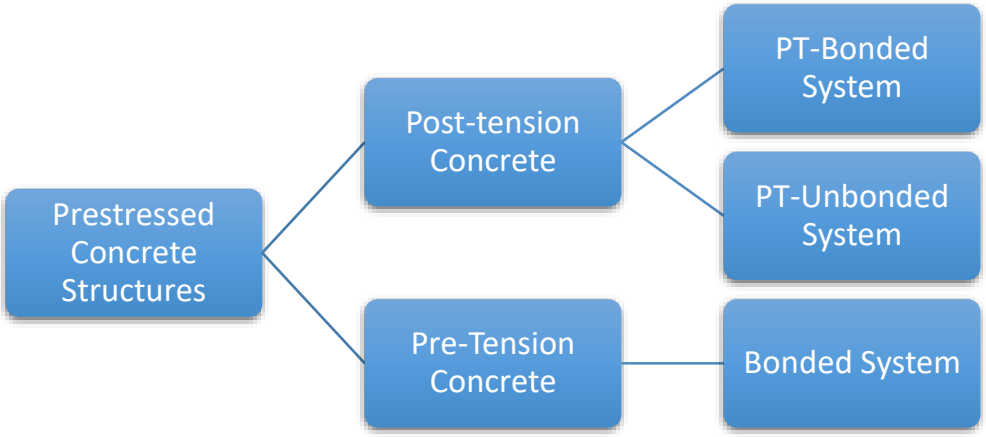

Figure 2-1 Prestressed concrete systems

Pre-tension concrete members are members whose prestressing steel tendons are stressed before the concrete casting. Then, the concrete is cast and when the concrete reaches the designed compressive strength, the tendons are cut down from between the surface of concrete and the buttresses. This system is achieved using bonded tendons only because the concrete is poured around the tendons after the tendons stressing and the stresses are transferred through the created bond to the concrete. This prestressing technique takes place at precast plants (Post-Tensioning Institute Manual, 2006).

On the other hand, the post-tension concrete element's tendons are prestressed after the casting of concrete. Empty ducts are inserted with their designed profile in the member's mold before the concrete pouring. After the pouring and hardening of concrete and reaching the desired concrete compressive strength, steel strands are inserted in the fixed empty ducts. Afterward, the tendons are stressed with the aid of hydraulic jacks and are anchored to the concrete's surface using mechanical anchorage devices. Figure 2-2 shows a real picture of the hydraulic jack and the stressing machine. The tendons are eventually cut from between the buttresses and the concrete surface to transfer the stresses to the concrete element. The post-tensioning technique provides premium advantages when compared to the pre-tension system. The post-tension system ensures

the integrity between the different elements of the structure through the continuity of the tendon and the structure's continuous framing. Post-tension systems also eliminate joint troubles as this system provides a monolithic connection between the different members of the structure, slabs, beams and columns (Post-Tensioning Institute Manual, 2006). Figure 2-3 shows a post-tension concrete slab before concrete pouring.

Figure 2-2 Hydraulic jack and prestressing machine (PTE SYSTEMS INT'L. LLC).

Figure 2-3 Post-tension concrete slab before concrete casting (https://theconstructor.org/structural-engg/pre-engineered-building/, 2021)

The post-tension system can be performed by the usage of bonded or unbonded tendons. Bonded post-tension structures are made of plastic or steel ducts in which the steel strand is inserted. Grout is injected into the ducts after the stressing of the bonded tendons to create a bond between the 7-wires strand and the duct that is already bonded to the concrete surrounding. After concrete curing, the whole member becomes integrated and the relative movement between the tendon and the concrete becomes prohibited. The stress is transferred from the stressed tendon to the concrete surrounding it through the created bond (Ellobody et al. 2008).

For the unbonded post-tension concrete members, the tendons are mostly made up of 7-wires steel strands painted with corrosion inhibiting grease and covered with an extruded seamless plastic sheathing. The tendon's coating and sheathing provide corrosion protection and allow movement between the tendon and the concrete surrounding it. Hardened steel wedges and ductile iron anchors are used to support the tendons to the concrete member. Also, bolsters and chairs are used to maintain the concrete's tendons profile through its length (Post-Tensioning Institute Manual,

2006). The stresses in the unbonded tendons are transmitted to the concrete via end anchors, strain throughout the tendon's length and the cables profile (Ellobody et al. 2008).

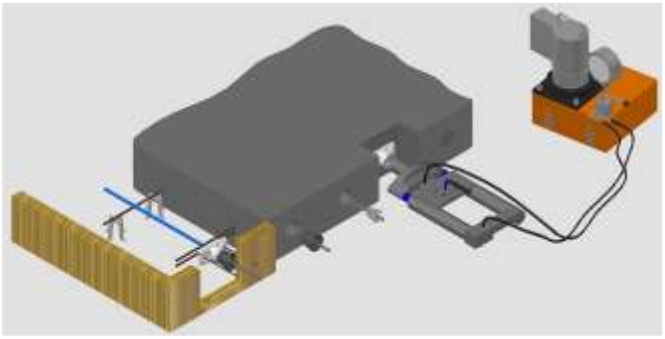

Figure 2-4 Unbonded post-tension slabs stressing stages (PTE SYSTEMS INT'L. LLC)

2.2 Applications of prestressed concrete members

Due to the various advantages that the prestressing technology offers, several types of structures are constructed using the prestressed technique such as office buildings, residential structures, parking, bridges, tanks, dams and foundations. Ocean Heights 2, Dubai, 2016 and Sydney Opera House, 1973 are examples of prestressed concrete structures shown in Figures 2-5 and 2-6 (Aedas, 2020) and (Cordelia Williamson, 2020).

Figure 2-5 6 Ocean Heights 2, Dubai, 2016 (Aedas,2020)

Figure 2-6 Sydney Opera House, 1973 (Cordelia Williamson, 2020)

The post-tension system is adopted in many rehabilitation applications of old or deteriorated buildings. Between the years 1965 and 2008, more than three million tons of bonded and unbonded

tendons were produced in the U.S., 73 % of the produced tendons are unbonded ones. Most of the buildings with prestressed concrete that were constructed in North America since the 1950s were made up of unbonded floor systems resulting in almost one billion square meters of floor area (**PTE** SYSTEMS INT'L. LLC). There are different types of post-tension concrete slabs such as one-way ribbed slabs, two ways waffle slabs, one-way solid slabs with band beams and transfer slabs which are widely used. Transfer slabs are usually located in a lower floor of a building. This slab is used to support columns of small spans from the upper floors; this transfer slab is to be supported on large spanned massive columns in the ground floor to provide wide spans in the building's entrances. Also, other slabs like industrial slabs and slabs on ground for residential and tennis courts are extensively constructed using the post-tensioning technique. Many high-rise building floors are made up of the post-tension slab system to reduce the building's mass and increase the story height. One of these high-rise buildings is the Landmark 72 in Korea, 2011. The Landmark 72 is made up of a 72-story building, 350 meters height and two 48-story towers. The floor size is 90x50m. Figure 2-7 shows the landmark 72 in a street view (Chung et al. 2017)

Also, the post-tensioning system is highly effective to be used for the consolidation of structures such as silos. Figure 2-8 shows an existing silo consolidated by post-tensioning tendons (Torok et al. 2019). The post-tension application has significantly grown to almost include everything such as stay cables, contaminated structures, rock and soil anchors, barrier cable applications, vertical post-tensioning located in walls with the aim to resist earthquakes.

Figure 2-8 Consolidated Silos (Torok et al. 2019)

Figure 2-7 landmark 72 in a street view, Korea (Chung et al. 2017)

2.3 Bonded vs. unbonded prestressing systems

Post-tension concrete systems are categorized into bonded and unbonded systems in the construction industry. The unbonded system consists of a greased mono-strand covered by extruded plastic sheathing, as shown in Figure 2-9. The stresses are transferred from the tendons to the concrete through the anchors as there is no bond between the tendon and the concrete; this makes the long-term integrity of the anchor to the concrete crucial during the tendon service life. The sheathing provides several advantages to the system. Firstly, it works as a barrier against moisture and sequentially protects the tendon from corrosion. Secondly, the plastic sheathing works as a breaker for the bond and provides protection from mechanical handling damage (Aalami, 1994).

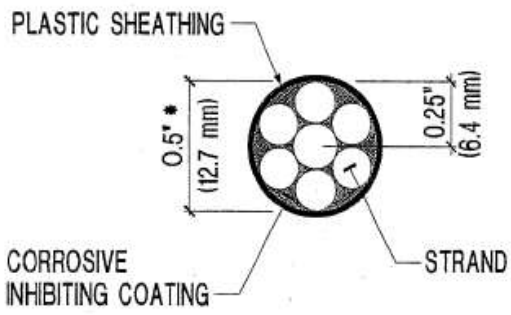

Figure 2-9 7-Wire Unbonded Tendon (12.7mm) (Aalami, 1994)

The bonded post-tension system is mainly characterized by the bond between the tendon and the concrete surrounding it. This bond is created by inserting a bonding matrix called the grout, in a duct that can be made of plastic or steel and can be either corrugated or flat. Corrugated ducts are shown in Figure 2-10. Mono-strands or multi-strands system are used for the bonded post-tension concrete members; the multi-strands system contains multiple tendons in each duct while the mono-strand system is a system that contains only one tendon in each duct, as shown in Figures 2-11 and 2-12

Also, the multi-strands system can be circular or flat, where the flat is used for the slab's applications while the circular is used for the beam's application (Aalami, 1994).

Figure 2-10 Corrugated Ducts for Bonded Post-Tension System (https://www.indiamart.com/proddetail/post-tension-gi-sheathing-duct-gi-corrugated-duct-21519115162.html, 2021)

Figure 2-11 Multi-strands application (http://www.tensionedconcrete.com.au/post-tensioning-services/, 2021)

Figure 2-12 Mono-strands system application (https://www.dywidag-systems.com/projects/2009-info-17/dsi-monostrand-system-prevents-loss-of-material/, 2021)

The bonded and the unbonded systems have different construction stages and steps. The unbonded system is considered faster in construction due to the bonded system's extra steps required for construction. The unbonded system only involves the tendons fixation followed by the pouring of concrete and then the tendon's prestressing. On the other hand, the bonded system includes extra construction phases such as the fixation of the empty ducts, the threading of the tendons inside the ducts and the grouting. These extra activities are considered additional labor operations and consequently additional costs and slower construction cycle (Aalami, 1994).

The bonded system has another problem related to the grouting where the ducts may be subjected to occasional problems like the blockage or failure of the duct during the construction. Also, the bonded system ducts are sensitive to the temperature changes and the environment, so they need supports at close intervals to maintain the tolerance of the vertical plan placement (Aalami, 1994).

The unbonded tendons are considered more flexible than the bonded tendons as the bonded tendons are inserted in flat ducts; the unbonded tendons become easier and faster for installment and for retaining the designed profile. The unbonded tendons are considered easier for maneuvering and accommodating for openings and untraditional member shapes due to their flexibility. There are some ducts used for the bonded system that are too flexible and hence require higher number of supports at frequent intervals. In the case of failure or repairing the unbonded tendons flexibility gives a privilege for its ease of replacement and repair. Simply the unbonded tendon can be pulled out of the concrete member and replaced with a new one; splicing and other techniques can be used to recover the ruptured or cut unbonded tendon. While the bonded tendon lacks the replacement flexibility due to the continuous bond between the tendon and the concrete (Aalami, 1994).

The unbonded tendon's design provides a high level of protection against moisture and consequently corrosion of the steel strands. In contrast, the bonded tendons may be subjected to the corrosion risk in case of pour grouting that does not cover the whole surface area of the tendon or that the grout may contain any corrosive material. Also, ferrous ducts would direct the bonded tendons to corrosion and hence results in a low durable structure (Aalami, 1994).

Apart from the corrosion protection provided for the unbonded tendon through greasing and plastic sheathing, the unbonded tendons are protected from corrosion at the anchorage zone. Zero encapsulated anchors now used are designed for the aggressive environments as they are isolated and void less anchors. The zero encapsulated anchors are made up of plastic sheath and plastic grease that cover the anchor and grease cap for the tendon's tail as shown in Figure 2-13. The bonded tendons may encounter higher losses due to friction than the unbonded tendons specially in case of a heavily profiled and a short tendon (Aalami, 1994).

Figure 2-13 Zero-Encapsulated Anchor components (https://gti-usa.net/, 2021)

The rest of the short-term losses, elastic shortening and seating losses, are the same for both systems, the bonded and the unbonded. There is a difference between the bonded and the unbonded systems for the shrinkage, creep of concrete and the steel relaxation losses. For the bonded tendons, the long-term losses depend on the strain of the adjacent concrete to the tendons, while for the unbonded tendons, the long-term losses depend on the average prestressing of the prestressed concrete element (Aalami, 1994).

2.4 Codes of practice provisions

ACI 318-19 code's provisions provide design requirements for the bonded and unbonded systems. The bonded and the unbonded systems have the same allowable initial and service stresses for concrete. Also, the maximum and minimum values of prestressing force are the same for both systems. The shear resistance and cover distance requirements are the same for the bonded and the unbonded systems. However, the ACI 318-19 differentiates between the maximum values of the bonded and the unbonded tendon's stress at the ultimate limit state. The ACI 318-19 provides an empirical equation that calculates the unbonded tendon's ultimate stress. The unbonded tendon's ultimate stress cannot be calculated according to the strain compatibility concept due to the absence of bond between the unbonded tendon and the concrete. The ACI 318-19 limits the ultimate stress of the unbonded tendon to a maximum value equal to the yielding stress, while the bonded tendon's ultimate stress is not limited to this maximum value.

Moreover, according to the ACI 318-19, the bonded prestressed concrete members are not required to have additional non-prestressing steel reinforcement, however, a minimum amount non-prestressing bonding reinforcement is required for unbonded prestressed concrete members for crack control. Also, this minimum reinforcement requirement maybe added to ensure the flexural

behavior at the ultimate stage instead of a tied arch behavior. Non-prestressing steel reinforcement maybe added to limit the spacing and the crack width during the service stage in case of high tensile stresses that exceed the concrete modulus of rupture. The minimum amount of non-prestressing steel reinforcement added to the unbonded tendon prestressed one-way slabs is calculated depending on the geometry of the section. The ACI 318-19 states the following equation to calculate the non-prestressing steel reinforcement required; $A_{s\,min} = 0.004A_{ct}$, Where A_{ct} is the area between the flexural tension face and the gross section's centroid.

The max design tensile strength of the bonded tendons prestressed member is higher than that of the unbonded ones according to ACI 318-19. The gap between the design strength of both systems may be filled with supplementary non-prestressing steel reinforcement to the unbonded prestressed member. Still, the bonded system is not in favor of the unbonded system as the cost of supplementary reinforcement is less than the cost of grouting (Bondy, 2012)

2.5 History of prestressed and post-tension concrete

The prestressing technology started to appear in 1886 when P.H.Jackson of San Francisco has produced the first prestressed concrete patent. Then later prestressed concrete developed in 1928 when Eugene Freyssinet of France introduced the usage of high tensile steel wires to the prestressed concrete members. Before high tensile steel acquaintance, there were many attempts to use normal strength concrete, but all attempts failed because of the prestressing losses due to shrinkage and creep. Creep is the continuous shortening of concrete with time under the effect of constant stresses and happens after the prestressing of the concrete member. While the shrinkage takes place due to the moisture loss of the concrete element over time and consequently causes shortening of the member. The shortening of concrete members due to shrinkage and creep reaches 0.1 % and when low-tensile steel is used, the steel tendons cannot be elongated by more than 0.15% during the prestressing process. So in the case of lower strength steel is used for concrete prestressing, two-thirds of the prestressing is lost because of the shortening to the concrete members. On the other hand, high strength steel wires can be elongated during the prestressing process to almost 0.7%, and even with the losses of concrete due to shrinkage and creep, 80% of the prestressing remains. Freyssinet also recommended using the high strength concrete with high

strength steel wires to reach a higher level of precompression and lower the losses due to creep and shrinkage (Post-Tensioning Institute Manual, 2006).

Afterward, the conical wedges were designed by Freyssinet in 1939 to anchor the steel wires to the prestressed concrete member's end. Also, Freyssinet introduced special jacks to be used in the prestressing and anchoring of the wires. Later, professor Gustave Magnel of Belgium, in 1940, established a new system made up of curved, multi-wire tendons to be inserted on rectangular flexible ducts. The improvement of the prestressing technology stopped during world war two but was resumed again after the war ended due to the high demand on prestressed concrete to replace the damaged structures in Europe in the post-world war years. France and Belgium had been the leading countries in the advancement of the prestressed concrete, still England, Germany, Switzerland, Holland, Russia and Italy followed (Post-Tensioning Institute Manual, 2006).

Post-tension concrete was first used in the U.S in 1949 to construct a landmark bridge in Philadelphia. The bridge is made of post-tension precast girders. Then, in the mid of 1950s, a post-tension building was constructed in the U.S using the lift-slab construction method. By the 1960s, the post-tension box girders majorly spread in California and other Western states. Also, the unbonded tendons were being broadly used for floor systems at the same period. In addition, in the 1960s, post-tension nuclear containment started to be used and by the 1970s, the importance of the usage of the post-tension technique for other applications such as post-tension foundations for large structures and the use of prestressed rock and soil anchors for tying back and down the structures were considered (Post-Tensioning Institute Manual, 2006).

Development of the post-tension technology through the years since its introduction is due to the following points; firstly, the strands system introduction, the single strand tendon cast fabrication from ductile iron and its development. The load balance design method and the banded tendon layout for two-way slabs introduction allowed a wider usage of the post-tensioning system. At last, the usage of computers for the analysis and design, the construction of the post-tensioning institute and the advancement of the corrosion resistance of the tendons increased the demand over the post-tensioning technique (Post-Tensioning Institute Manual, 2006).

2.6 Unbonded tendon's stress in the ultimate limit state

The unbonded system is broadly used in the construction industry and has many forms. The unbonded system is made of internal or external tendons. The external tendons are used for the retrofitting of concrete structures applications or the rehabilitation of old deteriorated structures, and being used for new construction applications. The wide usage of the unbonded post-tension system for many applications leads to the importance of investigating the design and analysis procedures followed for the unbonded post-tension concrete structures. The behavior of the bonded and the unbonded tendons is the same during the working stage, but majorly differs during overloading. The bonded tendon's ultimate stress (f_{ps}) depends on the concrete section and the bond between the bonded tendon and the concrete surrounding. The unbonded tendon's ultimate stress (f_{ps})depends on the whole section's deformation because of the relative movement between the tendon and the surrounding concrete (Au et al. 2004). In order to calculate the unbonded tendon's stress increase, the deformation analysis of the whole section is needed during the elastic, inelastic and ultimate limit state. The nominal resistance moment of unbonded post-tension members is recommended by many codes of practice to be predicted and verified at the ultimate stage. This could be done through non-linear analysis or numerical techniques, but an empirical equation is required for code determinations. A general approach governed by most codes of practice to determine the unbonded tendon's ultimate stress is from the following equation; $f_{ps} = f_{pe} + \Delta f_{ps}$, where f_{pe} is the effective prestress under the effect of the final prestress after the reduction due to losses and the moment due to dead loads only. Δf_{ps} is the ultimate stress increase by the cause of additional loading. For the calculation of the final prestressing value after the reduction of the losses and for the estimation of the creep losses, the moment due to dead loads has to be considered (Naaman et al. 1991).

Ozkul et al. (2008) mentioned that the general method acquainted for estimating the unbonded tendons ultimate stress is challenging because the change in the unbonded tendons ultimate stress depends on the whole concrete member's deformation and not the single section. Also, the stress increase of the unbonded tendon depends on the interaction between the stressed tendons and the concrete member. Accordingly, a relation between the unbonded tendon stress and the whole member deformation must be proposed to conduct a rational analytical model that could predict the increase in the unbonded tendon stress for any loading level or limit state. The analytical

models should also depend on the material's properties and the structure's mechanism (Ozkul et al. 2008).

According to Yang et al. (2013), the developed analytical models used to calculate the unbonded tendon stress increase depend on the idealized plastic region strain compatibility with the aid of an equivalent plastic hinge length and/or a bond reduction factor. The coefficient of bond reduction had been introduced as a constant or a function of the span-to effective depth ratio (L/d_p). The absence of bond between the unbonded tendon and the concrete affects the deformation of concrete and the propagation of cracks. The equivalent plastic hinge length is the zone where most of the deformations take place. The plastic hinge length is the zone that is a function of the neutral axis depth c of the section at the ultimate state. The value of the c is difficult to be determined as it is related to the tendon's stress increase. By origin in 1949, Baker had introduced the coefficient λ for bond reduction and defined it as the ratio between the average and the maximum stress of the concrete adjacent to the steel tendon. The bond reduction coefficient value was developed with a safe limit λ =0.1 at the ultimate limit state (Baker, 1949). Later, Janney et al. (1956) suggested for the bond reduction factor a ratio between the neutral axis and the prestressed tendons depth at the ultimate stage, where $\lambda= c/d_p$.

Au et al. (2004) developed a study demonstrating the different approaches governed to calculate the unbonded tendon's ultimate stress. The first approach is based on the span-to-depth ratio and the loading type. This approach adopts some assumptions, one of these assumptions is that the ultimate stress is constantly distributed through the entire tendon's length as there is no friction between the unbonded tendon and the concrete. The second assumption developed provide that the unbonded tendon's total elongation between the anchorages is impacted by the curvature distribution throughout the length of the member. The last assumption provides that the plastic deformation at the plastic hinge length zone is the main cause of the total elongation as the elastic region deformation is neglected. Through this approach, plastic hinge length is calculated with the aid of different factors such as the span of the member, the prestressing steel depth and the loading coefficient arrangement. Then, the compatibility of strain and equilibrium of forces concept used to calculate the unbonded tendon's ultimate stress. Au et al. (2004) stated that the derived model by Harajli (1990) was examined against the experimental test results of the unbonded tendons

ultimate stress carried by Warwaruk et al. (1962) Mattock et al. (1971) and Du et al. (1985), in which the proposed equation results were concluded to be fairly accurate. The model proposed by Harajli (1990) was furtherly investigated by Lee et al. (1999) to introduce a new design equation to calculate the unbonded tendon's ultimate stress. Throughout this new proposed equation, the arrangement of loads coefficients values proposed by Harajli were changed, the moment equilibrium equation replaced the force equilibrium equation and a new coefficient (K) which was found by regression of previous researches was introduced. The validity of Lee's proposed equation was tested against the available tests results. Lee's equation for the calculation of the unbonded tendons ultimate stress showed a very high correlation coefficient than the ACI 318-95 equation. The authors stated that the code's equation needs further investigation. However, the K coefficient values were derived from the regression analysis of past tests results.

The second design approach depends on the neutral axis's depth, Pannell (1969) has related the plastic region's length to of the neutral axis's depth and the ratio of the plastic hinge length to the neutral axis depth was found to have a constant value with different span-to-depth ratios. Pannell (1969) recommended this ratio to have a value equals 10. The British Code BS 8110 and the Canadian Code A23.3-94 used pannell's (1969) recommendation as a base to calculate the unbonded tendon's ultimate stress. Later, Au et al. (2004) performed a comparison between a data set to assess the applicability of having a constant value for the ratio between the plastic hinge length and the depth of the neutral axis. The conclusion of this research was that it is applicable to use the ratio as a constant value. The differences between the values of the ratio are due to the usage of different techniques, different materials and different measurement methods. Also, it was concluded that the ratio of the plastic hinge length to the depth of the neutral axis slightly decreases as the span-to-depth ratio decreases. Then Au et al. (2004) proposed a new equation derived from the development of the Pannell's (1969) approach. The authors proposed a value for the ratio between the plastic hinge length to the depth of the neutral axis equal 9.3 depending on a correlation analysis carried out on test data. In addition, the authors used the neutral axis's depth calculated depending on the unbonded tendon effective stress and not the neutral axis's depth Pannell derived from the unbonded tendon ultimate stress as it is still unknown. Sequentially, they proposed a new equation to calculate the unbonded tendon's ultimate stress and this equation was concluded to be applicable for materials like fiber-reinforced polymer (Au et al. 2004).

2.7 Literature Review

Burns and Pierce, (1967) carried out an experimental study that included 15 prestressed beams (I-shaped and ribbed sectioned) with unbonded tendons in addition to supplementary reinforcement. The main variable mentioned in this study is the amount of non-prestressed reinforcement. This study concludes that the ACI 318-63 equation gave very conservative values for the prediction of the unbonded tendon's ultimate stress (Burns et al. 1967).

Cooke et al. (1981) have conducted an experimental study to compare between one-way slabs of bonded and unbonded tendons. The study included 12 slab samples, where 9 were prestressed with unbonded tendons and the other three were prestressed with bonded tendons. The nine unbonded slabs were of different spans; the first three had a 4.6m span, the second three slabs had a 3.4m span and the last three were of 2.2m span. The bonded slabs had a span similar to the second group (3.4m). The widths of each slab in each group were 353, 705 and 1182 mm. All slabs had a depth of 180mm thick; the first two slabs of each group had three tendons of diameter 12.7mm, and the third had three tendons of diameter 7.9mm. All tendons had a straight profile with an eccentricity of 121mm. No non-prestressed steel reinforcement was added in all the samples. The specimens were subjected to two-line loads applied from two points. This experimental study showed that both the bonded and unbonded post-tension slabs had almost similar ultimate behavior. Each group of the unbonded post-tension slabs had a tendon length to effective depth ratio of 40, 30 and 20, respectively and prestressing steel index of $(q_e = \frac{\rho_{ps} f_{pe}}{f_c^{/}})$=0.25, 0.125 and 0.025, respectively. The tendon length to depth ratio is the effective factor in affecting the stress in steel as the slab deflects and not the span to depth ratio. The span to depth ratio of the three groups are 26.7, 20.2 and 13.3. All of the strands were stressed to 65 % of the strand's ultimate stress. The fourth unbonded post-tension slab showed flexural strength of 1.6 % higher than the similar bonded post-tension slab. Both slabs have a similar prestressing steel index. The two slabs showed similar average crack spacing of 163mm, the maximum crack width of the bonded post-tension slab at failure was 3.8mm while the crack width at the failure of the unbonded post-tension slab was 7.0mm. The group with the lowest prestressing steel index developed either one or two cracks and a very shallow concrete crushing zone. As the crack occurred for these three slabs the load dropped off significantly resulting in flexural instability. Upon more loading, the crack widened more with

a small increase in load until crushing of concrete. The bonded post-tension slab of similar dimensions and reinforcement showed flexural instability and had a flexural strength of 33 % more than the unbonded post-tension slabs of similar prestressing steel and span ratio. The unbonded slabs with middle value for the prestressing steel index showed a better flexural behavior with less cracks than the slabs with the highest prestressing steel index. These slabs had ductile failure and was companioned by concrete crushing before failure. The strength of the bonded slab in flexure was higher than that of the unbonded slabs by 5 %. Overall, the f_{ps} increases with the decrease in the prestressing steel index and the decrease in the tendon length to effective depth ratio. The slabs with prestressing steel index 0.125 were the most ductile and had higher deflection values than slabs with the highest and the lowest prestressing steel index. The slabs with the highest prestressing steel index showed large neutral axis depth and hence slight deflection. The unbonded slabs with the lowest prestressing steel index, showed less deflection than slabs with the highest prestressing steel index; this is due to the smaller plastic hinge length of the unbonded post-tension slabs with low prestressing steel index. (Cooke et al. 1981).

Naaman et al. 1991, has carried out a state-of-art review study that covered some of the research carried to discuss the different factors that affect the increase in the unbonded tendon's ultimate stress. They have mentioned the study carried by Pannell (1969), that has conducted an experimental and analytical study to investigate the span-to-depth ratio on the behavior of the unbonded prestressed beams in flexure. The study included 38 beams with main variables; span-to-depth ratio, the effective prestress and the reinforcement amount. Pannell (1969) derived an equation to calculate the unbonded tendon's ultimate stress, Equations 2-1 and 2-2. Where the unbonded tendon's stress at the ultimate limit state is given by:

$$f_{ps} = \frac{f_c^{/}\left[\frac{\left(\frac{A_{ps} f_{pe}}{b d_p f_c^{/}}\right) + \lambda}{L + \frac{\lambda}{\alpha}}\right]}{\rho_{ps}}$$

Equation 2-1

Where,

$$\lambda = \frac{\psi \rho_{ps} \varepsilon_{cu} E_{ps} d_p}{L f_c^{/}} \qquad \text{Equation 2-2}$$

The ε_{cu} is the concrete top fiber strain at the ultimate stage, ψ which is the plastic hinge length to the depth of the neutral axis c, α=0.85 β1 (For cylindrical compressive strength), or α=0.68 β1 (For cubic compressive strength), where β1 is the stress reduction factor as defined in the ACI code. ρ_{ps} is the prestressed reinforcement ratio (A_{ps}/bd_p), $f_c^{/}$ is the concrete compressive strength and d_p is the distance from the prestressed steel's centroid to the top of the compression fiber, Equations 2-1 and 2-2 (Naaman et al. 1991).

Then, Naaman et al. (1991) mentioned the experimental test carried by Tam and Pannell (1976) on eight beams that are partially prestressed using unbonded tendons and a single point load located at the mid- span. They included three main variables in their study, the effective prestress f_{pe}, the span-to-depth ratio and the amount of prestressed and non-prestressed steel used. They concluded that the value of the ratio between the length of the plastic hinge and the depth of the neutral axis is more practical to be taken as 10.5 and that all beams generated fine cracks similar to the beams prestressed using bonded tendons. Sequentially a new equation was developed based on Pannell's (1969) previous equation that considers the effect of the supplementary non-prestressed reinforcement. Equation 2-3 shows the equation developed by Pannell and Tam (1976) (Naaman et al. 1991).

$$f_{ps} = \frac{f_c^{/}\left[\frac{\left(\frac{A_{ps} f_{pe}}{bd_p f_c^{/}}\right)+\lambda}{L+\frac{\lambda}{\alpha}} + \frac{\left(\frac{A_{ps} f_{pe}}{bd_p f_c^{/}}\right)+\lambda}{\alpha+\lambda}\right]}{\rho_{ps}} \qquad \text{Equation 2-3}$$

The A_s and f_y are the area and the non-prestressed reinforcement's yield stress.

Naaman et al. (1991) indicated that Elzanaty and Nilson (1982) carried out an experimental test on eight small- scaled models of unbonded post-tension beams. The test was of two series; one included under- reinforced beams and the other series include over-reinforced beams. They were

studying the effect of varying the value of the unbonded tendon's initial stress on the behavior of the partially prestressed beams in flexure. They concluded that the usage of the bonded reinforcement is effective in distributing the cracks. For the over-reinforced series, the ACI 318-77 code equation results give conservative values while the same equation gives un-conservative values for the under-reinforced series of beams. In addition, the authors developed a procedure to estimate the increase in stress at the working stage based on the moment of inertia concept and the results were concluded to be in excellent agreement with the test results (Naaman et al. 1991)

Moreover, Naaman et al. (1991) mentioned that Du and Tao (1985) who had conducted an experimental study on 22 partially prestressed beams with unbonded tendons, in order to examine the effect of the non-prestressed reinforcement on the tendon's ultimate stress. They tested the specimens under third-point loading and maintained the span-to-depth ratio of all of the specimens as 19.1. The main variables were the amount of prestressing steel, non-prestressing steel reinforcement and the concrete's compressive strength. They conducted an equation to predict the unbonded tendon's ultimate stress. Although their proposal included calculating the unbonded tendon's ultimate stress increase depending on the moment curvature factor, they did not illustrate how this relation was derived and did not clarify it as an assumption for the equation (Naaman et al. 1991).

Naaman et al. (1991), have mentioned that Chouinard (1989) performed a third-point loading test on six partially prestressed beams. This test included the non-prestressed reinforcement as the only variable. The author was testing the effect of increasing the amount of reinforcement on decreasing the unbonded tendon's ultimate stress, so five of the beams were over-reinforced. They observed that within the region of constant moment at the prestressing steel level, close to the mid span of the beams with no supplementary reinforcement, one or two wide cracks were formed and high strain was developed. On the contrary, beams with non-prestressed reinforcement developed more uniform strain distribution with a larger number of fine cracks (Naaman et al. 1991).

The state of art review for the computation of unbonded tendons ultimate stress in simply-supported members conducted by Naaman et al. (1991) resulted the following conclusions: (1) the unbonded tendon's ultimate stress (f_{ps}) is limited to the minimum value of the yield stress (f_{py}), or the effective prestress of the prestressed tendons (f_{pe}). (2) The non-prestressing steel has an

influence on the value of the unbonded tendon's ultimate stress that must be considered (Naaman et al. 1991)

Naaman et al. (1991) proposed a strain reduction coefficient, which is the unbonded tendon increase in strain to the concrete's average strain at the prestressing steel level. The proposed coefficient is to be used for beams that are fully or partially prestressed with either unbonded internal or external tendons for both uncracked and linear elastic cracked range of behavior (Naaman et al. Part 2, 1991).

Naaman et al. (1991) proposed an equation for calculating the unbonded tendon's ultimate stress (f_{ps}) by including the early introduced coefficient for the strain reduction and the ratio of the neutral axis to the prestressing steel depth at the ultimate limit state. According to the earlier studies, the variables such as the span-to-depth ratio and the loading conditions are the most effective variables and the strain reduction coefficient used in the proposed equation considers these factors. The results of the proposed equation were compared to data from previous studies. The author's equation showed excellent correlation in comparison to other previously proposed equations (Naaman et al. Part 2, 1991)

Harajli and Kanj (1991) tested 26 unbonded partially prestressed concrete beams. They included the reinforcement index, span-to-depth ratio and the loading type as the main variables. As a result of this experiment, they concluded the following: both the span-to-depth ratio and the plastic hinge length have the same important effect on the unbonded tendon's ultimate stress (f_{ps}). Also, they concluded that the parameter $\rho_{ps} / f_c^{/}$, which is included in ACI318-83 is not a rational parameter for design (Harajli et al. 1991)

Harajli and Hijazi (1991), performed an analytical study to investigate the unbonded tendon's ultimate stress in partially prestressed beams. They introduced a theoretical model to understand the behavior of beams which are partially prestressed with unbonded tendons in flexure. With the theoretical model, they made a parametric study to investigate some factors' effect, such as span-to-depth ratio, types of load application, cross section geometry, reinforcing ratio, partial prestressing ratio, effective prestress, concrete stress and types of steel. It was found that the span-to-depth ratio, amount of bonded steel reinforcement and the loading pattern have the most

significant effect on the unbonded tendon's ultimate stress. They concluded that the larger the span-to-depth ratio, the lower the unbonded tendon's ultimate stress (f_{ps}) (Harajli et al. 1991).

Moon and Burns (1997) carried out a computational procedure including the non-linear time-dependent constitutional law of concrete and the usage of the hybrid type element method to propose an equation that could predict the unbonded prestressed concrete member's behavior. This method proposed by Moon and Burns was embedded in a program that they developed (TAPS) in addition to three numerical solved examples for verification. The results were compared to 30 experimental test data in order to assess the stress at failure and the load-deflection response. The experimental test results were compared to the proposed equation results and Naaman and Alkhairi proposed equation results. The conclusion was that the plastic hinge length and the bonded reinforcement have a significant effect on the value of the tendon's ultimate stress increase.

Manisekar et al. (2006) have mentioned that Naaman, Burns, French, Gamble and Mattock, the subcommittee of the ACI-ASCE (2002) have carried out a procedure to represent the state of the art and the best trade-off to calculate the unbonded tendon's ultimate stress (f_{ps}). The authors highlighted that the unbonded tendon's ultimate stress cannot be obtained with the same procedure as the bonded tendons due to the absence of bond between the concrete and the tendon. Consequently, the application of the compatibility of strain is time-consuming. The authors proposed two alternative equations for calculating the unbonded tendon's ultimate stress (f_{ps}) that give approximate results but saves time and effort. The first equation is applicable for slabs and other cases, giving approximate conservative results. The second proposed equation is applicable for all cases and is a more refined prediction equation. They also concluded that for any load case and span, a minimum value for the stress increase would be limited to 52.5 MPa.

Manisekar et al. (2006) reviewed the computed values of the unbonded tendon's ultimate stress derived from predicted equations and compare it against six sets of experimental data through the state of art review. They focused on the plastic hinge length's influence on the increase of the unbonded tendon's ultimate stress. Alqam et al. (2019), commented that Manisekar et al. (2006) compared the results to an old version of the American Code ACI 318-83, and their conclusion was contradictory to the previous research carried.

Harajli (2006) evaluated the accurate influence of the effective plastic hinge length on the increase of the unbonded tendon's ultimate stress. He developed an equation for calculating the unbonded tendon's ultimate stress, considering all of the important parameters. With the aid of a large database of simple and continuous members with internal or external unbonded tendons, an evaluation of the design expressions was carried out. This resulted in an accurate equation to calculate the effective plastic hinge length for simple and continuous unbonded members. Also, Harajli carried a comparative study and concluded the ACI Building Code's equation (18-4) and (18-5) give in accurate values for the ultimate stress and at some cases gives unsafe results.

Ellobody et al. (2008) has carried a parametric study to compare the unbounded tendon's ultimate stress using a non-linear finite element model to the computed ultimate stress using the British Standards (BS8110-01, 1997) equations. This mechanical non-linear finite element model was verified by carrying a comparison between its results and the results of an experimental test. The experimental test consisted of two slabs, each of different compressive strength for the concrete. The slabs were experimented under a flexural test. The finite element model predicted ultimate loads higher than the loads derived from the experimental test by 2-4%. The finite element model then was used to test 4 variables that would affect the structural behavior of one-way slabs pre-stressed using unbonded tendons. These variables are the concrete strength, slab depth, tendon forces and boundary conditions. Throughout this research, it was found that the ultimate loads predicted by the codified equations are smaller than that predicted by the FE model, with a mean value for the ratio the finite element model's ultimate load to the ultimate load calculated by the British Standard equation of 1.27. From these findings, it can be concluded that the conservation of the code design equation is due to limiting the design stress of the tendon to 0.8 of the tendon's ultimate stress and that in reality the cable's stress at the ultimate load will be between the yielding stress and the ultimate stress. Also, this research showed that the BS8110-01, provides a conservative equation to calculate the stress losses of the unbounded cables (Ellobody et al. 2008)

Zheng and Wang (2010) have carried an analytical investigation for determining the increase in the unbonded tendon's ultimate stress (f_{ps}). According to the carried simulation analysis, they concluded that the span to depth ratio has a minor influence on the ultimate stress increase in the unbonded tendons in the case of two-third point or uniform loading (Zheng et al. 2010)

He and Liu (2010) have introduced a simple methodology for computing the internally and externally unbonded tendon's ultimate stress (f_{ps}). They have proposed three different closed-form solutions depending on the loading type to calculate the increase in the unbonded tendon's ultimate stress. The study included the calculation of the ultimate stress in the unbonded tendon according to ACI 318-08, and compared to beam tests data of 89 specimens from old studies. It was found that ACI code equation shows conservative values and in some cases, it gives un-conservative values. The authors proposed equation showed a very good correlation with the experimental data, and it was concluded that the ratio of the eccentricity of the tendon at mid-span to the neutral axis depth at ultimate nominal strength has a significant effect on the unbonded tendon's ultimate stress (He et al. 2010).

Lee and Kim (2011) have carried out a review study for the existing methods and equations for calculating the unbonded tendons ultimate stress (f_{ps}) and they developed their own modified model for the unbonded tendons ultimate stress calculation (f_{ps}). The authors verified the model proposed by comparing the models results to a large data of results from previous studies related to the prestressed concrete member's flexural strength. The model proposed gave adequate results compared to the previous tests data, and reflected the impact of important factors such as the loading patterns, the strength of the concrete and the ratio of the non-prestressing steel reinforcement. The authors proposed model provided an adequate estimation for the unbonded tendons ultimate stress of members which are over reinforced (Lee et al. 2011)

Sisi (2013) carried out a parametric study to predict the unbonded tendon's ultimate stress. The main factors studied are load pattern, strength of concrete, mechanical reinforcement ratio and the ratio of span-to-depth. The conclusion of this study is as follows, firstly, the addition of bonding reinforcement and decreasing the number of unbonded tendons significantly increases the unbonded tendon's ultimate stress. Secondly, the higher the concrete strength, the higher the unbonded tendon's ultimate stress. Also, uniform and two-point loading give higher ultimate stress values than one-point loading (Sisi, 2013).

Yang et al. (2013) had proposed new factors to introduce a more straightforward approach for the unbounded tendon's ultimate stress calculation. In the new equation proposed, the tendon's ultimate stress is expressed as a factor multiplied by the yielding stress of the tendon, where this

factor is greater than one. This assumption is due to the fact that most of the beams with low reinforcement ratio index and lightweight concrete slabs showed ultimate tendon stress higher than the yielding stress. These new equations derived were tested through the test data of 188 members made of normal-weight and lightweight normal stress concrete. The results of this study showed that the proposed equations give results of great compliance with the test results and that the ACI 318-11 equations underestimate the unbonded tendon's stress increase at the ultimate stage. Also, the ACI 318-11 equations were concluded to give conservative values for unbonded tendon ultimate stress for the normal and lightweight concrete (Yang et al. 2013).

Alqam et al. (2019) have carried out a research covering the background information that resulted in driving equations for predicting the unbonded tendon's ultimate stress. The review study focused on simple prestressed beams with internal and external unbonded tendons. The authors observed that the unbonded tendons ultimate stress is highly influenced by the span-to-depth ratio and the plastic hinge length, according to the authors of the included researches. The authors concluded that a minor development took place in the non-linear analysis models proposed by the authors reviewed in this research (Alqam et al. 2019)

2.8 ACI equation history

Naaman et al. (1991) has carried a review study covering the advancement of the unbonded tendon's ultimate stress in the ACI provisions. The ACI Building Code in the 1963 version suggested an equation for the prediction of the unbonded tendon's ultimate stress, Equation 2-4 in the Ksi units and Equation 2-5 in the MPa units.

$$f_{ps} = f_{pe} + 15\ Ksi,\ or, \qquad \text{Equation 2-4}$$

$$f_{ps} = f_{pe} + 105\ MPa \qquad \text{Equation 2-5}$$

Experiments were carried out by Warwaruk et al. (1962) which included 82 partially prestressed simply-supported beams; 41 of these beams were prestressed with unbonded tendons. The loading type, concrete compressive strength and the reinforcement amount were the main variables in the investigation. The authors recorded that the beams with no reinforcement failed due to the development of one major crack, while the beams with supplemental reinforcement have developed a large number of cracks before the failure. They also reported that the beams

prestressed with unbonded tendons remained in the elastic range until failure. They plotted several parameters against the prestressing steel stress and a prediction equation was derived.

$$f_{ps} = f_{pe} + (30000 - \frac{\rho_{ps}}{f'_c} x10^{10})\, psi, and\, f_{ps} \leq 0.6\, f_{pu} \qquad \text{Equation 2-6}$$

Where ρ_{ps} is the ratio of the prestressing steel reinforcement and f'_c is the concrete compressive strength.

Equation 2-6 was compared to ACI 318-63 code Equations 2-4 and 2-5, it was reported to be conservative. Later, a strain reduction coefficient was used to reduce the concrete top fiber's strain at the ultimate stage. Afterward, Mattock et al. (1971) carried out an investigation study where they tested seven simply-supported partially prestressed beams and three continuous beams. The span to depth ratio was fixed for all specimens. The main variables were the availability or the absence of the bond, and the supplemental non-prestressed reinforcement. The following conclusion was reported, the experiment results showed 30 % higher f_{ps} for the unbonded tendons when compared to the ACI 318-63 equation. Secondly, they concluded that as the ρ_{ps}/ f'_c ratio increases, the difference between the predicted and the observed f_{ps} decreases. Also, this experiment proved that the ACI 318-71 reflects the behavior of the beams that are simply-supported with unbonded tendons satisfactorily. They also observed that the cracks width and their distribution are similar for both the unbonded and the bonded prestressed beams, given that non-prestressed reinforcement was present. It was then recommended that 0.4 % of the total area at the critical section to be a minimum reinforcement that must be added while using unbonded tendons. Mattock et al. (1971) also concluded that both ACI Building Code equation, Equation 2-4 and Equation 2-6 are too conservative at low ratios of reinforcement and they developed and proposed a new equation which is

$$f_{ps} = f_{pe} + (\frac{1.4 f'_c}{\rho_{ps}}) + 10000 \text{ psi} \qquad \text{Equation 2-7}$$

This equation was later adapted in the ACI Building Codes with minor modifications in versions 1971 and 1977 presented in Equation 2-8,

$$f_{ps} = f_{pe} + (\frac{f_c^{/}}{100\rho_{ps}}) + 10000\ psi, and\ f_{ps} \leq f_{pe} + 60000\ psi$$ Equation 2-8

Later, Mojtahedi et al. (1978), carried out a comparison study between the results observed from testing simply-supported beams, continuous beams and continuous unbonded prestressed slabs. The authors tested the span-to-depth ratio's effect, and they reported that the span-to-depth ratio has a major effect on the ultimate stress at the nominal bending resistance. The authors emphasized their finding by conceptually modelling a triangular truss to comprise two symmetrical compressive members and a tie to simulate the unbonded prestressed cracked beam. The results show that the strain in the tie at the mid-span hinge decreases as the span to depth ratio increases. Their results also show that the equations from Equation 2-6 till equation 2-8 overestimate the tendon's increase in stress for a span-to-depth ratio of 45 and at low reinforcement ratios, while these equations underestimate the ultimate stress increase at a low span-to-depth ratio. As a result, the ACI 318-83 modified the 1977 equation to accommodate the span-to-depth ratio to be as follows in Equation 2-9:

$$f_{ps} = f_{pe} + (\frac{f_c^{/}}{\mu\rho_{ps}}) + 10000\ psi$$ Equation 2-9

Where μ=100 for $L/d_{ps} \leq 35$ and μ=300 for $L/d_{ps} > 35$, where L is the span and d_{ps} is the depth from the centroid of the prestressed steel to the top of the extreme compression fiber (Naaman et al. 1991)

This equation has not been changed since 1983, and later Zhang et al. (2010) commented that the ACI equations used to calculate the unbonded tendon's ultimate stress are derived from fitting experimental data, and these formulas developed could approximately estimate the ultimate stress in fixed ranges. These formulas do not consider factors such as reinforcement contribution, concrete and steel modulus of elasticity and the structure deformation. The structure deformation is a key factor because the cracked concrete section's deformation is totally different from that of a section at the elastic range. The nonlinear deformation is a key factor in affecting the ultimate stress on the unbonded tendons (Zhang et al. 2010).

According to the ACI 318-19 the equation for the calculation of the ultimate stress of the unbonded tendons for members with span to depth ratio less than or equal 35 is the least of the following:

$$f_{ps} = f_{pe} + 70 + \frac{f'_c}{100\rho_{ps}} MPa$$ Equation 2-10

$$f_{ps} = f_{pe} + 420MPa$$ Equation 2-11

$$f_{ps} = f_{py}$$ Equation 2-12

While, the equation for the calculation of the ultimate stress of the unbonded tendons for members with span to depth ratio greater than 35 is the least of equations 2-13, 2-14 or 2-12.

$$f_{ps} = f_{pe} + 70 + \frac{f'_c}{300\rho_{ps}} MPa$$ Equation 2-13

$$f_{ps} = f_{pe} + 210MPa$$ Equation 2-14

3 Design of PT Slab Specimens

3.1 Slab specimen

In order to carry a comparison between the ultimate limit state behaviors of post-tension slabs with bonded and unbonded tendons, an experimental program is designed with the aim of measuring the bonded and unbonded tendons stress at failure. As mentioned earlier slabs are one of the most common applications of post-tensioning. Also, it is concluded that most of the previous experimental researches carried out to assess the behavior of the bonded and unbonded tendons used beams specimens, not slab ones. So, slab specimens are chosen for the testing program and according to the available lab floor space and testing capacity, simply-supported slabs with a 4.0-meters span and 1.0-meter width are designed. Based on the chosen span, a thickness of 0.16m has been calculated in order to have a span-to-depth ratio equals 25.

The testing program includes six slabs:

1) Set 1 (BS1 and BS2): slabs with bonded tendons and no non-prestressing steel reinforcement
2) Set 2 (UBS1 and UBS2): slabs with unbonded tendons and no non-prestressing steel reinforcement
3) Set 3 (UBSR1 and UBSR2): slabs with unbonded tendons and non-prestressing steel reinforcement

According to the ACI 318-19 provisions, a minimum amount of non-prestressing steel reinforcement has to be included in the unbonded prestressed slabs. The minimum amount of steel required is 0.004 A_{ct}, where A_{ct} is the area between the flexural tension face and the centroid of the cross section. The designed non-prestressing steel reinforcement is taken no. 10 mm @ 200 mm lower mesh (0.006 A_{ct}) with a concrete cover of 20mm.

A set of two slabs is tested for each type in order to get almost statistically correct results. The two sets with the bonded tendons and the unbonded tendons without non-prestressing steel reinforcement (sets 1 and 2) are tested to compare the results and the behavior of the bonded and the unbonded tendons under similar conditions. The third set of unbonded slabs with non-prestressing steel reinforcement (set 3) simulates the ACI 318-19 requirements for unbonded prestressed slabs. Figures 3-1 and 3-2 show plans and elevations of the experimental slab

specimens with and without non prestressing reinforcement with the reinforcement details and the prestressing tendon's configuration.

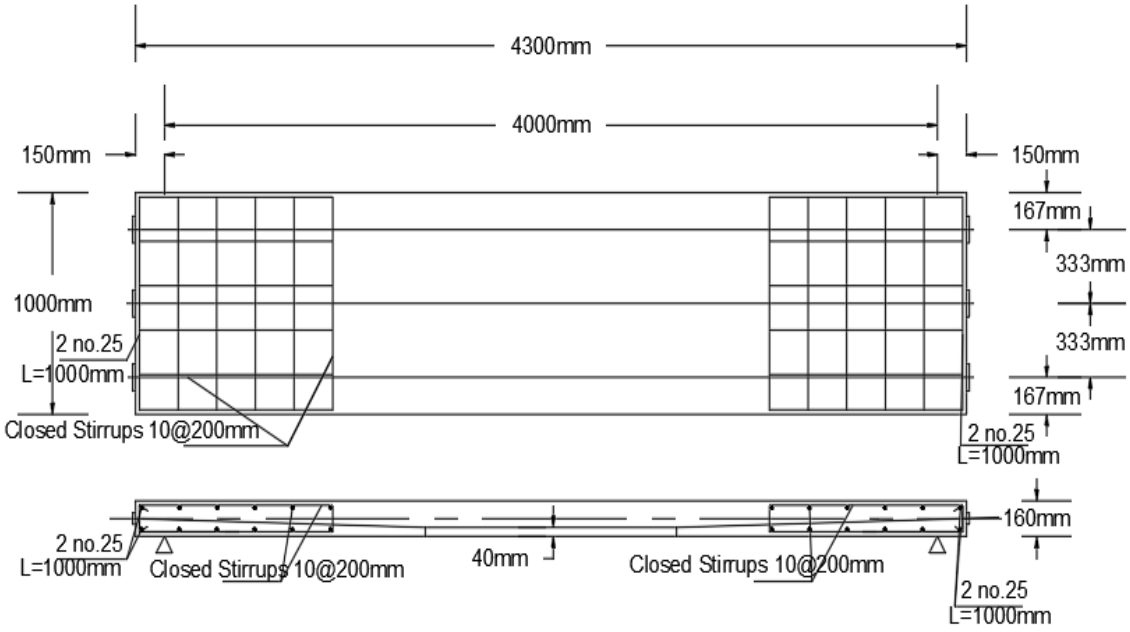

Figure 3-1 Post-tension bonded or unbonded slab cross-section and plan with all reinforcement and tendon details

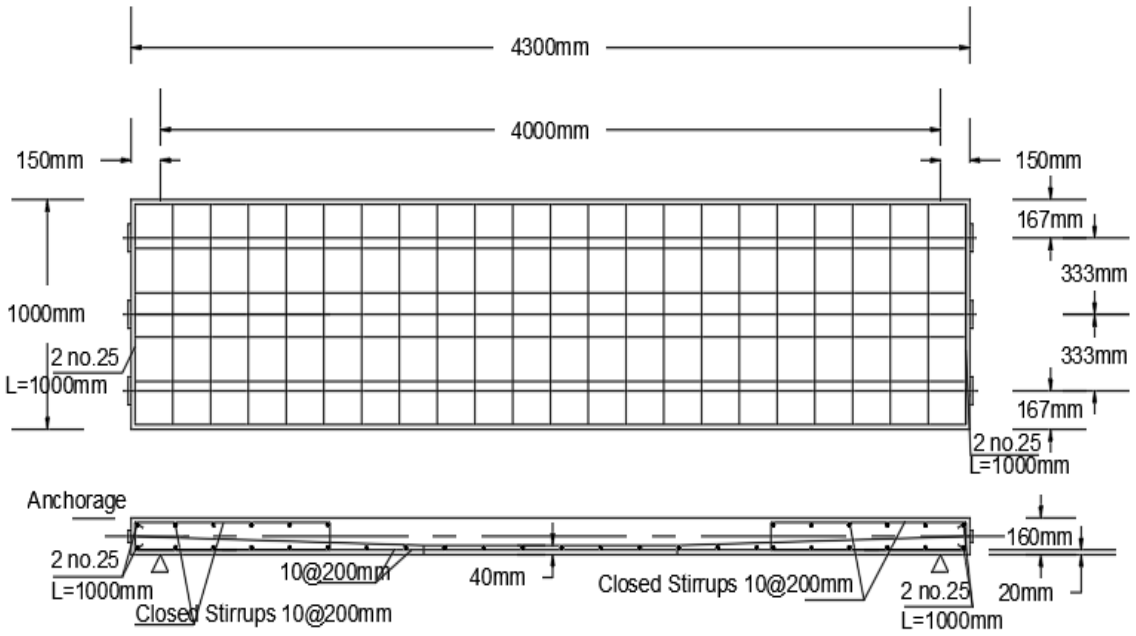

Figure 3-2 Post-tension unbonded slab cross-section and plan with non-prestressing steel reinforcement with all the reinforcement and tendons details.

Normal weight concrete with compressive strength of 30 MPa at 28 days and tendons with an ultimate strength of 1860 MPa are used for the tested slabs. The slab specimens have 4.0m span with an extension 0.15m from each side of the intended for the supports, which makes the total length of the specimen equals to 4.3m. Each slab contains 3 tendons of a diameter 12.7mm. The tendons are located with spacing 0.333m and with a spacing from the slab edge of 0.167m. Each tendon has one dead end and one live end in terms of the prestressing anchors.

A doubled-harped tendon shape is chosen with a maximum eccentricity at the slab's mid-span of 40mm and zero eccentricity at the slab ends. The tendon takes an inclined line profile with a length of 1.5m at the slab ends and a straight line profile with a length of 1.30m at the middle part of the span. The double-harped shape profile is chosen because the slabs will be tested under four points loading scheme; the tendon takes the shape of the generated bending moment due to this used type of loading. Figure 3-3 shows the loading test set-up, where the load from the testing machine P_{Exp} is distributed over two loading beams to generate two point loads $P_{Exp}/2$ on the specimens.

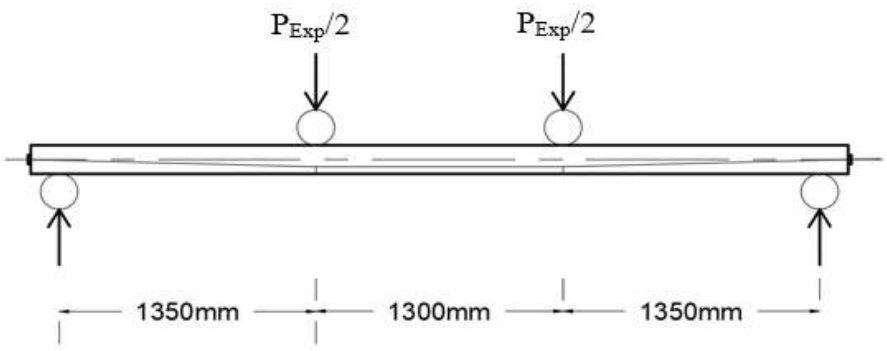

Figure 3-3 Four-point loading flexural test set-up

Anchors are used at the ends of the tendons; traditional anchorage system is used for the bonded tendons and supplied by STRANDS, Egypt. For the unbonded tendons, encapsulated zero void anchorage system is used to provide full protection for the unbonded tendons; this system is supplied by GTI Company, USA. Figures 3-4 and 3-5 show the traditional anchors for the bonded system and encapsulated anchors for the unbonded system.

Figure 3-4 Anchor for the bonded system provided by Strands (Egypt).

Figure 3-5 Encapsulated Anchor for the Unbonded System provided by GTI (USA).

Spiral stirrups are located around the cables at the end of the slabs to resist the stresses generated at the anchorage zone as shown in Figure 3-6. Closed rectangular stirrups made up of bars no. 10 mm @ 200 mm spacing in both directions are also used to account for the stresses generated at the anchorage zone and for the stresses that will be generated while hanging the slabs to move them inside the lab. Reinforcement added in the anchorage zone are all designed according to the ACI 318-19 provisions. In addition, 2 no. 25 mm transverse bars are added parallel to the slab edge ahead of the anchorage bearing face according to the ACI 318-19 requirements. Figures 3-1 and 3-2 show the location of the closed stirrups in the tested slabs in plan and cross sections.

Figure 3-6 Spiral Stirrups around the duct of prestressing tendon (https://www.tmgglobals.com/post-tensioning)

3.2 Preliminary specimen design

According to the ACI 318-19 provisions, the jacking force (P_J) should be the least of the following three values:

1) the maximum jacking forces recommended by the supplier
2) $0.94\ f_{py}$ and,
3) $0.8 f_{pu}$.

The value of the transfer force (P_i) must be less than $0.7 f_{pu}$. So, in order to ensure that the tendons stress will surpass yielding during testing, the highest of all these mentioned values is chosen to be the jacking force for the tendons which is the maximum jacking force recommended by the supplier; 150 kN per tendon and 450 kN per slab specimen (3 tendons).

In order to check the permissible stresses at the transfer stage, the short-term losses are preliminary calculated to be around 5 %, so the transfer force per slab is 427.5 kN. The compressive and tensile stress limitation at the transfer stage are calculated according to the ACI 318-19 provisions and the equations used to calculate the actual stresses at the top and bottom concrete fibers at the transfer stage are as mentioned in Equations 3-1 and 3-2.

$$f_{Top} = -\frac{P_i}{A} + \frac{P_i \times e \times y}{I} - \frac{M_{ow} \times y}{I} \leq 0.25\sqrt{f_c'} \qquad \textit{Equation 3-1}$$

$$f_{Bottom} = -\frac{P_i}{A} - \frac{P_i \times e \times y}{I} + \frac{M_{ow} \times y}{I} > -0.6 f_c' \qquad \textit{Equation 3-2}$$

Where the A is the gross area of the cross section ($b \times t$) where b is the slab width which is equal 1.0m and t is the slab thickness which is 0.16m, e is the eccentricity of the tendon from the centroid of the section (0.04m), M_{ow} is the moment due to the own weight of the slab (8 kN·m), y is the distance from the centroid of the slab to the top or bottom fibers of which the stress is calculated and I is the moment of inertia of the slab's cross section ($\frac{b \times t^3}{12}$).

At the transfer stage, the compression and tensile stress are calculated to ensure that they will not exceed the allowable stresses. The compressive strength of concrete at the age of 7-days is estimated to be 24 MPa, (about 80 % from the 28-days compressive strength). So the allowable compressive stress and tensile stresses are;

$$-0.6f_c^{/} = -0.6 \times 24 = -14.4MPa \qquad \text{Equation 3-3}$$

$$0.25\sqrt{f_c^{/}} = 0.25 \times \sqrt{24} = 1.22MPa \qquad \text{Equation 3-4}$$

The actual stress calculated at the concrete top fiber equals -0.53 MPa while the stress at the bottom fiber equals -4.8 MPa; both are less than the maximum permissible stresses according to the ACI 318-19.

The decompression stage follows the transfer stage, where the stress at the tendon location reaches zero. At this stage, the stress of the tendons decreased by the value of the short and long-term losses and sequentially, resulting the effective prestressing force (P_e). To calculate the load value from the loading machine (P_{Exp}), the stress is calculated at the location of the tendon and equated to zero as in the following equation:

$$f = -\frac{P_e}{A} - \frac{P_e \times e \times y}{I} + \frac{M_{Total} \times y}{I} = Zero \qquad \text{Equation 3-5}$$

Where the A is the gross area of the cross section ($b \times t$) where b is the slab width which is equal 1.0m and t is the slab thickness which is 0.16m, e is the eccentricity of the tendon from the centroid of the section (0.04m). M_{total} is the moment due to the own weight of the slab (8 kN·m) plus the moment due to the two point loads from the machine ($\frac{P_{Exp.}}{2} \times 1.35m$) where $P_{Exp.}$ is the load from the machine as shown in Figure 3-3, y is the distance from the centroid of the slab to the top or bottom fibers of which the stress is calculated and I is the moment of inertia of the slab's cross section ($\frac{b \times t^3}{12}$).

Then, the service stage follows up. The same equations as the transfer stage are used while using the effective prestressing force (P_e) and changing the tensile and compressive stress limits

according to the ACI 318-19. The tensile stress is limited to insure that the section is an uncracked one. In this stage, M_{Total} here is the moment due to own weight of the slab in addition to the moment from the two-point loads ($P_{Exp}/2$). The Equations 3-6 and 3-7 represent the stresses calculated at the top and bottom concrete fibers as follows:

$$f_{Top} = -\frac{P_e}{A} + \frac{P_e \times e \times y}{I} - \frac{M_{Total} \times y}{I} > -0.6 f_c' \qquad \text{Equation 3-6}$$

$$f_{Bottom} = -\frac{P_e}{A} - \frac{P_e \times e \times y}{I} + \frac{M_{Total} \times y}{I} \leq 0.62\sqrt{f_c'} \qquad \text{Equation 3-7}$$

Where the A is the gross area of the cross section ($b \times t$) where b is the slab width which is equal 1.0m and t is the slab thickness which is 0.16m, e is the eccentricity of the tendon from the centroid of the section (0.04m). M_{total} is the moment due to the own weight of the slab (8 kN·m) plus the moment due to the two point loads from the machine ($\frac{P_{Exp.}}{2} \times 1.35m$) where $P_{Exp.}$ is the load from the machine, y is the distance from the centroid of the slab to the top or bottom fibers of which the stress is calculated and I is the moment of inertia of the slab's cross section ($\frac{b \times t^3}{12}$).

Afterward is the yielding stage, where the stress in the tendons reaches the yielding stress and then follows the ultimate stage. Figure 3-7 illustrates the different stages the prestressing concrete section encounters.

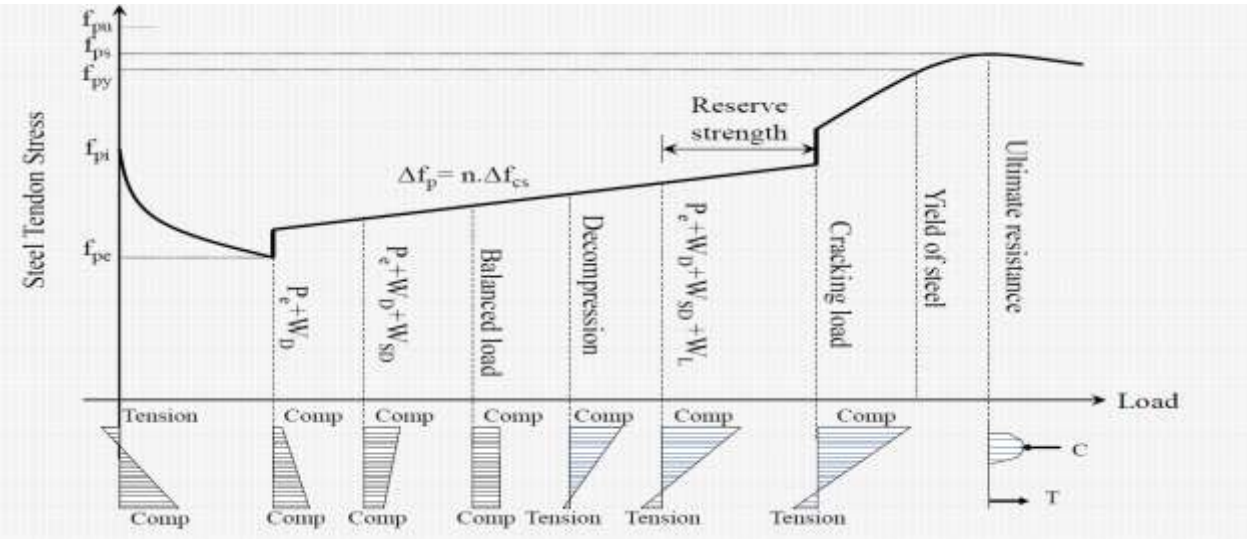

Figure 3-7 The Stress versus the Load curve showing the different prestressing stages. Sayed-Ahmed (2019), Design of PC members, Lecture notes, AUC.

At the ultimate stage, the tendon stress should have surpassed the yield stress. For the bonded tendons, the ultimate stress can be calculated using the strain compatibility concept. The strain in the prestressed concrete section is calculated according to the ACI 318-19 provisions, due to the effective prestress $\varepsilon_{pe,}$ the strain due to decompression ε_{dc} and the strain due to loading post decompression which is proportional to the distance from the neutral axis ε_{cs}. The three types of strain are combined to produce the total strain at failure ε_{ps} as shown in Equation 3-8.

$$\varepsilon_{ps} = \varepsilon_{pe} + \varepsilon_{dc} + \varepsilon_{cs}$$

$$\text{Where, } \varepsilon_{pe} = \frac{f_{pe}}{E_{ps}} \text{ ,}$$

$$\varepsilon_{dc} = \frac{P_e}{A_c E_c} + \frac{P_e \times e^2}{E_c I} \text{ and}$$

$$\varepsilon_{cs} = \varepsilon_{cu} \frac{d_p - c}{c} = 0.003 \frac{d_p - c}{c}$$

Equation 3-8

Where the f_{pe} is the effective prestress and its value is 1292 MPa and E_{ps} is the prestressing steel modulus of elasticity taken as 190,000 MPa. A_c is the area of concrete cross section, e is the eccentricity of the tendon (40mm), I is the moment of inertia of the concrete cross section, and E_c is the concrete modulus of elasticity 4500 $\sqrt{f'_c}$.

The effective stress is the stress after the deduction of the short and long-term losses. The long-term losses are assumed as 10%, so the effective prestressing force and stress are 382.5 kN and 1292 MPa, respectively. The ε_{pe} and ε_{dc} are calculated and their values are 0.006800 and 0.000189. Based on the strain compatibility concept, ε_{cs} is calculated by proportioning the distance to the neutral axis. Figure 3-8 illustrates the said compatibility and the equilibrium between the tension and compression force. d_p is the length from the top of concrete to the centroid of the prestressing tendons (120mm).

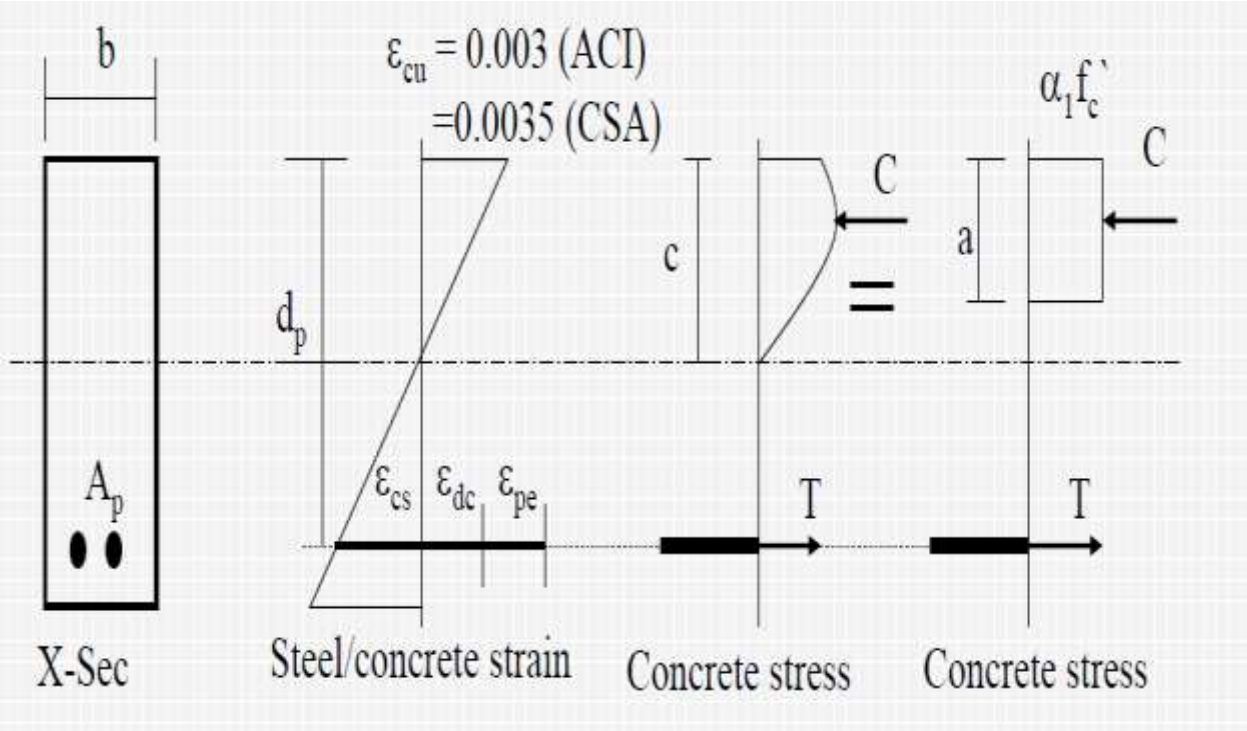

Figure 3-8 Strain Compatibility. Sayed-Ahmed (2019), Design of PC members, Lecture notes, AUC.

Equilibrium Equation 3-9 is generated by equating the tension force to the compression force in the cross section from the equilibrium of forces concept.

$$A_{ps} \times f_{ps} = \alpha_1 \times f_c^{/} \times a \times b \text{ , then } A_{ps} \times f_{ps} = \alpha_1 \times f_c^{/} \times \beta_1 \times c \times b$$

$$\text{and } \beta_1 = 0.85 - \frac{0.05(f_c^{/} - 28)}{7}, If\ 28 < f_c^{/} < 55MPa \qquad \text{Equation 3-9}$$

Where A_{ps} is the prestressing tendons area, f_{ps} is the tendons stress at ultimate, α_1= 0.85 according to the ACI, $f_c^{/}$ is the concrete strength, and b is the width of the section. According to the ACI 318-19 provisions $a = \beta_1 \times c$, the β_1 value depends on the concrete strength and is calculated according to the ACI 318-19 provisions. f_{ps} is calculated from the curve of the 1860 MPa steel tendon, (Figure 3-9).

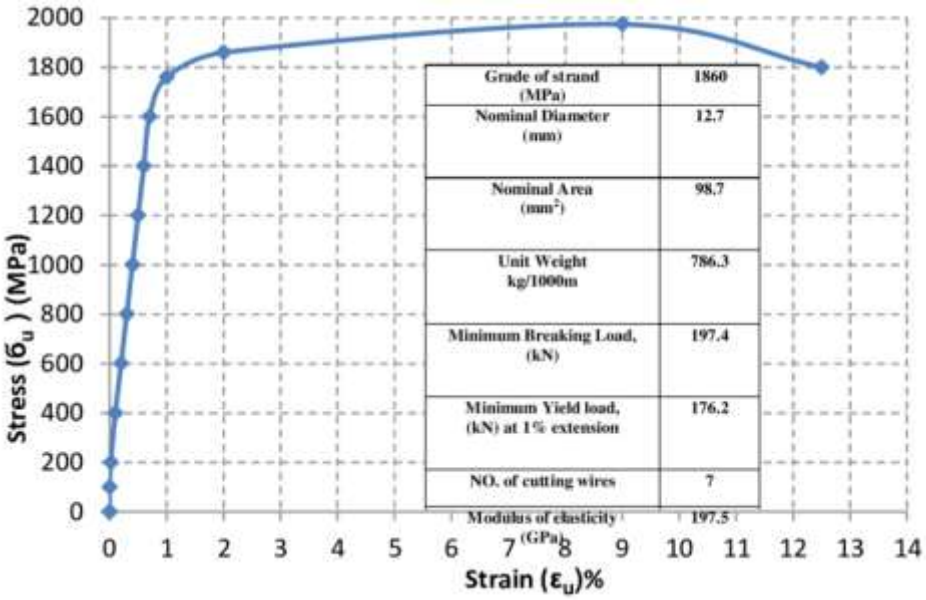

Figure 3-9 Seven Wires Strand Low Relaxation Stress-Strain Curve (https://www.researchgate.net/figure/Figure-5-stress-strain-curve-of-grade-270-low-relaxation-seven-wire-strands-at-127_fig1_338261560, 2021)

From equation 3-9, c ε_{cs} values are computed. Sequentially, ε_{ps} is calculated and compared to the yielding strain with ε_{py} =0.008, where

$$\varepsilon_{ps} < 0.008, \text{ then } f_{ps} = E_{ps} \times \varepsilon_{ps}$$

$$\text{Or, } \varepsilon_{ps} > 0.008 \text{ then } f_{ps} = 1848 - \frac{0.517}{\varepsilon_{ps} - 0.0065}$$

By computing in Equation 3-9 with the bonded specimen's strain values and assuming that the stress in the tendons has surpassed the yielding limit the following equation is derived with c value equals 25.09 mm.

$$296.1 \times \left[1848 - \frac{0.517}{\left(0.000189 + 0.0068 + 0.003 \frac{120 - c}{c} \right) - 0.0065} \right] = 0.85 \times 30 \times 0.835 \times c \times 1000$$

Equation 3-10

So, the value of the total strain ε_{cs} equals 0.011348 and sequentially ε_{ps} equals 0.017537 which is larger than ε_{py} =0.008, so the assumption is correct. The tendon stress is calculated and it is equal to 1801 MPa. To calculate the failure load P_{Exp}, the moment due to prestressing force at failure is

equated to the moment due to loading and due to the own weight of the slab. The following equation illustrates the procedure discussed above for bonded slabs BS1 and BS2.

$$A_{ps} \times f_{ps} \left[d_p - \frac{a}{2} \right] = M_{ow+} \frac{P_{Exp.}}{2} \times 1.35m \qquad \text{Equation 3-11}$$

From the strain compatibility and force equilibrium Equations 3-10 and 3-11, a value for the $P_{Exp}/2$ at failure for BS1 and BS2 is calculated, the failure load is 37.3 kN, and the P_{Exp} equals 74.7 kN.

On the other hand, the stress at the ultimate stage for the unbonded tendons cannot be calculated using the strain compatibility concept due to the lack of bond between the concrete and the unbonded tendon. Instead, an empirical equation is provided by the ACI 318-19, the equations used here are the equations for the span-to-depth ratio less than 35. These empirical equations can be used if the f_{pe} is greater than or equal to 0.5 f_{pu}, all the specimens satisfy the code limitations to use the empirical equations for the calculation of the unbonded tendon's ultimate stress where $f_{pe} = 1292MPa > 0.5 \times 1860 = 930MPa$

The ultimate stress of the unbonded tendons for each specimen of the unbonded system without reinforcement UBS1 and UBS2, is calculated in MPa according to the ACI 318-19 provisions. The equations stated by the ACI 318-19 gives the unbonded tendon ultimate stress to be 1483 MPa.

Then, by equating the tension force to the compression force, using Equation 3-9. The moment and the $P_{Exp}/2$ are calculated using the same procedures adopted for bonded tendon specimens. The value of a is found to be 17.22 mm, $P_{Exp}/2$ is calculated to be 30.3 kN, and the P_{Exp} equals 60.6 kN.

For the unbonded slabs with non-prestressing steel reinforcement (UBSR1 and UBSR2) another part is added to the previous calculations which accounts for the contribution of the non-prestressing steel reinforcement that contributes to the ultimate strength of the slab. So, the equilibrium of forces Equation 3-12 is given by:

$$A_{ps} \times f_{ps} + A_s \times f_s = \alpha_1 \times f'_c \times \beta_1 \times c \times b \qquad \text{Equation 3-12}$$

Where A_s is the area of non-prestressing steel reinforcement no.10 mm @ 200 mm and f_s is the stress of the non-prestressing steel reinforcement at the ultimate limit state. The strength of steel f_s is assumed by f_y =360 MPa, then the value of c is conducted and the strain of the non-prestressing steel reinforcement ε_{cs} is calculated as shown in Equation 3-13.

$$\varepsilon_{cs} = \varepsilon_{cu}\frac{d-c}{c} = 0.003\frac{d-c}{c} \qquad \text{Equation 3-13}$$

Where d is the distance from the extreme compression fiber to the centroid of the non-prestressing steel reinforcement bars.

Accordingly, the value of c is calculated for the two specimens and the strain of the non-prestressing steel reinforcement is checked against the yielding strain (0.002). Also, before this step the used ultimate stress of the unbonded members is chosen according to the three given empirical equations by the ACI 318-19. The calculations resulted in unbonded tendon's ultimate stress of 1483 MPa and a value for the c equals to 28.58mm.

Since the strain of the non-prestressing steel of the two specimens is higher than the yielding strain then, the assumption for the non-prestressing steel strength is correct. Then, the moment, the failure load $P_{Exp}/2$ and P_{Exp} are calculated using the same previous procedures but including the contribution of the non-prestressing steel reinforcement which results in $P_{Exp}/2$ equals to 45.3 kN and P_{Exp} equals 90.6 kN.

The six post-tension slabs are designed for shear. The design for shear for the slabs is done according to the ACI 318-19 provisions, $V_u = V_c + V_s$. Where V_c is the shear causing inclined cracks. The value of V_c is calculated after ensuring the condition for using the approximate equation is satisfied. The condition is $A_{ps} \times f_{pe} \geq 0.4\left[\left(A_{ps} \times f_{pu}\right) + \left(A_s \times f_s\right)\right]$. So V_c is the lesser of the following three equations:

$$(0.05\sqrt{f'_c} + 4.8(\frac{V_u \times d_p}{M_u}))b \times d_p$$

$$(0.05\sqrt{f'_c} + 4.8)b \times d_p \qquad \text{Equation 3-14}$$

$$(0.42\sqrt{f'_c})b \times d_p$$

Where d_p is the distance from the extreme compression fiber to the centroid of the prestressing steel bars (d_p shall not be permitted to be more than 0.8h). V_u and M_u are the ultimate shear and moment calculated due to the external loads only, respectively. So, $V_u = P_{Exp}/2$ and $M_u = \frac{P_{Exp.}}{2} \times 1.35m$

V_s is calculated to provide transverse reinforcement for the concrete members that have $V_u > \phi V_c$, so Vs and the shear reinforcement are calculated according to the ACI 318-19 provisions as:

$$V_s \geq \frac{V_u}{\phi} - V \quad \text{and}$$

$$V_s = \frac{A_v \times f_{yt} \times d_p}{s}$$

Equation 3-15

Where A_v is the area of shear reinforcement within spacing s in mm^2, f_{yt} is the specified yield strength of transverse reinforcement in MPa and d_p is the depth of the member from the extreme compressive stress layer to the centroid of the prestressing steel.

V_u value for all the specimens is greater than $0.5(\phi V_c)$ with Ø equals 0.75. Yet there is no need to provide any shear reinforcement A_{vmin} as the depth of the section is less than 250m and V_u for all cases is calculated to be less than ϕV_c. The steps indicated above are calculated for the three different types of specimens and the results are presented in Table 3-1 below.

Table 3-1 Design for shear steps and results

Name	$P_{Exp}/2 = V_u$	$(A_{ps} \text{ X } f_{pu}) + (A_s \text{ X } f_s)$	$\left(0.05\sqrt{f'_c} + 4.8\left(\frac{\text{VuXdp}}{\text{Mu}}\right)\right)$ XbwXd	$\left(0.05\sqrt{f'_c} + 4.8\right)$ bwXd	$\left(0.42\sqrt{f'_c}\right)$ bwXd	least V_c	Ø V_c
BS1 & BS2	37.9	220.3	84.7	608.9	276.1	84.7	63.5
UBS1 & UBS2	30.7	220.3	84.7	608.9	276.1	84.7	63.5
UBSR1 & UBSR2	43.5	276.9	84.7	608.9	276.1	84.7	63.5

4 The Experimental Investigation

4.1 Introduction

Through this chapter, the experimental work is discussed in details, showing all the steps followed to test six one-way simply-supported post-tension slabs with bonded and unbonded tendons. This chapter is divided into three main parts, where each part contains a stage of the post-tensioning program discussing the steps carried to construct, prestress and test the slab specimens. The three main parts or stages are

- The construction of formworks and the casting of concrete
- The prestressing of the bonded and the unbonded tendons
- The test setup and testing program of the post-tension slabs

4.2 Casting of concrete slabs

This part illustrates the procedures of the construction of the post-tension slab specimens. The detailed steps of the formwork construction, reinforcement detailing, anchor fixation, and cables installation are discussed.

The six post-tension slab specimen's fabrication with all the details of the reinforcement of the non-prestressing steel reinforcement bars, the rectangular stirrups, the spiral stirrups and the prestressed cables, the anchors fixation, the settlement of the strain gauges all took place at the AUC structural engineering laboratory. The concrete casting and curing for the specimens were then carried out and followed by the prestressing tendons stressing.

Six post-tension one-way slabs simply-supported with a 4.0m span and a 1.0 m width are tested under four-point loading flexural test as shown in Figure 3-3. Three sets, each consisting of two replica of the same slab are designed. The first set of slabs (BS1 and BS2) contains bonded tendons and without non-prestressing steel reinforcement. The second set of slabs (UBS1 and UBS2) contains unbonded tendons without non-prestressing steel reinforcement. The last set of slabs (UBSR1 and UBSR2) contains unbonded tendons and non-prestressing steel reinforcement of bars (no.10 mm @ 200mm) in the two directions according to the ACI 318-19 requirements. Each slab contains three prestressing tendons of a diameter 12.7mm. The six slabs are designed and constructed according to ACI 318-19 provisions. As shown in Figures 3-1 and 3-2, the six slabs

include closed stirrups bars (no.10 mm @ 200mm) distributed in both directions at the slab's ends in addition to 6 mm diameter spiral stirrups around the steel cables which extend for a distance of 0.3 m from the slab edge. Table 4-1 shows the different details of the six one-way post-tension slab specimens. All slabs include spiral stirrups and no.10mm @ 200mm rectangular stirrups at the end anchorage zone as shown in Figures 3-1 and 3-2.

Table 4-1 The description of the six post-tension slab specimens

Name	Number of Specimens	Dimensions of specimen	3 Tendons (12.7mm diameter)	Non-prestressing RFT
BS1	2	4.3mx1.0mx0.16m	Bonded	None
BS2	2	4.3mx1.0mx0.16m	Bonded	None
UBS1	2	4.3mx1.0mx0.16m	Unbonded	None
UBS2	2	4.3mx1.0mx0.16m	Unbonded	None
UBSR1	2	4.3mx1.0mx0.16m	Unbonded	no.10mm @ 200mm in both directions
UBSR2	2	4.3mx1.0mx0.16m	Unbonded	no.10mm @ 200mm in both directions

The formwork for the slab specimens is fabricated from plywood and pine wood panels. The plywood panels are of dimensions 1.2x2.4m and are used for the bottom side of the specimen's formwork. The pine wood panels are of different dimensions, and they are used for the side edges of the specimen. Also, the pine wood panels are used for supporting the formwork during casting to prevent the failure of the side edges or the leakage of concrete during pouring. The pine wood panels of dimensions (5.7m x 17cm x 5cm) are used for the forming of the slab specimen's sides. In contrast, the pine wood panels of dimensions (4.8m x 10cm x 2.5cm) are used to support the formwork from failure, buckling, or leakage during casting of the concrete. They are used to support the plywood panels to have a stable and perfectly horizontal specimen. Figures 4-1 shows the plywood panels and pine wood panels before their cutting and forming. The pine wood panels used for the slab specimen sides are cut down to the needed dimensions. The internal dimensions of the wooden formwork of the slab specimens are 4.3m in length. The extra 0.3m are divided to 0.15m added to the two sides of the slab specimen to count for the support fixation length during testing, 1.0 m in width and 0.16m in depth. Figure 4-2 shows the formwork for a slab specimen

with the four sides fixed from pine wood panels (the base of the slab specimen is made up of two panels of plywood) and shows the check for all the dimensions using a measuring tape.

*Figure 4-1 pine wood Panels (left) and plywood panels of dimensions (1.2*2.4m)(right)*

Figure 4-2 Slab specimen formwork (left) and checking the internal dimensions of the slab specimen formwork (right)

The steel reinforcement bars (no.10mm) are cut to the needed dimensions for the stirrups and the mesh bars. The stirrups located at the edges of the slabs are erected firstly outside the specimens and then fixed in their place inside the slab specimens when the six longitudinal stirrups are tied to the six stirrups in the transverse direction forming a cage as shown in Figure 4-3. These cages of stirrups are installed to serve the anchorage zone, support the slab from any failure during the specimen movement to the testing location, and prevent the tendon from separating from the concrete during failure. The non-prestressing steel reinforcement added to the two specimens UBSR1 and UBSR2 were cut to the needed lengths of 4.3m to be settled in the longitudinal direction while steel bars of length 1.14m were provided in the transverse direction. The additional 0.14m is to form a side leg for the bar for better support inside the specimen formwork. Extra two bars of the length of 4.3m are tied to the top of the transverse reinforcement bars to prevent the bars from tilting or movement during concrete pouring. Figure 4-3 shows the detailing of reinforcement of the two unbonded slabs with non-prestressing steel reinforcement, UBSR1 and UBSR2. The steel stirrups cages were erected in their places in the six specimen's formwork, and the non-prestressing steel bars were provided in UBRS1 and UBRS2 specimen's formwork. All of the steel bars were tied to each other using steel wires (Figure 4-4).

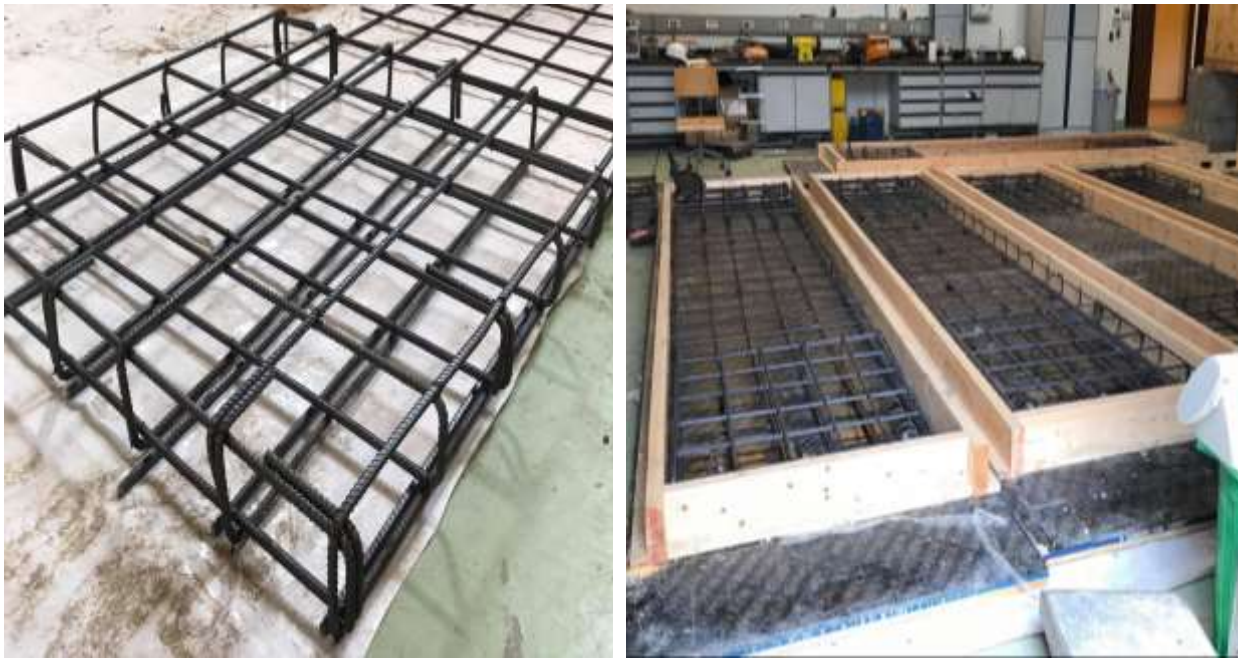

Figure 4-3 Stirrups of bars no.10 mm in the two dimensions forming a cage (left) and detailing of reinforcement of the two unbonded slabs with non-prestressing steel reinforcement (right)

Figure 4-4 Wires connecting the steel bars in the slab specimen

The spiral stirrups are formed to cover a length of 0.3m from the slab edge and are located around the prestressing tendons starting from the back of the end anchor. The spiral stirrups' pitch is 0.04-0.05m, while the diameter of these spiral stirrups is 0.07m to 0.09m. Figure 4-5 shows the spiral stirrups before the erection and shows how the spiral stirrups were formed in the lab manual. The bar of diameter 6mm is tied around a cylindrical tube to form the spiral shape.

Figure 4-5 Spiral Stirrups Before Erection showing the total length of the stirrup (left) and spiral stirrups formed in the lab manually (right)

Afterward, holes were formed in the two sides of the six slab specimens to install the bonded and unbonded anchors in their designed position. The hole in the formwork sides is to allow the prestressing tendons to point out of the slabs edge by 0.3m to be able to apply prestressing force to the tendons later. Figure 4-6 shows the unbonded tendons pointing out of the formwork edge by

0.3m. A drill formed the holes, and the first hole is formed at a location of distance 0.1667m from the slab edge, then the second hole is located at a distance of 0.333m from the center of the first hole, and the third hole is at a distance 0.333m from the center of the second hole. Also, this figure shows the drilling of the holes using a drill. After this, the anchors are supported in their spots and fixed with the spiral stirrups.

The bonded and the unbonded tendons were then cut down to divide the tendons in which each of length 5.0m, as shown in Figure 4-7. Then, all of the unbonded tendons are fixed in their places. The unbonded tendons are made up of the seven-wires strands covered with grease and protected with an extruded plastic sheathing (Figure 4-7). Two bars of 25mm diameter were added to all the slab specimens parallel to the slab edge right behind the anchors with a length equals to the slab edge length of 1.0m. These two bars are added to resist the bursting and the spalling forces as per the ACI 318-19 provisions. The ACI 318-19 requires the addition of these two bars with a diameter not less than 13mm. Figure 4-8 shows the two bars location aligned at the slab edge behind the anchors, the spiral stirrups, and the unbonded anchor. For the two bonded post-tension slab specimens, the bonded anchors are tied to the hose that will allow the grout into the duct after prestressing. The bonded anchor is tied to the hose using wires and plastic tape. The hose tied to the anchor is also connected to an orange hose that has a length larger than the depth of the specimen to insert the grout through it after the hardening of concrete and the prestressing of the tendons. Afterward, the 7-wires steel strands cable is inserted in the corrugated plastic duct then the whole setups of the bonded tendons are installed in their designed positions, as shown in Figure 4-8.

Figure 4-9 shows the whole setup of the BS2 after the final installation of all the elements. The ducts' profiling is maintained by the usage of steel bars and plastic chairs to maintain a clear distance (cover) of 0.04m from the bottom slab edge to the center of the tendons. The chairs are located at two points to maintain two points harped profile. The double harped profile starts with an inclined line from the slab edge with a vertical height of 0.08m measured from the bottom slab edge (anchor location at the middle of the slab depth) until reaching a vertical height of 0.04m from the slab bottom edge at a distance 1.5m from the slab side edge. Then the tendon remains in a straight line profile with a constant vertical height of 0.04m from the slab bottom edge for 1.3m.

Then the inclined line profile is maintained again until reaching the other side edge of the slab with 0.08m vertical height measured from the slab bottom edge. Figure 4-9 shows the profile of the tendons maintained for a slab specimen.

Figure 4-6 The bonded tendons pointing out of the slab specimen edge with length 30 cm (left) and drilling the holes (right)

Figure 4-7 Prestressing cables are cut down to 5.0m each (left) and the unbonded tendons covered with grease and extruded plastic sheathing (right)

Figure 4-8 Unbonded anchors installed in their designed spots with the spiral stirrups and the two bars of diameter 25mm are shown after fixation in their final position (top) and the bonded tendons inserted in the corrugated plastic duct are fixed with the designed profile in their designed locations (bottom)

Figure 4-9 The full setup of the BS1 after installment showing the designed tendon profile installed using chairs and steel bars

Strain gauges are used to measure the deformation at different locations. Four strain gauges are added to each slab. Three 10 mm long strain gauges are added on the slab tendons, while one 60 mm long strain gauge is added on the slab's concrete top surface. Two 10 mm long strain gauges are added on two of the three tendons in each slab at mid-span, while the third 10 mm long strain gauge is added at the dead-end of one of the tendons. The strain gauges are intended to measure the strain in the tendons and sequentially convert it to stress at different loading stages. Short-term and long-term losses are intended to be calculated through these strain measurements. Figure 4-10 shows the strain gauge that will be fixed on the steel tendons. The procedure of installing the strain gauge on the bonded and the unbonded tendons is as follows. For the bonded tendon, the 7-wires strands wire is cleaned, and the strain gauge is fixed on one wire only using glue and plastic tape. Figure 4-10 shows a strain gauge supported on one wire of the seven wires strand. Then the cut part of the plastic corrugated duct is resorted, and plastic tape is used to connect the restored cut duct to the rest of the bonded tendon's duct, as shown in Figure 4-10.

Also, to protect the strain gauges wires during pouring, the wires are inserted in a plastic tube with a length larger than the slab specimen's depth as shown in figure 4-11. For the unbonded tendons, the plastic sheathing is removed and the grease is cleaned from the surface of the 7-wires strands. Then, the strain gauge is attached to one wire of the 7-wires strands with the same procedures

followed for the bonded tendons. Figure 4-11 shows the unbonded tendon after the installation of the strain gauges in their designed spots.

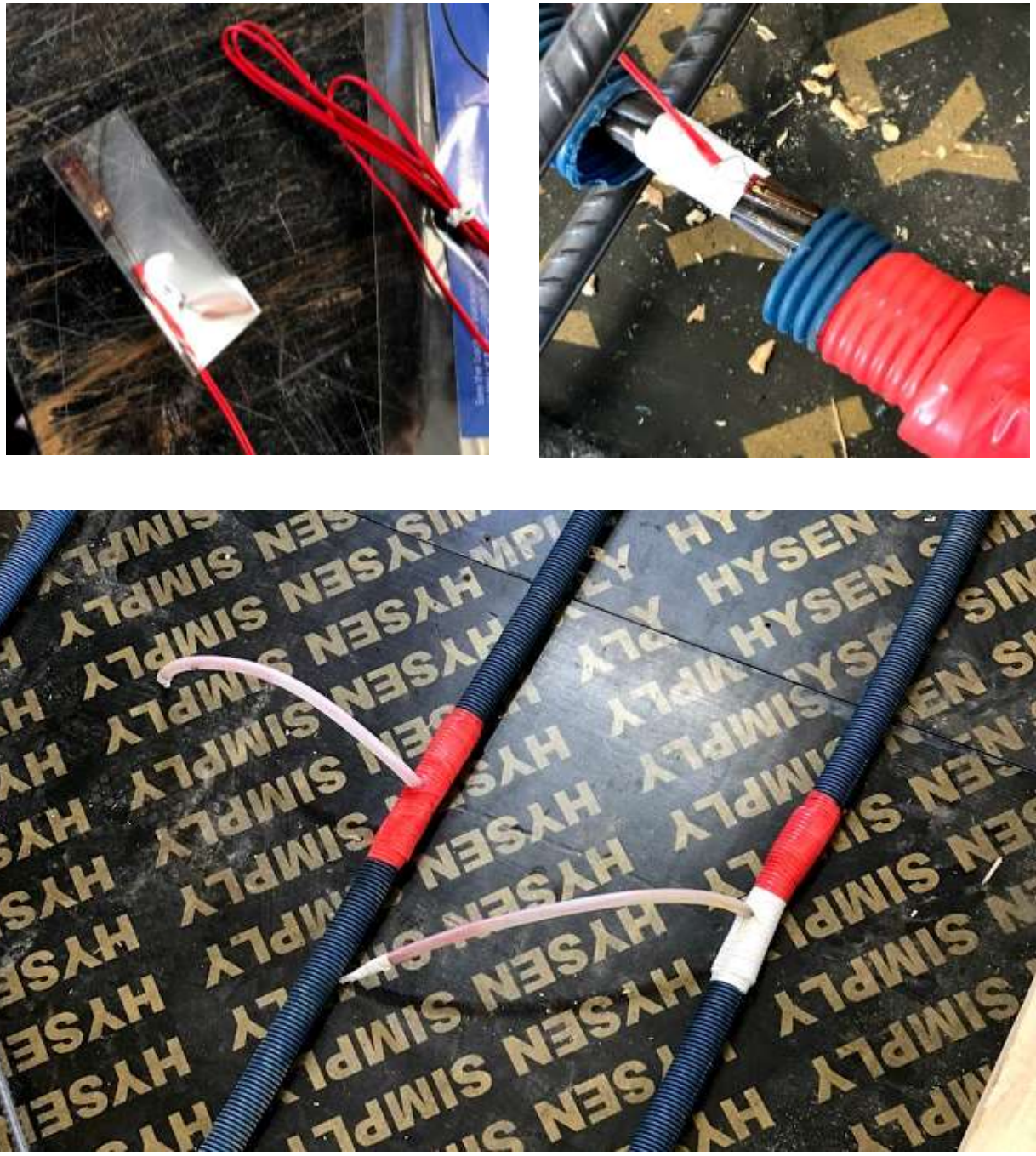

Figure 4-10 10 mm long strain gage and its connection to one wire of the 7-wires stand (top) and the strain gage's final look (bottom)

Figure 4-11 Strain gauge wires inserted inside the plastic tube (left) and strain gauges fixed on the unbonded tendons in their designed spots (right)

Supporting panels of pinewood are fixed at the top of the specimens as shown in Figure 4-12 to prevent the failure of the slab specimen sides. Also, the plastic tubes containing the strain gauge's wires are tied to the supporting pine wood panels in order to keep the wires out of the slab specimens after pouring and hardening of concrete.

Figure 4-12 The slab specimens after the installment of all of the elements and the supporting wood panels attached to them the plastic tubes containing the strain gauge's wires.

Hooks are used to hold the slab specimen for moving the specimens to the flexural test location. The hooks are located at a distance of 0.25m in both directions from the slab corner. Figure 4-13 shows the location of the hooks inside the UBSR 1 slab specimen. The hooks' location is the same

on both sides of the same slab specimens and the same for all the slab specimens. The six one-way post-tension slabs with all the details after completion are shown in Figure 4-13.

Figure 4-13 Shows the hooks' location in the UBSR 1 specimen (top) and the six one-way post-tension slab specimens before concrete casting (bottom)

Concrete is poured after the fixation of the tendons, non-prestressing steel reinforcement bars, rectangular and spiral stirrups, bonded and unbonded anchors, and the strain gauges. Ready-mix concrete with 30 MPa strength (f_{cu}) is ordered from CEMEX with a volume of 5 cubic meters. The concrete is delivered in a rotating drum and was cast to the six slab specimens (Figure 4-14). The concrete is moved from the concrete drum to the specimens using the crane and the bracket, as shown in Figure 4-15. The vibrator was used for concrete compaction, while the trowel is used for leveling and finalizing the concrete with a smooth surface. Figure 4-15 shows the compaction and smoothening of the concrete surface.

Six concrete cubes of standard dimensions (0.15X0.15X0.15m) are poured to be later tested under compression force in order to determine the compressive strength of the concrete on the day of prestressing (7-days) and on the day of testing (28-days). The molds were prepared as shown in Figure 4-16, then the concrete was cast in the molds, compacted, and the surface was leveled.

Figure 4-14 Rotating drum delivering concrete to the AUC lab

Figure 4-15 Concrete casting for the slab specimens (left) and concrete compaction and surface smoothening (right)

Figure 4-16 Standard concrete cube molds (left) and concrete standard cubes casting and compaction (right) (top) and concrete standard cubes leveling (bottom)

After finalizing the concrete casting, compaction, and leveling of the surface, the six post-tension slab specimens are covered with water for curing. Figure 4-17 shows the concrete slab specimens after concrete casting, and shows the post-tension slab specimens covered with wet polyethylene sheets to keep the concrete surface always hydrated. The curing of the slab specimens lasted for seven days.

Figure 4-17 Post-tension Slab specimens after concrete casting (left) and post-tension slab specimens covered with polyethylene sheets for curing (right).

The concrete mix design specifications and details are presented (Table 4-2) and as received from CEMEX Ready Concrete Company.

Table 4-2 Description of the ordered 5 m3 of concrete mix

Material Name	Unit	Mix Design	Actual (m^3)	Actual Truck(m^3)
ISOFLEX 390(Type G)	kg	8.40	6.96	34.8
ISOFLEX 3550(Type F)	kg	2.95	1.00	5.0
Portland Cement 42.5	kg	350	350.0	1750
Natural Sand	kg	750	743.6	3718
Dolomite Crushed 10-20mm	kg	557	556.0	2780
Dolomite Crushed 5-10mm	kg	557	559.2	2796
Water for Concrete	kg	193	190.6	953

4.3 Prestressing of the slabs

After 7-days, prestressing of the slab specimens took place. On the same day, standard cubes of concrete are tested under compression to get the concrete's compressive strength at the age of 7-days and compare it to the strength of $0.7x f_{cu}$= 0.7x30 MPa= 21 MPa. The tested standard cubes'

results, compressive force, and compressive stress, the average compressive strength and the corresponding cylindrical compressive strength are presented in Table 4-3

Table 4-3 Compressive force and stress for three standard cubes at 7-days

Cube Number	Compression force (kN)	Compression stress (MPa)
1	531.3	23.6
2	602.3	26.8
3	644.7	28.7
Average f_{cui}	592.8	26.4
Corresponding f'_{ci}	474.24	21.1

The compression stress is calculated as the compression force divided by the standard concrete cube's cross-sectional area (0.15mx0.15m). While the concrete mix's compression strength on 7-days is considered the average of the compression stress of the three tested standard concrete cubes. The average compressive strength of the concrete at 7-days is 26.4 MPa, corresponding to 21.1MPa cylindrical compressive strength. Figure 4-18 shows one of the three standard concrete cubes in the compression testing machine after cracks occurred due to reaching the failure load.

Figure 4-18 Standard concrete cube under compression load, showing cracks

The compressive strength of the concrete at 7-days (f'_{ci}) is checked against the ACI 318-19 requirement, which states that the prestressing of the cables cannot be done before the concrete reaching compressive strength not less than 17 MPa (Cylindrical compressive strength) in case of the usage of mono-strands. After the concrete compressive strength verification for exceeding the code specified limit for prestressing, the prestressing of the post-tension slabs is confirmed and started. First of all, the bonded tendons anchors are cleaned from any excessive concrete mortar that got into the anchor opening during concrete casting. Figure 4-19 shows the cleaning process of the bonded tendons anchors. Then, the wedges are inserted in the anchor openings for the bonded and the unbonded tendons for the dead and live ends.

Figure 4-19 Cleaning process for the bonded tendon anchor opening from concrete mortar (left) and wedges installation into the bonded and the unbonded anchors (right)

Afterward, all of the bonded and the unbonded tendons are marked, one mark is directly after the wedge face on the tendon, and then ten marks are added with a distance of 1 cm between every two consecutive marks. Then, for the live ends, the hydraulic jack is fixed, and the tendons are stressed. The sequence of the tendons stressing is as follows; each tendon is stressed to the maximum required force, and then the next tendon is stressed. The force applied by the hydraulic jack equals 335 bars which are equivalent to 150 kN. The elongation of each tendon is measured using a caliber after stressing the tendon, and from the dead-end, slippage of the tendon from the dead-end side was checked to make sure that there is no slippage that took place. Figure 4-20 indicates the live ends, the numbered ends, while the other side is the dead end. The numbers 1,2,

and 3, indicate the prestressing sequence of the tendons mentioned above. Also, figure 4-20 shows the hydraulic jack connected to one of the tendons. The following table 4-4 illustrates the elongation measured from the live end in millimeter for each tendon.

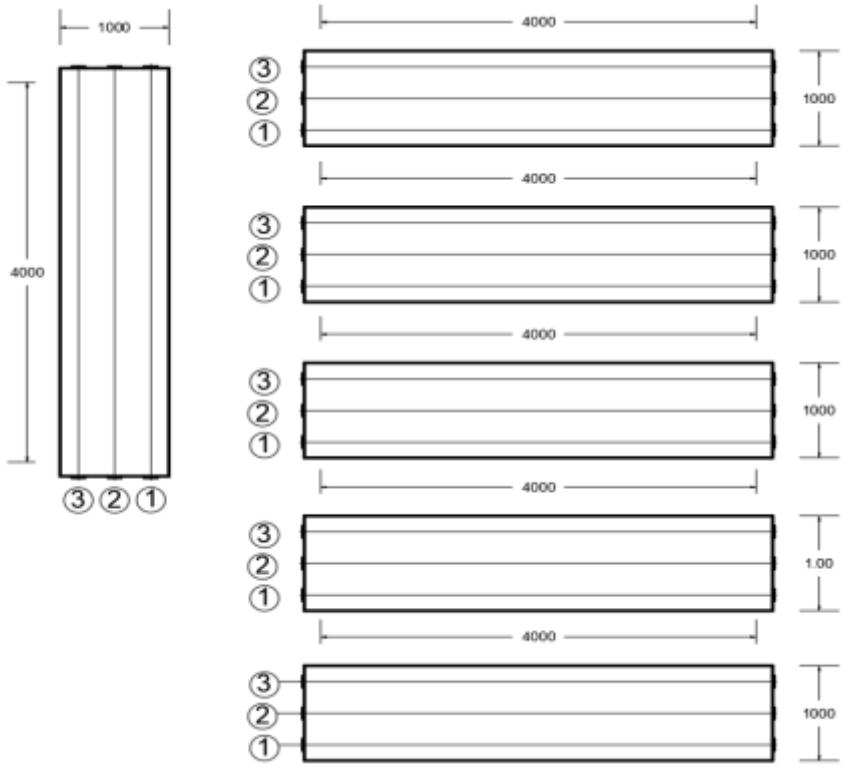

Figure 4-20 The setup of the slab specimens with an indication for the dead and live ends (All dimensions are in millimeters) (top) and the hydraulic jack connected to one of the unbonded tendon to apply the prestressing designed force (bottom)

Table 4-4 Measured elongation of each tendon of the six specimens

Specimen	Tendon no. 1 (mm)	Tendon no.2 (mm)	Tendon no.3 (mm)
UBSR1	33.5	33	34
UBSR2	33	31	32
UBS1	32.5	34	36
UBS2	34	32.5	35
BS1	33	35	36
BS2	34	34	35

The six specimens were inspected for four consecutive days after the prestressing to check for the occurrence of any tendons' slippage, or any formation of cracks. Then the grouting activity took place the next day, where the six bonded tendons are filled with grout after the cables' stressing. The material used for mixing the grout is cement, water, and an expanding grout admixture. All of the ingredients are mixed in a machine used to fill the ducts with grout under pressure. Figure 4-21 shows the admixture bag, and the mixing and grouting machine. The six bonded tendons are grouted as the hose of the grouting machine is inserted to the specimen hose's opening connected to the tendon from one side, and grout was filled until the grout exceeded from the specimen's hose opening on the other end of the tendon as shown in Figure 4-22. After grouting, the slabs are left for 48 hours for the grout to consolidate. The specimens at that time are ready to be tested under four-point loading flexural test.

Figure 4-21 Expanding admixture used for the grout mix (left) and mixing and grouting machine (right)

Figure 4-22 The grouting procedure for one of the six bonded tendons

4.4 Test setup

Before performing the test, the standard cubes' compressive strength is determined where three standard cubes are tested for compression to give the following results presented in Table 4-5. The average compressive strength of the three tested standard cubes is 40 MPa, and sequentially the cylindrical compressive strength equals 32 MPa.

Table 4-5 Compressive force and stress for three standard cubes on testing day

Cube Number	Compression force (kN)	Compression stress (MPa)
1	859	38.2
2	996.2	44.3
3	843.4	37.5
Average f_{cu}	899.53	40.0
Corresponding $f_c^{/}$	719.62	32.0

The loading of the slabs during testing is modeled through three HEB 300 steel beams. The load is transferred from the loading machine to an HEB 300 of span 1.60m, then to another two beams of span equal to the slabs' width, 1.0m. The setup of the loading beams in elevation and plan are shown in Figure 4-23. The slabs are simply supported on supports located with an edge distance of 0.15m. Rubber pads are located between the two testing beams and the slab specimen. Figure 4-23 also shows the real test setup of the slabs. This setup is chosen to apply two-line loads on the

slab specimen to produce a trapezoidal bending moment diagram. The two points of supports for the slab specimen are real roller supports presented by cylinders supported on grooved plates.

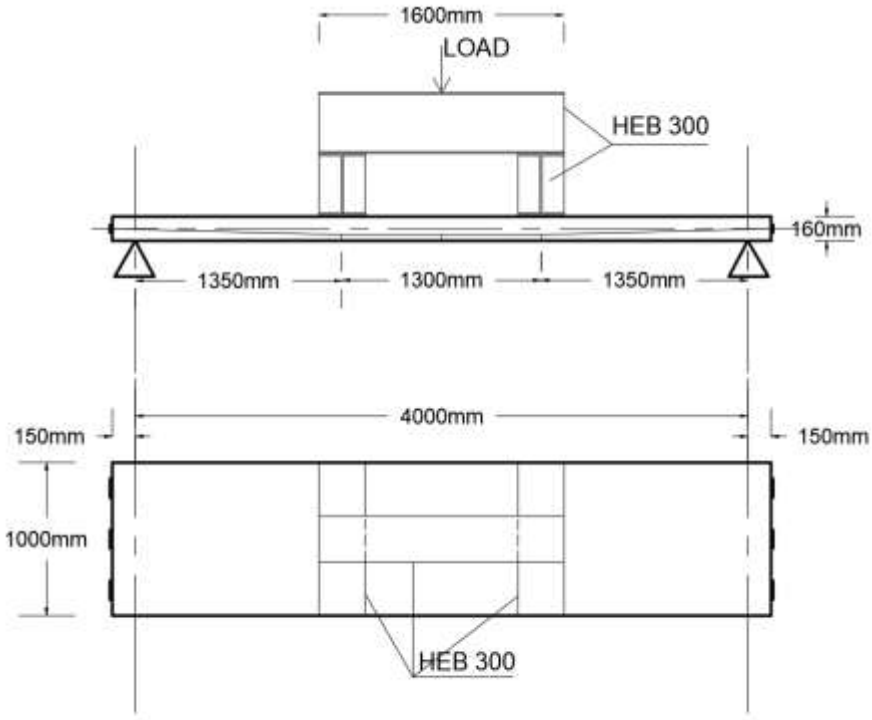

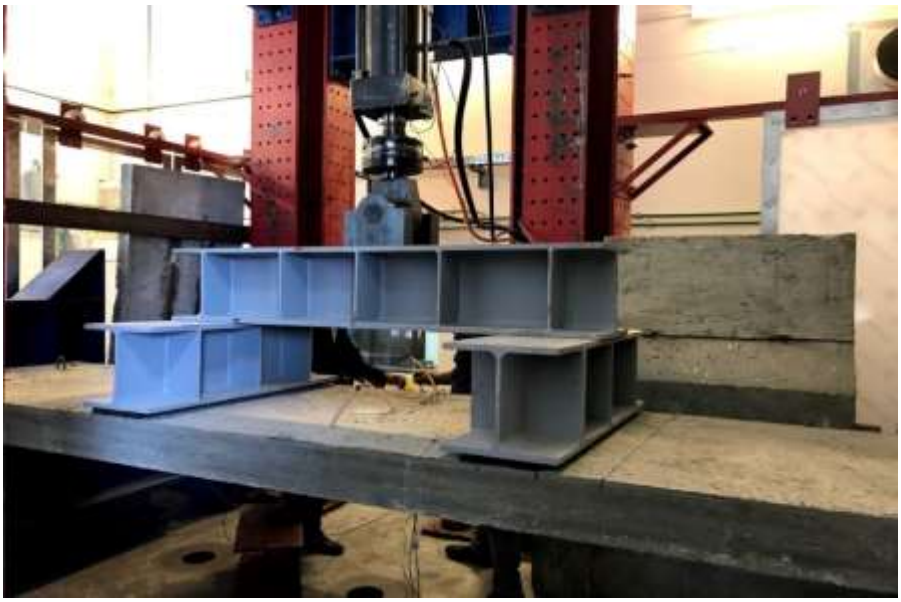

Figure 4-23 The planned setup for the tested specimens showing the locations of the loading beams and their sizes and dimensions (All dimensions are in millimeters) (top) and the setup prepared in reality at the AUC structural engineering lab (bottom)

The linear variable differential transducer (LVDT) is added on the concrete bottom surface at mid-span in order to measure the displacement that takes place at different stages till failure. A 60mm long strain gauge is also supported on the concrete top surface at mid-span as shown in Figure 4-24 to measure the deformation at the compressed fibers.

Figure 4-24 Strain gage attached to the concrete top surface

The six specimens' construction has been carried according to the code provisions and the practical aspects followed in Egypt as discussed and presented in this chapter. After discussing the whole construction phase during this chapter, the flexural test was then performed on the six specimens, and the results are presented in the following chapter five, illustrating the behavior and the failure mechanism of each system.

4.5 Revised slab strength

After determining the exact elongation in the tendons due to prestressing, failure loads calculated previously for the tested specimens are recalculated using the exact prestressing force in each

tendon and the values of the compressive strength at 7-days and 28-days. The recalculated failure loads for each system are the loads that will be used for the comparison later in chapter five.

From the measured elongation of each tendon, the strain is calculated, followed by the calculation of the stress in each tendon to be converted to a jacking force as shown in Equation 4-1, giving the following results presented in Table 4-6.

$$\varepsilon = \frac{elongation}{length\ of\ tendon}$$

$$E_{ps} = \frac{f_J}{\varepsilon} \qquad \text{Equation 4-1}$$

$$P_J = f_J \times A_{ps}$$

Where the elongation is obtained from the Table 4-4, the measured elongation, the exact length of the tendon is 4.308 m and its Young's modulus E_{ps} is 190,000 MPa. The stress and the Jacking force are calculated for each tendon and presented in Table 4-6.

Table 4-6 The calculated strain, stress and jacking force for the three tendons in each specimen

Specimen	Tendon 1			Tendon 2			Tendon 3		
	Strain in tendon no. 1	Stress in tendon no. 1 (MPa)	Jacking force in tendon no.1 (kN)	Strain in tendon no. 2	Stress in tendon no. 2 (MPa)	Jacking force in tendon no.2 (kN)	Strain in tendon no. 3	Stress in tendon no. 3 (MPa)	Jacking force in tendon no.3 (kN)
BS1	0.007667	1456.8	143.8	0.008132	1545.1	152.5	0.008364	1589.2	156.9
BS2	0.007899	1500.8	148.1	0.007899	1500.8	148.1	0.008132	1545.1	152.5
UBS1	0.007551	1434.7	141.6	0.007899	1500.8	148.1	0.008364	1589.2	156.9
UBS2	0.007899	1500.8	148.1	0.007551	1434.7	141.6	0.008132	1545.1	152.5
UBSR1	0.007783	1478.8	146.0	0.007667	1456.7	143.8	0.007899	1500.8	148.1
UBSR2	0.007667	1456.7	143.8	0.007203	1368.6	135.1	0.007345	1395.5	137.7

The jacking force on the slab is the sum of the jacking forces of the three tendons. The calculated jacking force for each slab is calculated and presented in the following Table 4-7.

Table 4-7 Total jacking force calculated for each specimen

Specimen	Jacking Force (kN)
BS1	453.1
BS2	448.8
UBS1	446.6
UBS2	442.2
UBSR1	437.9
UBSR2	416.6

The short and long-term losses are now precisely calculated. The losses are calculated according to ACI 318-19 provisions, which refers to the Post Tensioning Institute Manual, (2006). The short-term losses are the elastic shortening, anchorage slippage and friction. While the long-term losses are shrinkage of concrete, creep of concrete and the relaxation of the steel tendons. So, the initial prestressing force (P_i) is the prestressing force after the short-term losses and the effective prestressing force (P_e) at the service stage is the prestress force after the long-term losses.

4.5.1 Short-term losses

The short-term losses are calculated, starting by the elastic shortening losses, which is calculated according to the following Equation 4-2.

$$\Delta_{shortening} = \frac{P_J \times L}{A \times E_c}$$ *Equation 4-2*

Where $\Delta_{shortening}$ is the change in length due to elastic shortening of the concrete specimen, L is the span of the slab specimen, E_c is the modulus of elasticity of the concrete calculated as $4500\sqrt{f'_{ci}}$ (f'_{ci} equals 21 MPa), A is the cross sectional area of the slab specimen and P_J is the jacking force.

Then, the change in length that took place for the concrete slab specimen due to elastic shortening is divided by the length of the tendon, 4.308 m to calculate the strain in the tendon. Afterward, the stress of the tendons is calculated by multiplying the modulus of elasticity by the strain. At last, the reduction of force in the tendons is the stress multiplied by the cross sectional area of the three tendons (each tendon's cross sectional area =98.7 mm^2) which adds up to 296.1 mm^2. The reduction of force is multiplied by two-thirds, because the prestressing was performed in a

sequential scheme, so the first tendon will suffer a full loss of force due to elastic shortening then the second tendon will lose only two-thirds of the value of the reduced force. While the last tendon will lose one-third of the reduction of the force due to elastic shortening, then the average value of the three tendons reduction in force is calculated and presented in Table 4-8.

Table 4-8 Elastic shortening results calculated for each specimen

Jacking force (kN)	$\Delta_{shortening}$ (mm)	Tendon's Strain	Tendon's Loss of Stress (MPa)	Tendon's Loss of Force (kN)	2/3 Tendon's Loss of Force (kN)
453.1	0.515998	0.000137	26	7.7	5.1
448.8	0.585984	0.000136	26	7.6	5.1
446.6	0.583112	0.000135	26	7.6	5.1
442.2	0.577367	0.000134	25	7.5	5.0
437.9	0.571753	0.000133	25	7.5	5.0
416.6	0.543942	0.000126	24	7.1	4.7

The losses due to anchorage slippage are neglected because anchorage's inspection after the tendons prestressing, shows no slippage for any tendon of the six slab specimens.

The last form of the short-term losses is the friction losses that occurs due to the wobble and the curvature effects. The coefficients for the wobble and the curvature are k and μ, respectively which are determined from the Post Tensioning Institute Manual, (2006). For the unbonded and bonded tendons, μ is taken 0.07 and 0.22, respectively. The k factor is taken 10×10^{-4} and 7.5×10^{-4} per feet, or 0.003 and 0.00246 per meter, for the unbonded tendons and the bonded tendons, respectively. The tendon force at the mid-span of the slab specimen (x=2.15 m) after the friction losses is calculated as follows:

$$P_x = P_J \times e^{-(\mu\alpha + Kx)}$$ Equation 4-3

Where P_x is the force at distance x after the reduction of the friction losses and α is the angular angle of tendon curvature in radians. The friction losses due to the curvature effect are neglected because the tendon is only inclined by 2˚ making the tendon almost straight. The friction losses are calculated for the six slab specimens and the results are presented in Table 4-9.

Table 4-9 Friction losses calculated results for each specimen

Specimen	Jacking force (kN)	Wobble coefficient (k)	P_x (kN)	Friction Losses=P_J-P_x (kN)
BS1	437.9	0.00300	435.1	2.8
BS2	416.6	0.00300	413.9	2.7
UBS1	446.6	0.00300	443.7	2.9
UBS2	442.2	0.00300	439.4	2.8
UBSR1	453.1	0.00246	450.7	2.4
UBSR2	448.8	0.00246	446.4	2.4

The short-term losses for each slab specimen are added and calculated as a percentage from the jacking force for each specimen and presented in Table 4-10.

Table 4-10 Total short-term losses calculated as percentage for each specimen

Specimen	Jacking Force (kN)	Elastic shortening losses (kN)	Friction losses (kN)	Total short-term losses (kN)	Short-term losses %
BS1	453.1	5.1	2.4	7.5	1.66
BS2	448.8	5.1	2.4	7.5	1.66
UBS1	446.6	5.1	2.9	7.9	1.78
UBS2	442.2	5.0	2.8	7.9	1.78
UBSR1	437.9	5.0	2.8	7.8	1.78
UBSR2	416.6	4.7	2.7	7.4	1.78

The compression and tensile stress should not exceed the permissible stresses defined by ACI 318-19 provisions. The cylindrical compressive strength of concrete at the age of 7-days equals 21 MPa. So the allowable compressive stress and tensile stresses are calculated in Equations 4-4 and 4-5.

$$-0.6f'_{ci} = -0.6 \times 21 = -12.6MPa$$ Equation 4-4

$$0.25\sqrt{f'_{ci}} = 0.25 \times \sqrt{24} = 1.14MPa$$ Equation 4-5

The initial force is calculated after the reduction due to the short-term losses and presented in addition to the jacking forces in Table 4-11:

Table 4-11 The jacking force and calculated initial force for each specimen

Specimen	Jacking force (kN)	Initial Force (kN)
BS1	453.1	445.6
BS2	448.8	441.3
UBS1	446.6	438.6
UBS2	442.2	434.4
UBSR1	437.9	430.1
UBSR2	416.6	409.2

The stress at the bottom and top surfaces of the concrete slab specimens is calculated and checked versus the calculated allowable compressive and tensile stress according to the ACI 318-19. The following Table 4-12 represents the stresses at the top and bottom fiber of each of the six slab specimens, the six specimens did not surpass the permissible stresses during the initial stage:

Table 4-12 Top and bottom stresses calculated for each specimen at the initial stage

Specimen	Top Stresses f_{Top} (MPa)	Bottom Stresses f_{Bottom} (MPa)
BS1	-0.4825	-5.0875
BS2	-0.4959	-5.0203
UBS1	-0.5042	-4.97875
UBS2	-0.5175	-4.9120
UBSR1	-0.5290	-4.8550
UBSR2	-0.5963	-4.5180

4.5.2 Long-term losses

To calculate the effective prestressing force (P_e), the long-term losses must be calculated first. The long-term losses are due to shrinkage and creep of concrete and relaxation of tendon's steel. The shrinkage losses are calculated as

$$\Delta_{Pshrinkage} = \varepsilon_{shrinkage} \times A_{ps} \times E_{ps}$$ Equation 4-6

Where $\varepsilon_{Shrinkage}$ is the strain due to shrinkage which equals $200X10^{-6}$, A_{ps} is the three tendon's cross section area which equals to 296.1 mm^2 and E_{ps} is the tendon's steel modulus of elasticity which equals to 190,000 MPa. Giving shrinking losses equals 11.3 kN which is 2.5% from the original jacking force. The second type of long-term losses is the concrete creep, which is calculated by Equation 4-7.

$$\Delta_{Pcreep} = \phi \times A_{ps} \times \frac{E_{ps}}{E_c} \times f_{cs}$$ Equation 4-7

Where $\emptyset$ is a factor equals 1.6 for post-tension members, E_c equals $4500\sqrt{f'_c}$ where f'_c equals 32 MPa and f_{cs} is the concrete stress due to sustained loads only at the tendon location and is calculated by

$$f_{cs} = -\frac{P_i}{A} - \frac{P_i \times e \times e}{I} + \frac{M_{ow} \times e}{I}$$ Equation 4-8

A is the cross sectional area of the slab specimen ($160000mm^2$), e is the eccentricity of the tendon, which is equal to 40mm, I is the moment of inertia of the slab cross section ($341333333.3mm^4$), M_{ow} is the moment due to own weight of the slab specimens which equals (8 kN·m). According to each slab's initial prestressing force, the stresses due to sustained loads are calculated and results are presented in Table 4-13, along with the prestress loss due to creep of concrete.

Table 4-13 Initial force, forces due to sustained loads only, creep stresses and creep losses percentage for each specimen

Specimen	p_i (kN)	f_{cs} (MPa)	Δp_{Creep} (kN)	Creep losses percentage (%)
BS1	445.6	3.9	14.0	3.08
BS2	441.3	3.9	13.8	3.07
UBS1	438.6	3.9	13.7	3.06
UBS2	434.4	3.8	13.5	3.05
UBSR1	430.1	3.8	13.4	3.05
UBSR2	409.2	3.5	12.6	3.01

The last type of long-term losses for post-tension members are losses due to tendon's steel relaxation. This type of losses is as follows

$$\Delta_{Pr} = f_{pi} \times \frac{\log(t)}{K} \times (\frac{f_{pi}}{f_{py}} - 0.55) \qquad \text{Equation 4-9}$$

Where Δ_{pr} is the reduction is stress due to steel relaxation, f_{pi} is the initial stresses after the reduction of the short-term losses, t is the time and is determined in hours with a maximum value (1000 hours), the time is taken as the number of hours for 30 days which gives 720 hours. K is a factor that depends on the type of steel used, the type of steel used is low relaxation steel, so K equals to 45. f_{py} is the yielding stress of the steel used which is equal $0.9 \times 1860 MPa = 1674 MPa$ The initial stress depends on the slab specimen and the results obtained for the steel relaxation losses calculated depending on the above equation are listed in Table 4-14. The total long-term losses and the effective prestressing force are calculated for the six slab specimens after the reduction of the long-term losses and are presented in Table 4-15.

Table 4-14 The initial prestressing forces, steel relaxation losses stresses in kN and percentage of steel relaxation losses for each specimen

Specimen	p_i (kN)	Δp_{Pr} (MPa)	Steel Relaxation Losses percentage (%)
BS1	445.6	33.3	2.18
BS2	441.3	32.2	2.12
UBS1	438.6	31.5	2.09
UBS2	434.4	30.4	2.035
UBSR1	430.1	29.3	1.98
UBSR2	409.2	24.2	1.72

Table 4-15 The jacking force, initial force, long-term losses force, the total losses forces and percentage and the effective force for the six specimens

Specimen	Jacking force (kN)	Initial Force (kN)	Steel Relaxation (kN)	Creep of concrete (kN)	Shrinkage of concrete (kN)	Total Losses (kN)	Total Losses (%)	Effective force (kN)
BS1	453.1	445.6	9.9	14.0	11.3	35.2	7.77	410.8
BS2	448.8	441.3	9.5	13.8	11.3	34.6	7.71	407.3
UBS1	446.6	438.6	9.3	13.7	11.3	34.3	7.68	404.9
UBS2	442.2	434.4	9.0	13.5	11.3	33.8	7.64	401.2
UBSR1	437.9	430.1	8.7	13.4	11.3	33.4	7.63	397.3
UBSR2	416.6	409.2	7.2	12.6	11.3	31.1	7.47	378.6

The calculations at the ultimate limit stage are repeated to get the failure loads for each specimen. The bonded tendon's slab specimen's failure is recalculated using the same procedures adopted in chapter 3 using the losses calculated in Table 4-15. Table 4-16 illustrates the values of the effective force and stress, ε_{pe}, ε_{dc}, c, a, and the failure loads for BS1 and BS2.

Table 4-16 The slab specimens with bonded tendons calculated results at the failure stage

Specimen	Effective force (kN)	Effective stress f_{pe} (MPa)	ε_{pe}	ε_{dc}	c (mm)	a (mm)	$P_{Exp}/2$ (kN)	P_{Exp} (kN)
BS1	410.8	1387	0.007302	0.000177	24.19	19.86	38.1	76.2
BS2	407.3	1375	0.007237	0.000175	24.18	19.85	38.1	76.2

For the unbonded tendons slabs without reinforcement and the unbonded tendons slabs with non-prestressing steel reinforcement the failure loads for the four specimens UBS1, UBS2, UBSR1 and UBSR2 are recalculated and the results are listed in Table 4-17.

Table 4-17 The slab specimens with unbonded tendons calculated results at the failure stage

Specimen	Effective Stress (f_{pe}) (MPa)	f_{ps} 1 (MPa)	f_{ps} 2 (MPa)	f_{ps} 3 (MPa)	f_{ps} used (MPa)	a (mm)	$P_{Exp}/2$ (kN)	P_{Exp} (kN)
UBS1	1367	1567	1787	1674	1567	17.06	32.4	64.8
UBS2	1355	1555	1775	1674	1555	16.92	32.1	64.2
UBSR1	1342	1542	1762	1674	1542	23.02	46.9	93.8
UBSR2	1279	1479	1699	1674	1479	22.33	45.6	91.1

The strain of the non-prestressing steel reinforcement in UBSR1 and UBSR2 are calculated to give 0.013296 and 0.012441, respectively. Both values have exceeded the yielding strain of the non-prestressing steel reinforcement, confirming the assumption stated before.

5 Results and Discussion

5.1 Introduction

Chapter five represents the results collected from testing the six slab specimens under four-point flexural loading. The test setup is prepared as discussed through chapter four and the sequence of testing is as follows, one slab of each set is tested, then the second round is testing the second slab of each set. The first slab to be tested is the bonded slab without non-prestressing steel reinforcement (BS1), followed by the unbonded slab with non-prestressing steel reinforcement (UBSR1) and then the unbonded slab without non-prestressing steel reinforcement (UBS1). Then this loop is repeated. The results, observations and data collected for each slab are discussed separately through the following section.

Table 5-1 represents the failure loads and the six slab specimen's deflections measured during the experimental testing. The theoretical failure loads are also represented in this table. These data will be discussed and clarified through this chapter.

Table 5-1 The experimental failure load, deflection and the theoretical failure loads for the six slab specimens

Specimen	Experimental load at failure (kN)	Maximum deflection at failure (mm)	Analytical ultimate load (kN)
BS1	-	-	76.2
BS2	45.6	87.8	76.2
UBS1	61.8	87.0	64.8
UBS2	64.8	91.6	64.2
UBSR1	103.8	98.1	93.8
UBSR2	101.6	93.6	91.1

5.2 Results of the experimental program

5.2.1 Bonded slab without non-prestressing steel reinforcement (BS1)

The testing program started with BS1 specimen, the set up was prepared as descripted in Chapter 4 and all the strain gages were connected in addition to the LVDT located at the soffit of the concrete slab and the (60mm) strain gage was bonded the top surface of the concrete specimen at mid-span. Only the strain gage located on the mid-span of the middle tendon was working in addition to the LVDT and the strain gage (60mm) at the top concrete surface. Figure 5-1 shows BS1 slab with the complete set-up before testing.

Figure 5-1 Bonded slab without non-prestressing steel reinforcement specimen BS1 before testing

During testing this specimen, the loading ram did not work correctly due to a mechanical error and the slab failed suddenly after almost 40 seconds from the start of loading and the loading ram did not record any load. Two cracks have propagated during loading, one beneath one of the loading beams and the second within the bending zone. The slab failed at the location of the point load at the location of the shear-bending zone. Figure 5-2 represents BS1 after failure showing the two formed cracks and the two cracks formed by viewing them from the slab's soffit. One of the three tendons was seen unbroken through the wide crack that is formed at the location of the point load at failure, as shown in Figure 5-3.

The LVDT located at the mid-span of the slab has recorded maximum deflection at failure 94 mm. While the strain gage fixed on the upper surface of the concrete recorded a maximum strain of 0.006, the strain gage did not work properly during test showing this incorrect value. The strain gage located on the middle tendon documented strain due to loading 0.0089. The strain due to loading is added up to the strain that took place due to prestressing which equals to 0.008132, in order to calculate the final strain of the tendon at failure which is 0.017032; it is greater than the yielding strain of the low relaxation high tensile steel tendon (0.008).

Figure 5-2 BS1 after failure (top) and formed cracks after failure in a view from the slab's soffit (bottom)

Figure 5-3 BS1 wide crack at failure viewing an unbroken tendon

5.2.2 Unbonded slab with non-prestressing steel reinforcement (UBSR1)

The second tested specimen is the unbonded slab with non-prestressing steel reinforcement (UBSR1); the testing setup is prepared as descripted in Chapter 4 and a (60 mm) strain gage is bonded to the concrete top surface at mid-span. Because all of the strain gages attached to the unbonded tendons were not working before the test, four LVDTs were used to measure the deflection along the slab span and sequentially determine the profile of the slab and the tendon at failure. One LVDT is located at the bottom surface at mid-span. Two LVDTs each are connected to the bottom surface of the concrete at the location of the loading beams. The last LVDT is located at the mid distance between the support and the loading beam. Figure 5-4 shows a sketch with the locations of the LVDTs and their set-up in reality.

The test started with a displacement-control scheme where a total displacement of 120mm is distributed over 480 seconds. Throughout this phase, the ram of the loading machine reached the total displacement of 120mm with a load of 97.5 kN without failure of the specimen, only few fine flexural cracks were seen on the soffit (tension surface) of the slab which were distributed all over the bending zone of the specimen.

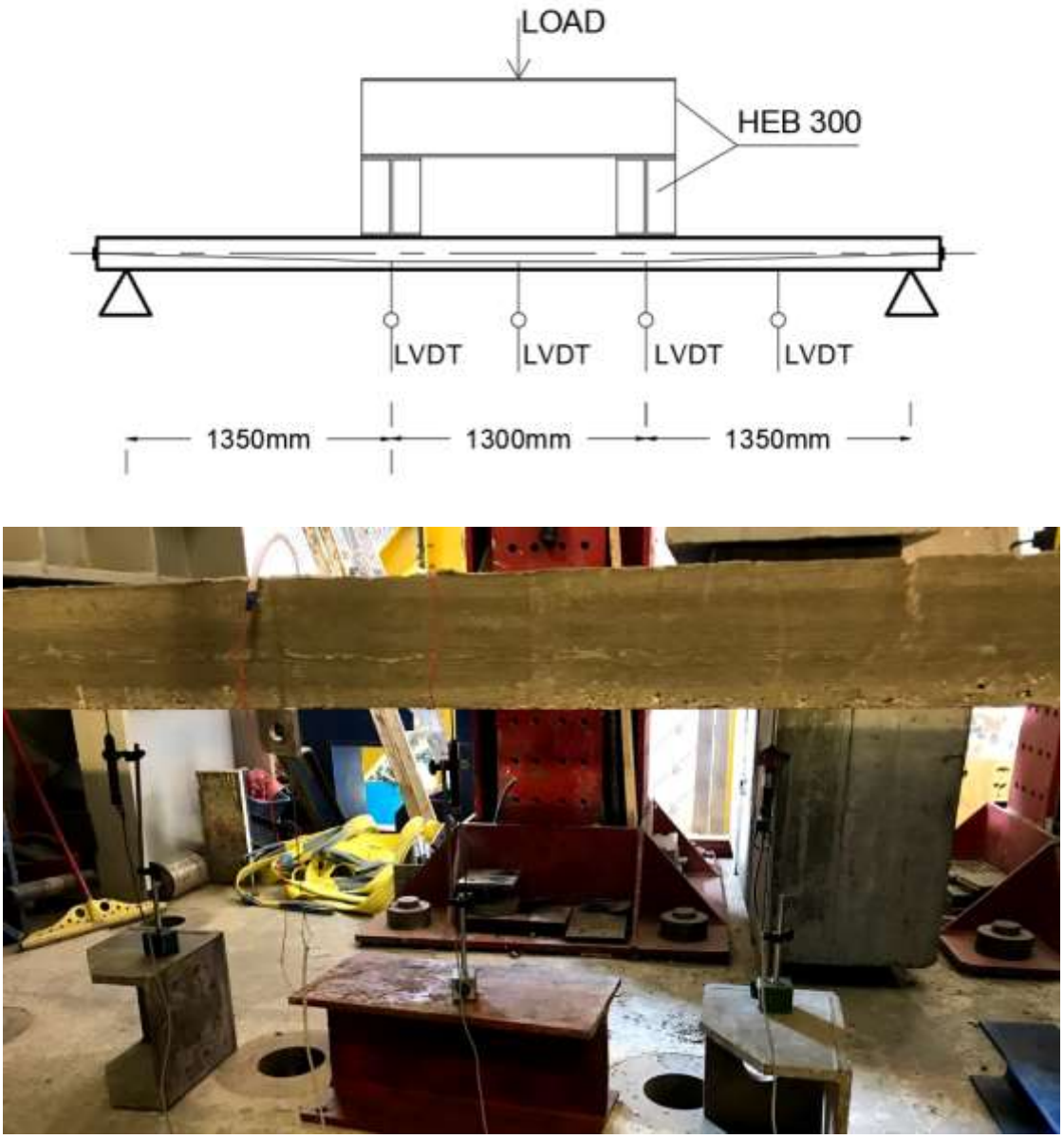

Figure 5-4 UBSR 1 with a sketch for the location of four LVDTs (top) and the LVDTs in their positions in reality (bottom)

The strain gage located on the concrete's top surface showed a strain of 0.004056, but no crushing occurred and after the removal of the load, the slab started to rebound back, leaving a permanent deflection. The permanent deformation is computed from the load-deformation curves drawn from the data collected from each LVDT. From the graph, the curve line is extended parallel to the elastic zone line to record a permanent deformation recorded in Table 5-2.

Table 5-2 Permanent deformations of UBSR 1

LVDT at the location of the loading beam (1)	LVDT between the support and the loading beam	LVDT at mid-span	LVDT at the location of the loading beam (2)
mm	mm	mm	mm
35	22	22	3.7164

The LVDT at the location of the loading beam (2) results are neglected because it showed very far results from the actual.

The test was then continued in a load-protocol scheme and the slab specimen failed at load 100 kN due tendon's yielding followed by concrete crushing at compression zone in the mid-span of the specimen. Figure 5-5 shows the failure mode of UBSR 1 presenting the concrete crushing in addition to the cracks located at the tension zone. 3.8 kN are added to the failure load value to consider the contribution of the loading beams' weight. So UBSR1's failure load is 103.8 kN.

Figure 5-5 Unbonded slab without reinforcement UBSR1 after failure showing the concrete crushing ant the compression zone and the cracks formed at the tension zone

Major cracks are observed in the mid-span bottom surface as shown in Figure 5-6. After failure of the slab and removal of the loading ram, the specimen has rebounded back, leaving some permanent deformation; this permanent deformation was not recorded by the LVDTs but still evident in the recorded videos, the rebound percentage is estimated to be around 50%. All of the anchors and the tendons were checked at both sides of the specimen. There was no failure on any of the anchors or even tendon slippage.

Figure 5-6 Major cracks at the bottom surface of the concrete slab at failure located at mid-span

The UBSR1 slab showed a final deformation measured by the LVDTS with a maximum value of 98.14 mm at mid-span. The measured deformations at failure are represented in Table 5-3. The load-deformation curve prepared from the data collected from the LVDT located at mid-span is presented in Figure 5-7.

Table 5-3 Deflection measured and calculated for UBSR1

LVDT Location	LVDT at the location of the loading beam (1)	LVDT between the support and the loading beam	LVDT at mid-span
Unit	mm	mm	mm
Total Deflection	96.54	80.48	98.14

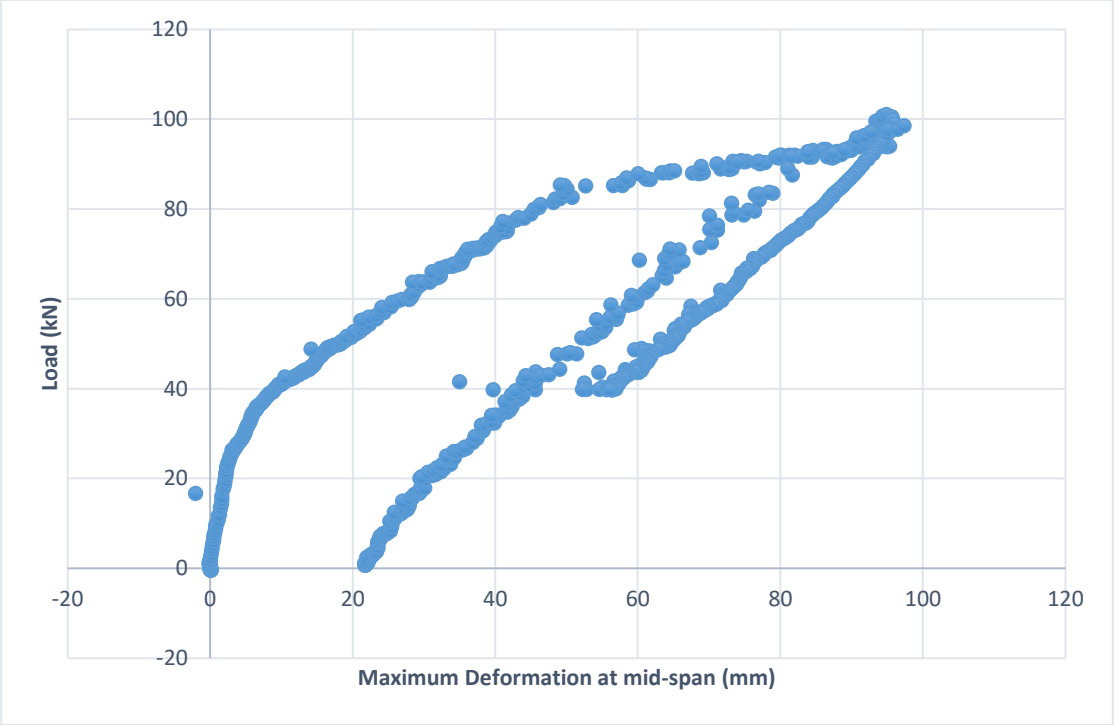

Figure 5-7 Load-Deformation curve for data collected from the LVDT located at mid-span

To calculate the strain in the cables, the profile of the slab and the tendon are drawn based on the measured LVDT's deflections along the slab span. Due to symmetry, half of the slab profile is drawn according to these measured deformations. The new length of the tendons at failure is 4.3136 m while the actual length is 4.3008m. The change in length and the tendon's strain are calculated and found to be 0.0128 m and 0.002976, respectively. Figure 5-8 shows the slab specimen's profile before applying loads and after reaching the maximum deflection right before failure, which corresponds to the extended length of the tendon after applying the maximum loads that the slab can withstand. The strain due to loading is added to the strain that took place due to prestressing and the total strain of each tendon is calculated and compared to the yielding strain of the high-strength steel tendons. The strain in the three tendons of UBSR 1 surpassed the yielding strain. Table 5-4 represents the total strain calculated in each tendon of the UBSR 1 specimen.

Table 5-4 Strain in each tendon at failure for UBSR1 specimen

Tendon number	Prestressing Strain	Strain at Failure	Total Strain
Tendon 1	0.007783	0.002976	0.01076
Tendon 2	0.007667	0.002976	0.01064
Tendon 3	0.007899	0.002976	0.01088

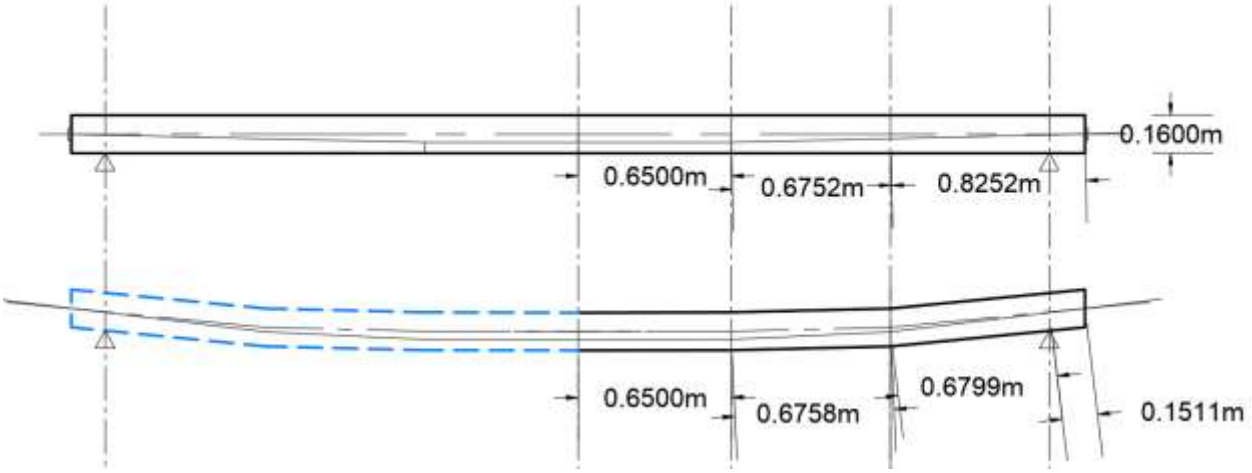

Figure 5-8 The elevation of UBSR1 before applying loads (The upper elevation) and after reaching the maximum deflection (The lower elevation)

The cracks are distributed all over the slab surface and are fine and short in length due to the presence of the non-prestressing steel reinforcement. The failure load recorded experimentally (103.8 kN) is larger than the analytical value calculated (93.8 kN) by almost 12%.

5.2.3 Unbonded slab without non-prestressing steel reinforcement (UBS1)

The test setup was prepared for the third specimen as planned in Chapter 4. The loading beams were positioned as mentioned before. All of the strain gages erected on the tendons were not working during the test and instead, LVDTs were used to measure the deformations along the slab's span and sequentially calculate the tendon's strain at failure. For this specimen, five LVDTs were used and positioned on the concrete's top surface. One LVDT is positioned at the mid-span of the slab specimen, then at a distance, 0.4 m from the mid-span, the second LVDT is supported followed by another LVDT at a distance of 0.9 m from the mid-span. The fourth LVDT is supported at 1.3 m from the mid-span and the last LVDT is positioned at 1.7 m from the mid-span. Figure 5-9 shows a sketch for the five LVDTs in their descripted positions and their positions in reality.

Two (60 mm) strain gages are supported on the upper and the bottom concrete surfaces at the mid-span in order to measure the concrete surface strain at the failure stage. Figure 5-10 shows the strain gage position on the concrete top surface. The test was carried using a load-protocol and the three loading beams were positioned as planned and are shown in Figure 5-10.

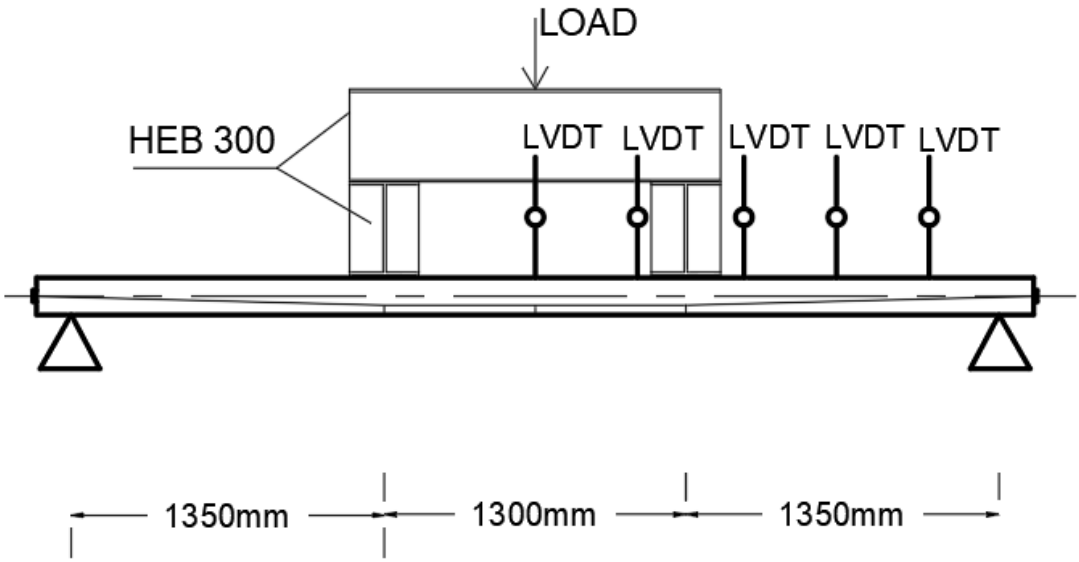

Figure 5-9 Sketch for the five LVDTs positioned for UBS1 at different locations (top) and their positons in reality (bottom)

Figure 5-10 Strain gage located on the concrete top surface (top) and loading beams full set up (bottom).

UBS1 failed due to tendon yielding followed by concrete crushing at the position of one of the loading beams, forming one wide crack on the tension surface at the load location. The concrete fractured completely while recording a maximum load of 58 kN, and 3.8 kN are added to this value

to account for the loading beams' weight, so the failure load is 61.8 kN. Figure 5-11 shows the position of the concrete failure, and the crack width that is formed at the position of failure. Through the crack formed at the bottom surface of the specimen, the prestressed unbonded tendon was seen unbroken. After failure and the removal of the load, the slab rebounded back, leaving permanent deformation. Any of the LVDTs did not record the permanent deformation. The crack that was formed almost closed back when the slab specimen rebounded back after the removal of the load. The rebound of the slab is around 80%, determined from the recorded videos during testing. All the anchors and tendons were checked at both sides of the specimen. There was no failure on any of the anchors or even tendon slippage.

The maximum displacement recorded by the LVDTs is at the mid-span with a value of 87.0 mm. Figure 5-12 shows the load-deformation curve conducted from the test results for the deformation recorded from the LVDT located at mid-span versus the results recorded by the loading ram. In this graph, the maximum value of deformation and the failure load are shown and also, the shape of the curve is similar to the load-deformation curve of the prestressing steel. Table 5-5 shows the maximum displacement recorded by the five LVDTs in addition to the deformation recorded at the yielding stage for of about 36 kN. The load at the yielding stage is determined from the load-deformation curve in Figure 5-12. The recorded readings by the LVDTs were used to draw the profile of the tendon after failure and to calculate the new length of the tendon. The actual length of the tendon is 4.3008m, while the length at failure is 4.3094 m. The same procedure followed for conducting the tendon's length for UBSR1 is repeated here to calculate the strain in UBS1 tendons. Figure 5-13 shows the tendon profile of UBS1 before testing, at the yielding stage and at the failure stage. The total change in length that took place at failure equals 0.0086m and the strain is 0.002. The strain is added to the strain derived by prestressing to calculate the tendon's total strain. Table 5-6 lists the prestressing strain in each tendon and the strain due to loading. Then, the total strain is compared to the yielding strain (0.008) and reveals that the strain of the three tendons surpassed the yielding strain of the seven wires low relaxation steel. Also, the total strain in each tendon at the yielding stage is calculated with the same procedure explained earlier and the results are presented in Table 5-7. The length of the tendon at the yield stage equals to 4.3016m and sequentially, the change in length equals to 0.0008m while the strain equals to 0.00019. The three

tendons show a total strain at yielding stage around 0.008 which is the yielding strain of the low relaxation steel.

Figure 5-11 UBS1 failure mode (top) and concrete bottom surface crack showing the prestressing tendon (bottom)

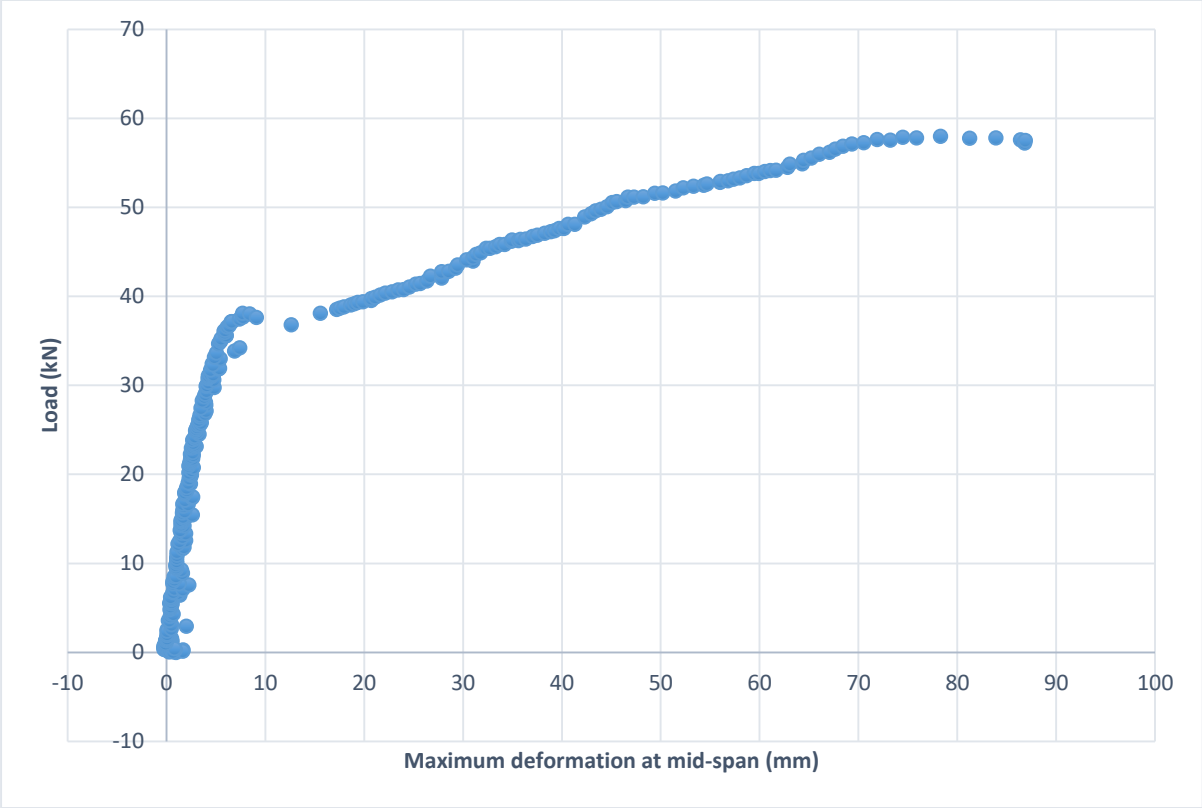

Figure 5-12 Load-Deformation curve for data collected from the LVDT located at mid-span

Table 5-5 Maximum deflection recorded by the five LVDTs

LVDT Location	LVDT at mid-span	LVDT at 40 cm from mid-span	LVDT at 90 cm from mid-span	LVDT at 130 cm from mid-span	LVDT at 170 cm from mid-span
Unit	mm	mm	mm	mm	mm
Maximum Deflection	87.0	72.017	54.107	13.76	0.22
Deflection at yielding stage	15.57	13.765	9.926	2.756	0.0821

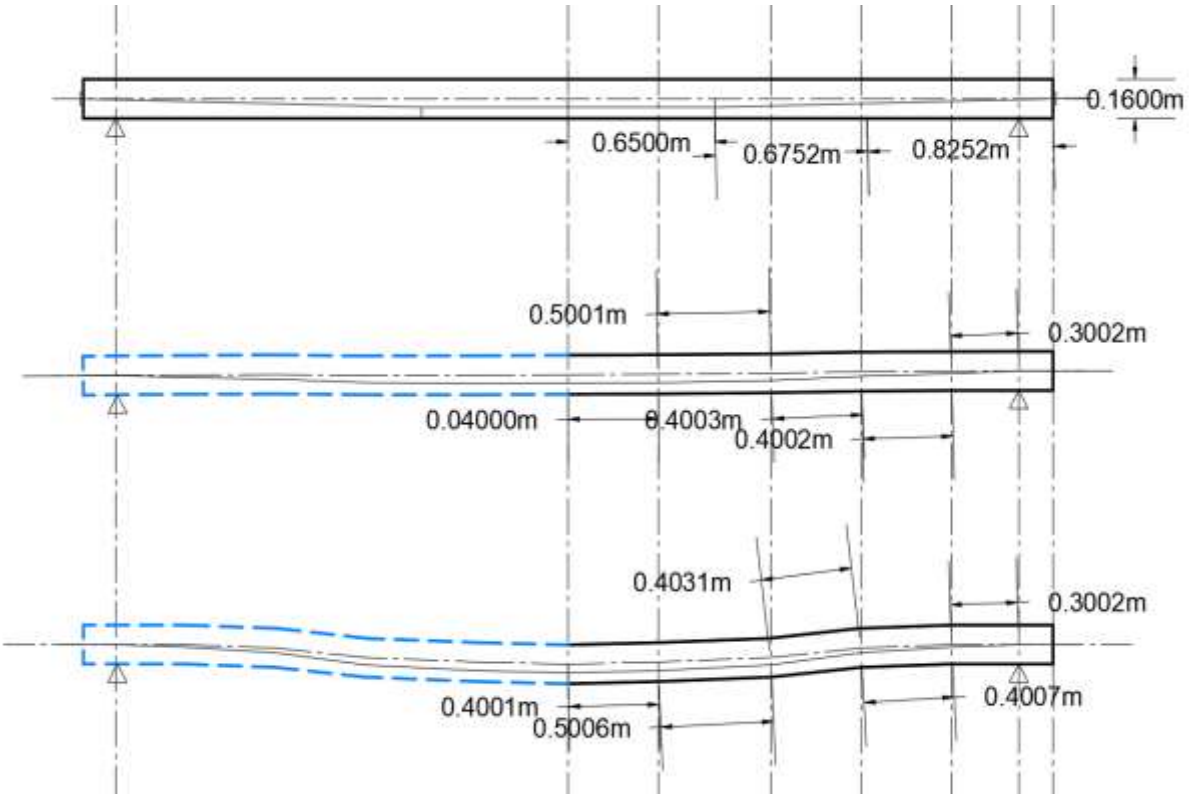

Figure 5-13 UBS1 tendon profile before testing (Upper figure), at yielding stage (Middle figure) and at failure stage (Bottom figure)

Table 5-6 Strain in each tendon at failure for UBS1 specimen

Tendon number	Prestressing Strain	Strain at Failure	Total Strain
Tendon 1	0.007551	0.002	0.00955
Tendon 2	0.007899	0.002	0.00989
Tendon 3	0.008364	0.002	0.01036

Table 5-7 Strain in each tendon at yielding stage for UBS1 specimen

Tendon number	Prestressing Strain	Strain at Yield stage	Total Strain
Tendon 1	0.007551	0.00019	0.0077
Tendon 2	0.007899	0.00019	0.0081
Tendon 3	0.008364	0.00019	0.0085

The strain gages supported on the concrete top and bottom surfaces, compression and tension surfaces, at the mid-span recorded maximum strain 0.0007 and 0.0009, respectively. These strains did not exceed the concrete limit strain 0.003, these recorded strains are not logic and obviously the strain gages did not work correctly during the test.

On comparing the experimental failure load value (61.8 kN) to the analytical value (64.8 kN) calculated in Chapter 4, it is concluded that the empirical equation used for determining the unbonded tendon's ultimate stress is accurate as the difference between the analytical and the experimental values is around 4%. Also, on comparing the unbonded system without non-prestressing steel reinforcement (UBS1) to the unbonded system with non-prestressing steel reinforcement (UBSR1), the effect of non-prestressing steel can be observed where they distribute the cracks and significantly increases the experimental capacity of the prestressed concrete member by almost 70%.

5.2.4 Bonded slab without non-prestressing steel reinforcement -2 (BS2)

The second slab of the first set BS2 is tested under four-point flexural loadings as planned for in Chapter 4, using three HEB-300. (10 mm) Strain gage is erected on the mid-span of one of the three tendons was working and connected during testing in addition to attaching two (60 mm) strain gages on the top and bottom surfaces of the concrete at the slab's mid-span. LVDTs are positioned similarly to specimen UBS1, as shown in Figure 5-14.

Encountered failure occurred at load of 41.8 kN with maximum displacement measured at mid-span 87.8 mm. The loading beams' weight 3.8 kN is added to the failure load conducting the actual failure load of value 45.6 kN. The slab firstly started to bend down, showing a maximum deformation at mid-span then a single crack began to form underneath one of the loading beams until complete failure. Figure 5-14 shows the moment of collapse of BS2. The failure load recorded during testing is less than the 76.2 kN analytical failure load value calculated according to the ACI code provisions. The experimental failure load recorded is obviously not correct.

BS2 entirely crushed to the ground after seconds from stopping the test, as shown in Figure 5-15. The slab was then checked to see if there are any other cracks and to know the state of the tendons after failure. One of the three tendons was seen not broken and only a wide crack at the location of failure was detected, as shown in Figure 5-15. All the anchors and tendons were checked at both sides of the specimen. There was no failure in any of the anchors or even tendon slippage.

Figure 5-14 BS2 set up complete with LVDTs positioned as demonstrated and strain gages shown on the top and bottom surfaces of the concrete (top) and its failure due to the formation of one single crack underneath one of the loading beams (bottom)

Figure 5-15 BS2 completely fallen down to the ground after a few seconds from stopping the test (top) and one of the tendons in BS2 was detected unbroken after failure (bottom)

The data recorded by the LVDTs and the strain gages is analyzed and the following results are observed.

First of all, the deflections recorded by the LVDTs at the locations explained before for UBS1 were used to draw the profile of the cable after failure and sequentially measuring the new length of the tendon, which is 4.3146 meters. The maximum deformation recorded by the LVDT located at the mid-span is presented versus the load in Figure 5-16, showing the maximum failure load and deformation.

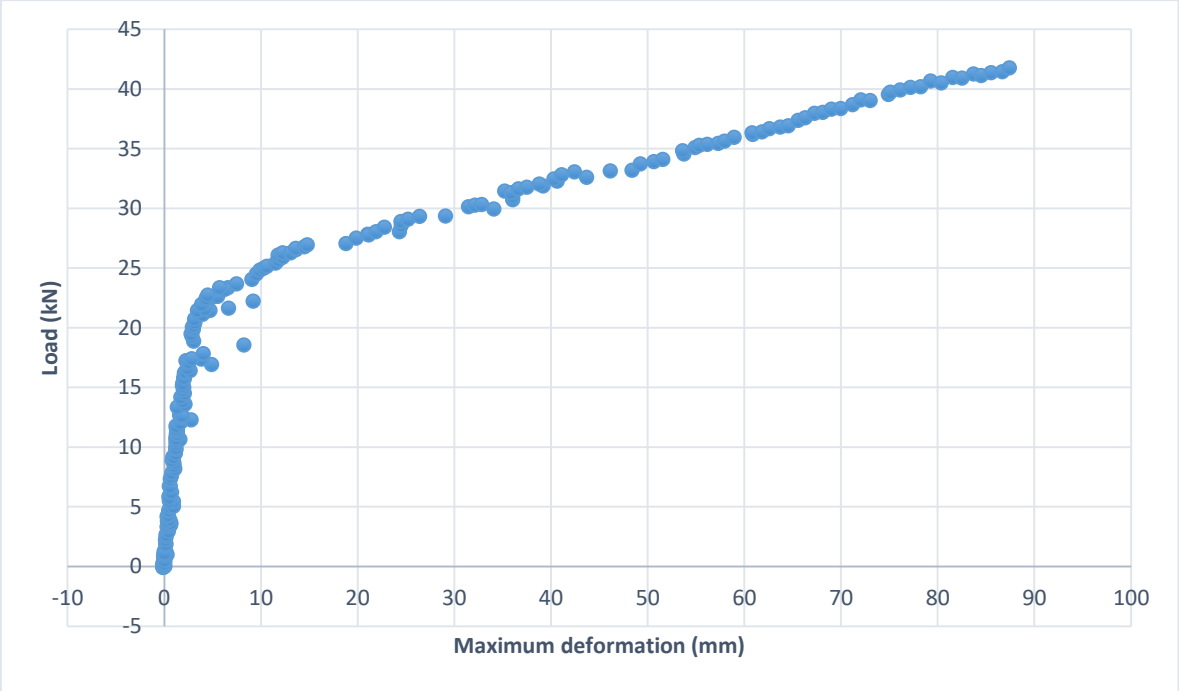

Figure 5-16 Load-Deformation curve for data collected from the LVDT located at mid-span

Figure 5-17 shows the tendon's profile before testing, at the yielding stage and right before the failure. Table 5-8 lists the deflection recorded by each LVDT at the moment of failure and at the yielding stage. Then, the change in length and the strain at failure are calculated to be 0.0138 m and 0.0032, respectively. The strain due to loading is added to the strain of each tendon that took place due to prestressing to calculate the final strain in the tendons. Table 5-9 illustrates the strain due to prestressing and due to loading and the final strain in each of BS2's three tendons. The strain in the three tendons has exceeded the yielding strain for the low-relaxation high-tensile steel (0.008).

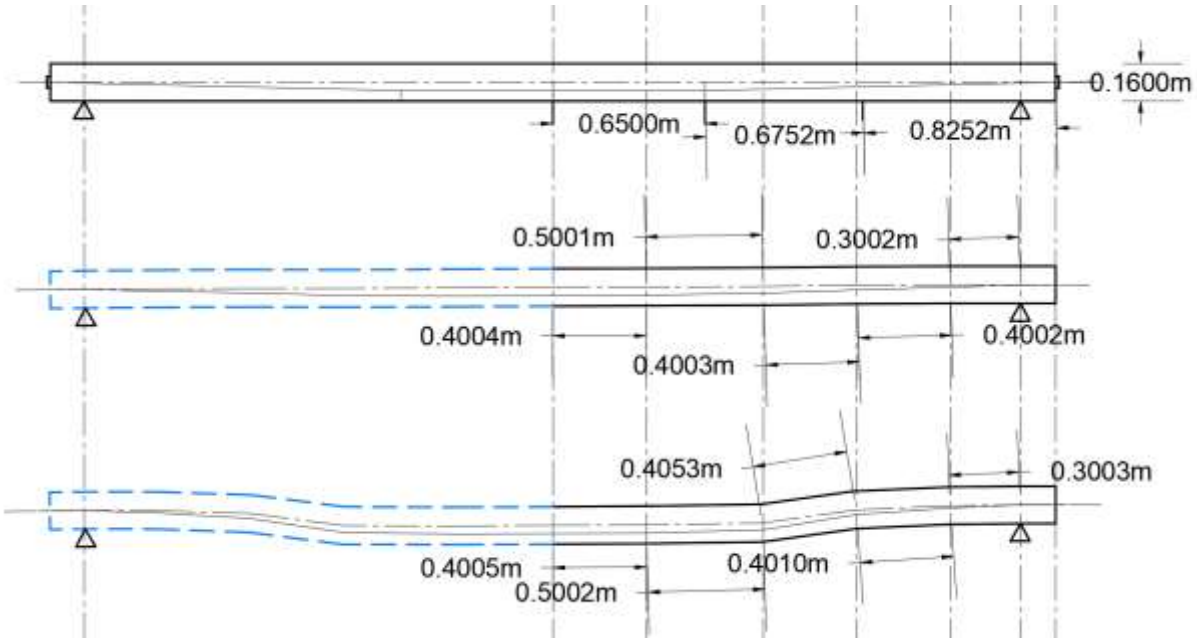

Figure 5-17 BS2 tendon profile before testing (Upper figure), at yielding stage (Middle figure) and at failure stage (Bottom figure)

Table 5-8 Maximum deflection recorded by the five LVDTS

LVDT Location	LVDT at mid-span	LVDT at 40 cm from mid-span	LVDT at 90 cm from mid-span	LVDT at 130 cm from mid-span	LVDT at 170 cm from mid-span
Unit	mm	mm	mm	mm	mm
Maximum Deflection	87.8	85.3	79.2	22.1	0.37
Deflection at yielding stage	11.49	9.51	6.85	2.17	0.06

Table 5-9 Strain in each tendon at failure for BS2 specimen

Tendon number	Prestressing Strain	Strain at Failure	Total Strain
Tendon 1	0.007899	0.0032	0.0111
Tendon 2	0.007899	0.0032	0.0111
Tendon 3	0.008132	0.0032	0.0113

In addition, the strain at the yielding stage is calculated from the new profile of the tendon at load equals 24 kN chosen from the load-deformation curve represented. The tendon's new length at the

yield stage equals 4.3024m, while the change in length and strain equal 0.0016 m and 0.00037, respectively. Table 5-10 represents the strain conducted for each tendon from the calculations at the yielding stage and the total strain of the three tendons is around 0.008.

Table 5-10 Strain in each tendon at yielding stage for BS2 specimen

Tendon number	Prestressing Strain	Strain at Yield stage	Total Strain
Tendon 1	0.007899	0.00037	0.00827
Tendon 2	0.007899	0.00037	0.00827
Tendon 3	0.008132	0.00037	0.00850

The (10 mm) strain gage attached to the steel tendon at mid-span recorded a maximum strain of 0.00577 during failure. After adding up this strain due to loading to the prestressing strain of tendon 0.00789, the final strain in this tendons equals 0.01366 exceeding the yielding strain 0.008. Figure 5-18 represents the maximum strain measured and shows the load-strain curve drawn for BS2's tendon presenting the 0.00789 strain that took place due to prestressing in addition to the strain due to loading versus the loading sequence recorded during testing. The strain determined from the strain gage supported on the tendon is compared to that calculated from the conducted profile at failure for the tendon and both values are close to each other.

The strain gages (60 mm) erected on the concrete upper and bottom surfaces, compression and tension surfaces, showed maximum strain values during failure equals 0.00162 and 0.0007, respectively. Same as for the last specimen, the strain gages did not work correctly during the test.

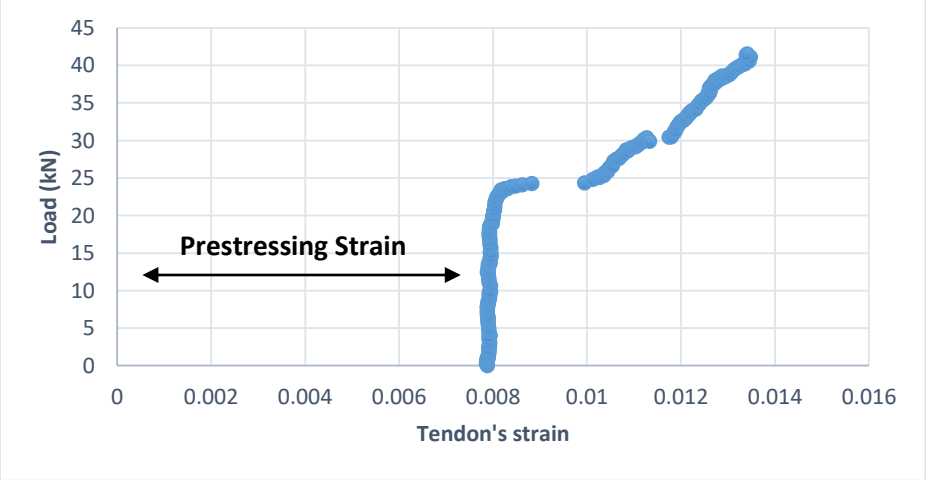

Figure 5-18 The tendon's strain-load for BS2

5.2.5 Unbonded slab with non-prestressing steel reinforcement-2 (UBSR2)

The second specimen of the second set, the unbonded slab with non-prestressing steel reinforcement UBSR2, is tested as planned in Chapter 4; the setup was erected similarly to all the past specimens. None of the strain gages fixed on the prestressed tendons were working during the test. LVDTs were secured in the positions illustrated for the UBS1 specimen. In addition, two (60 mm) strain gages were adhered to the upper and lower surfaces of the concrete, compression and tension surfaces, at the specimen's mid-span. Figure 5-19 shows the complete setup of UBSR2 before testing.

UBSR2 reached a maximum load at failure equals 97.8 kN, with maximum deflection measured at mid-span equals 93.6 mm. The loading beams' weight 3.8 kN is added to the recorded failure load to give 101.6 kN failure load. The experimental failure load is greater than the analytical value calculated in Chapter 4 by almost 8%. The failure took place underneath one of the loading beams. At the beginning of the loading, the slab started to bend down, with a maximum deflection at mid-span; then fine cracks started to appear distributed all over the bending zone of the slab until a wide crack propagated beneath one of the loading beams. Figure 5-19 shows UBSR2 after failure with the cracks at the bending zone and the wide crack at the location of the point load. Figure 5-20 shows the cracks formed at the soffit of the concrete slab after failure. The cracks at the bottom surface are all almost fine and distributed all over the slab due to the presence of the non-prestressing steel reinforcement, accompanied by one wide crack that propagated under the point load at the shear-bending zone. After failure and the removal of the loading ram, the slab specimen started to rebound back, leaving behind obvious permanent deformation. This permanent deformation was not recorded by the LVDTs connected to the specimen. The slab is estimated to have rebounded back by around 60%, this value is determined from the recorded video during the test. All the anchors and tendons were checked at both sides of the specimen. There was no failure on any of the anchors or even tendon slippage.

Figure 5-20 shows the load-deformation curve produced from the results obtained for UBSR2. The load-deformation curve shows the maximum deformation and the failure load stated above. The strain in the tendons is calculated from the recorded deflections by the LVDTs by the same procedure followed for the previous specimens. The new length of the tendons is calculated from

the new profile of the slab after failure, similar to what is done for the past three specimens. The new length is derived 4.3146 meters, the change in length and the strain equal 0.0137834 m and 0.0032, respectively. Table 5-11 shows the maximum deflection and the deflection during the yielding stage recorded by the five LVDTs supported on UBSR2.

Figure 5-19 The complete set up of UBSR 2 before the start of the flexural test (top) and after failure (bottom)

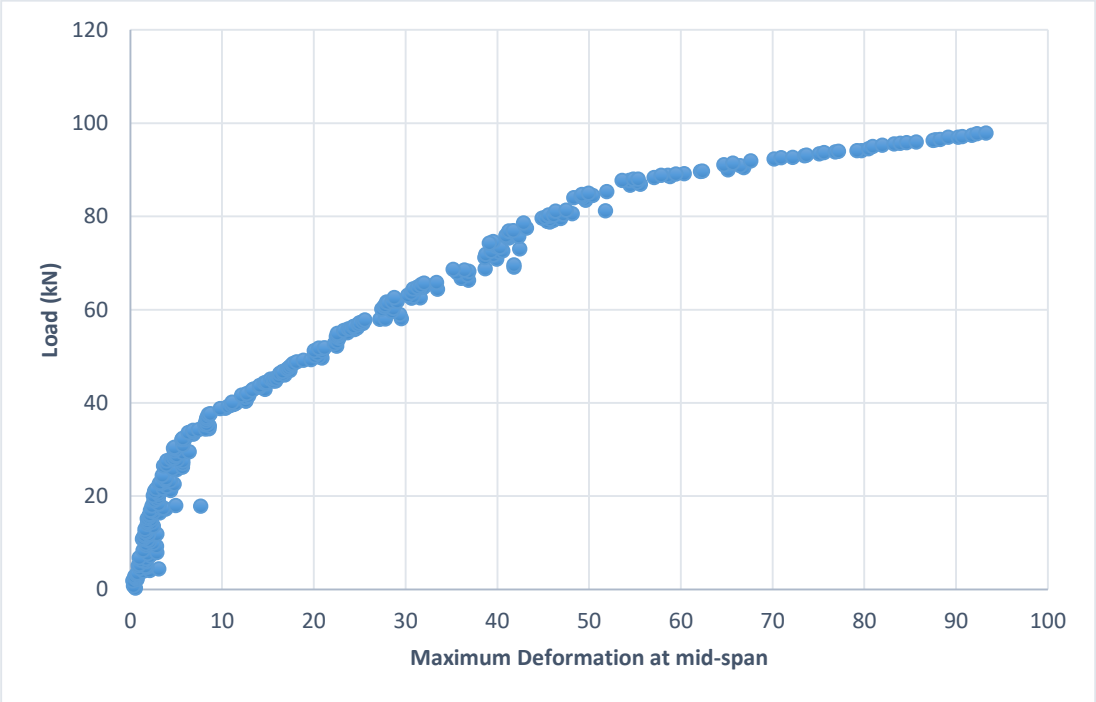

Figure 5-20 Cracks formed on the bottom surface of UBSR2 after failure (top) and The load-deformation curve for data collected from the LVDT located at mid-span (bottom)

Table 5-11 The maximum deflection recorded by the five LVDTs

LVDT Location	LVDT at mid-span	LVDT at 40 cm from mid-span	LVDT at 90 cm from mid-span	LVDT at 130 cm from mid-span	LVDT at 170 cm from mid-span
Unit	mm	mm	mm	mm	mm
Maximum Deflection	93.6	92.1	85.6	40.7	0.14
Deflection at yielding stage	12.59	10.74	7.88	2.90	0.04

The total strain in each tendon is calculated after adding up the strain that took place due to prestressing to the strain due to loading. Table 5-12 lists the total strain calculated in each tendon as illustrated above. The final strain calculated in the three tendons of UBSR2 has exceeded the yielding strain of the low-relaxation high-tensile steel (0.008). Figure 5-21 represents the tendon's profile and the elevation of the concrete before testing, and right before failure.

Table 5-12 Strain is each tendon at failure for UBSR2

Tendon number	Prestressing Strain	Strain at Failure	Total Strain
Tendon 1	0.007667	0.0032	0.010867
Tendon 2	0.007203	0.0032	0.010403
Tendon 3	0.007345	0.0032	0.010545

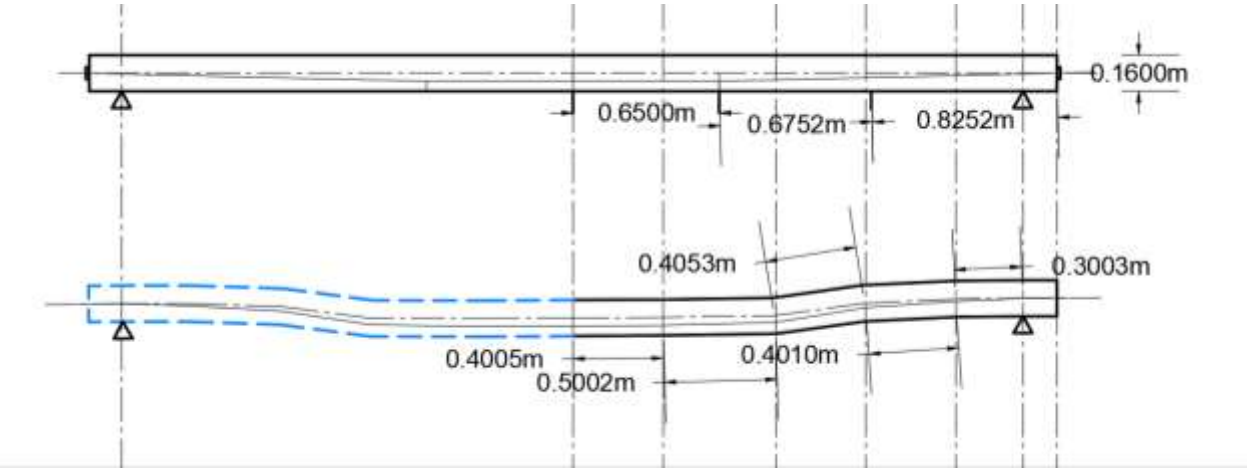

Figure 5-21 UBSR2 tendon profile before testing (Upper figure), at yielding stage (Middle figure) and at failure stage (Bottom figure)

The (60 mm) strain gage fixed on the bottom surface of UBSR2 was disconnected after reaching 80 kN by the loading machine and was showing unrealistic values during testing, while the strain gage erected on the upper surface on the compression surface recorded maximum strain equals 0.0036 as shown in the load-strain curve represented in Figure 5-22.

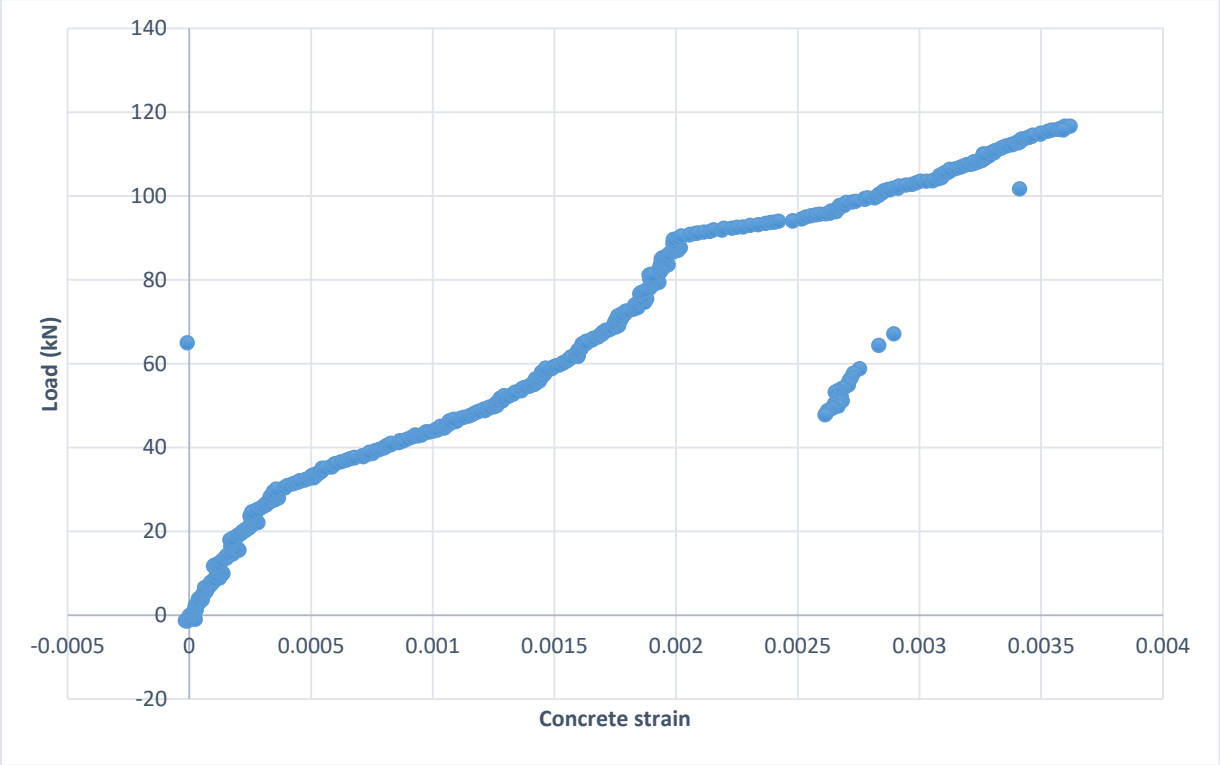

Figure 5-22 Concrete strain versus load at the concrete tension surface

The failure load, deformation, crack's shape, mode of failure and the total strain in the tendons values of both UBSR1 and UBSR2 are almost the same reflecting the accuracy of the carried tests and experiment. The average failure load of the unbonded slabs with reinforcement is 102.7 kN.

5.2.6 Unbonded slab without non-prestressing steel reinforcement-2 (UBS2)

The sixth specimen is the unbonded slab without non-prestressing steel reinforcement UBS2 and is tested under a four-point loading system. The set-up is prepared according to the planned program as mentioned in Chapter 4. None of the strain gages fixed on the tendons before concrete pouring were working during the test. LVDTs were used to measure the deflection as done for the specimen UBS1. Figure 5-23 shows the complete setup of UBS2 with the attached five LVDTs and the (60 mm) strain gages on the upper and the bottom surface of the concrete slab at mid-span.

Figure 5-23 The complete set up of UBS2 before testing

UBS2 failed at 61 kN with a maximum deflection recorded by the LVDT located at the mid-span equals 91.6 mm. The effect of the loading beams is added to conduct of a failure load of value 64.8 kN. The values of the failure load and the deformation are close to the recorded results for UBS1 and the difference between the analytical and the experimental failure load is less than 1% for UBS2. The slab failed due to the formation of one wide crack beneath one of the two loading beams. There was also one fine crack that appeared at the mid-span of the slab. Figure 5-24 shows the slab after failure showing the two cracks that have propagated and caused the failure.

After the failure and the removal of the loading ram, the slab rebounded back by almost 80% detected from the recorded videos during testing. The crack formed and caused failure has almost closed due to rebounding back after removing the load. Figure 5-25 shows the difference between the slab profile during failure and after the removal of the load. Figure 5-26 represents the load-deformation curve conducted from the recorded data for the deformation measured by the LVDT located at the mid-span and the data of the loads from the loading ram. From the curve, the maximum deformation and the maximum load reached and mentioned above are observed.

Figure 5-24 The wide crack that propagated on UBS2 beneath the loading beam (top) and the fine crack that propagated on UBS2 at almost mid-span (bottom)

Figure 5-25 UBS2 during failure showing maximum deflection (top) and after failure and the removal of the load (bottom)

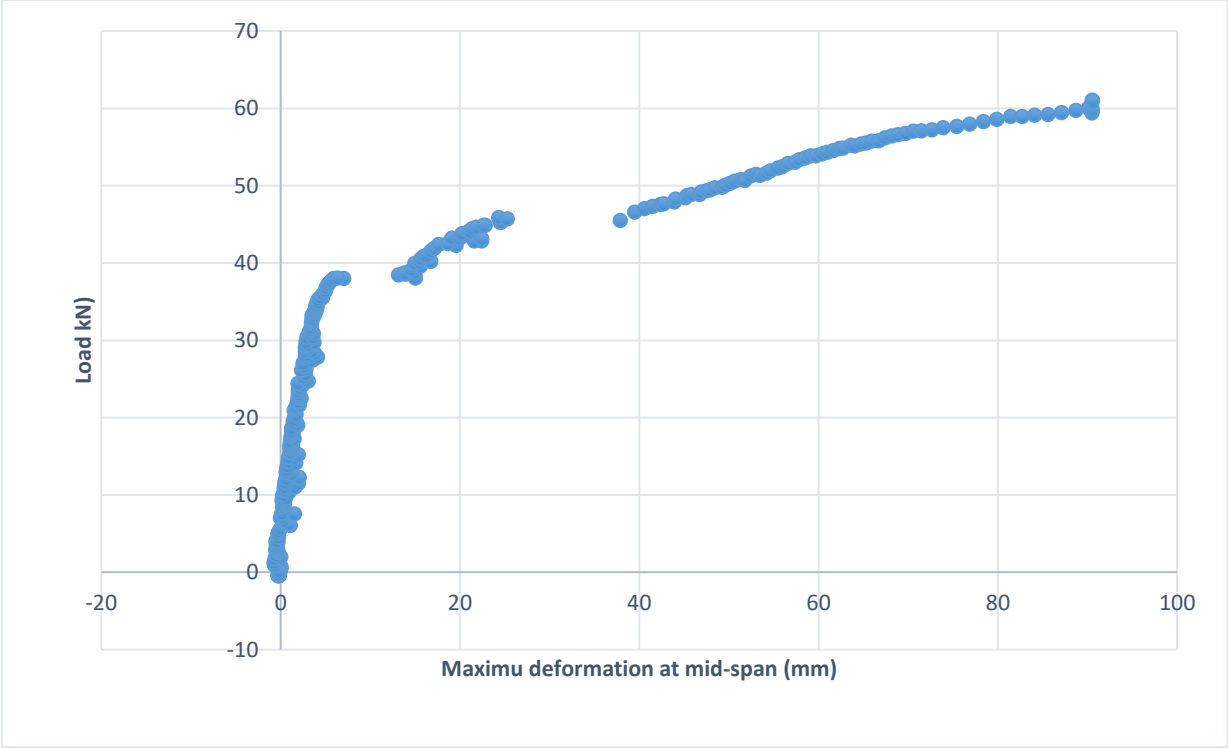

Figure 5-26 Load-Deformation curve for data collected from the LVDT located at mid-span

The value of the maximum deflection at failure and at yielding stage are recorded by the five LVDTs and shown in the following Table 5-13. The new length of the tendons at failure is calculated with the same procedure followed for the last four slabs. The new length calculated is 4.3136 meters, the change in length and strain equal 0.0128 m and 0.00298, respectively. The strain due to loading and the prestressing of each tendon are added to calculate the final strain in the prestressed tendons. Also, the new length, change in length and strain are calculated with the same followed procedure for the tendons at the yielding stage which is at load equals 40 kN (determined from the load-deformation curve) and the values are 4.3028m, 0.002m and 0.000465, respectively. The strain due to loading and due to the prestressing in addition to the final strain at the failure stage are presented in Table 5-14, while Table 5-15 represents the strain due to prestressing and loading and the final strain at the yielding stage. The total strain at failure calculated in the three tendons has exceeded the yielding strain governed by the low-relaxation high-tensile steel strands 0.008. The profile of the tendon before testing, at the yield stage and at the failure stage is presented in Figure 5-27.

Table 5-13 Maximum deflection recorded by the five LVDTs

LVDT Location	LVDT at mid-span	LVDT at 40 cm from mid-span	LVDT at 90 cm from mid-span	LVDT at 130 cm from mid-span	LVDT at 170 cm from mid-span
Unit	mm	mm	mm	mm	mm
Maximum Deflection	91.6	90.8	89.6	30.1	0.041
Deflection at yielding stage	18.52	17.13	14.16	5.36	0.004

Table 5-14 Strain at failure in each tendon for UBS2

Tendon number	Prestressing Strain	Strain at Failure	Total Strain
Tendon 1	0.007899	0.002976	0.0109
Tendon 2	0.007551	0.002976	0.0105
Tendon 3	0.008132	0.002976	0.0111

Table 5-15 Strain at yield stage in each tendon for UBS2

Tendon number	Prestressing Strain	Strain at Failure	Total Strain
Tendon 1	0.007899	0.00046	0.00835
Tendon 2	0.007551	0.00046	0.00800
Tendon 3	0.008132	0.00046	0.00859

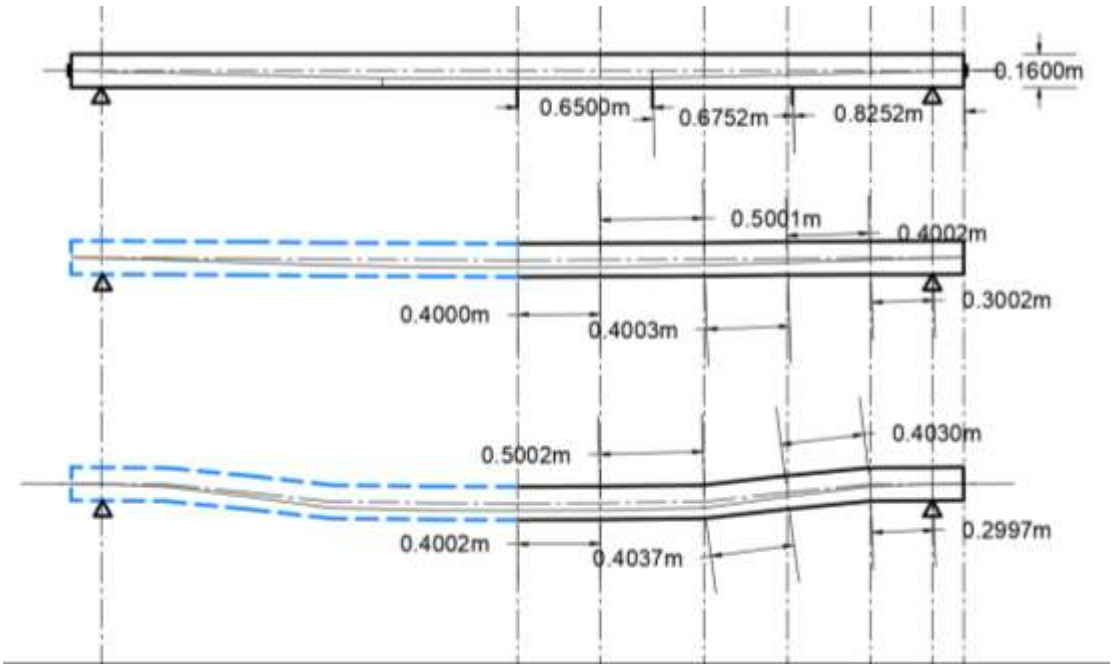

Figure 5-27 UBS2 tendon profile before testing (Upper figure), at yielding stage (Middle figure) and at failure stage (Bottom figure)

The strain measured by the strain gages (60 mm) fixed on the upper and lower surface of the concrete slab at mid-span were 0.0008 and 0.0012, respectively. These recorded strain values are not realistic and that means that the strain gages did not work correctly during the test.

The values recorded for the two specimens UBS2 and UBS1 are too close, having an average failure load of 63.3 kN. Also, the behavior and failure mode of both specimens are the same. The difference between the analytical and the experimental failure load for UBS2 is less than 1%. Also, the increase in the specimen's flexural capacity due to the addition of the non-prestressing steel reinforcement is around 60%.

5.3 Discussion of results

Table 5-16 Summary for all the data collected from the six tested slabs

Specimen	Experimental load at failure (kN)	Average Experimental load at failure (kN)	Maximum deflection at failure (mm)	Analytical load at failure (kN)	Average Analytical load at failure (kN)	Cracks description
BS1	-	45.6	-	76.2	76.2	-
BS2	45.6		87.8	76.2		One wide crack
UBS1	61.8	63.3	87.0	64.8	64.6	One wide crack
UBS2	64.8		91.6	64.2		One wide crack and one fine crack
UBSR1	103.8	102.7	98.1	93.8	92.4	One wide crack and other few fine cracks
UBSR2	101.6		93.60	91.1		One wide crack and other few fine cracks

After illustrating the behavior of the six specimens and discussing their failure modes, a comparison between the tested specimens is carried in terms of the value of loads reached for each specimen at failure and at the yielding stage. Also, the maximum deformations recorded during failure are compared. The analytical load values calculated in chapter 4 for each specimen are represented in addition to the cracks description. All of the results conducted from the experimental work and the analytical calculations are presented in Table 5-16 as a summarization of the work carried in this research.

5.3.1 Failure loads

5.3.1.1 Analytical and experimental loads

The experimental program carried through this research shows failure loads for the unbonded system with non-prestressing reinforcement (UBSR), with an average value of 102.7 kN, higher than the other two systems. The unbonded system with no non-prestressing steel reinforcement (UBS) shows higher failure loads with an average of 63.3 kN, than the bonded system (BS), 45.6 kN. According to the analytical calculations carried in Chapter 4, the bonded system (BS) should show a higher failure load than the unbonded system with no non-prestressing steel reinforcement (UBS) due to the ACI 318-19 code limitation on the unbonded tendon's ultimate stress maximum value limiting it to the tendon's yield stress. Obviously, the failure load recorded for BS is not correct and accordingly, the stress in the three tendons is calculated from the strain derived from the drawn tendon's profile at the failure stage for BS2. The same procedure followed in Chapter 4 for calculating the experimental load $P_{Exp.}$ is followed to calculate the correct failure load, which is conducted to be 74.2 kN. This calculated value is more logical than the recorded one and confirms the analytical calculations carried according to the ACI 318-19 provisions.

5.3.1.2 ACI 318-19 unbonded tendon's ultimate stress empirical equation

The differences between the analytical and the experimental failure loads for UBSR and UBS were all around 10%, proving the accuracy of the carried experimental program and the provisions provided by the ACI 318-19. UBSR two specimens show higher experimental failure loads than the analytical ones by almost 10%. For UBS two specimens, the experimental and the analytical loads were almost the same with very minor percentage of difference. Although the recorded failure loads for UBS shows that the empirical equation used to calculate the unbonded tendon's

ultimate stress governed by the ACI 318-19 is accurate, still the limitation on the maximum value of the unbonded tendon's ultimate stress is not correct because all of the tendons in the UBSR and UBS systems have surpassed the tendon's yield stress.

5.3.1.3 Effect of adding non-prestressing steel reinforcement

The non-prestressing steel reinforcement enhances the capacity of the unbonded members significantly. Analytically, the addition of non-prestressing steel reinforcement (0.006 A_{ct}) increases the unbonded slabs' capacity by around 40 % and experimentally, it increases the capacity by around 60%. Also, non-prestressing steel reinforcement added for UBSR two specimens provides a uniform distribution of the cracks and makes them finer than the UBS and BS systems.

The non-prestressing steel reinforcement also allows for a better capacity for the unbonded system than the bonded system. So, the unbonded tendons can be used widely to benefit from its various advantages while having a higher flexure capacity than the bonded system by around 35%.

5.3.2 Ductility

To assess the ductility, the elongations of the three systems are compared. As the tendon's length in all of the specimens is the same, the deformations of the systems are compared instead. From the previously mentioned load-deformation curves, it can be observed that the unbonded system with non-prestressing reinforcement has the highest average deformation (95.8mm), followed by the unbonded system with no non-prestressing reinforcement (89.3mm). In contrast, the bonded system shows the least average deformation of 87.8mm.

The behavior of the unbonded slabs with non-prestressing steel reinforcement and with no non-prestressing steel reinforcement showed better behavior during failure than the bonded slabs. The unbonded slabs with non-prestressing steel reinforcement (UBSR) rebounded back after failure and the removal of the load by an average of around 55% and the unbonded slabs with no non-prestressing steel reinforcement (UBS) have shown a higher percentage, 80%, of rebound after failure and the removal of the load. On the contrary, the bonded slabs (BS) completely failed to the ground after seconds from stopping the test.

The UBS specimens have a higher rebound capacity than the UBSR specimens due to the presence of the non-prestressing steel reinforcement. The non-prestressing steel reinforcement have developed plastic deformation during failure so the rebound was limited for the UBSR specimens.

The unbonded slabs without non-prestressing reinforcement showed very good behavior at the failure stage and showed very high ductility levels so, the requirement of the ACI 318-19 for the addition of non-prestressing steel upon the usage of unbonded tendons can be removed.

6 Conclusion

6.1 Introduction

Through this thesis, the post-tension concrete slabs with bonded and unbonded tendons were investigated in depth. The first chapter represented the problem raised due to the ACI 318-19 provisions that limit the capacity of the unbonded post-tension concrete members to be less than the bonded post-tension concrete members. The research aims to persuade the Egyptian designers and contractors to use the unbonded tendons as widely as the bonded tendons to benefit from the various advantages of the unbonded system. Chapter two reviewed the prestressing concept and the difference between traditional concrete and prestressed concrete. Also, a detailed comparison is carried between the bonded and the unbonded system, including a comparison between the ACI 318-19 provisions for each system. Then, a literature review is presented to highlight all of the previous work carried to investigate the behavior of the unbonded tendons at failure. Through chapter three, an experimental program is designed to reach the objectives of the thesis. The experimental program included a 4.0 m span simply-supported six post-tension concrete slabs with bonded and unbonded tendons. The slab specimens were divided into three sets; the first set is made of two post-tension slabs with bonded tendons, the second set includes a set of two slabs with unbonded tendons. The third set has two post-tension slabs with unbonded tendons and non-prestressing steel reinforcement. Slab specimens were chosen because there is no enough data for tests carried for slab specimens. All of the slab specimens are designed through chapter three according to the ACI 318-19 provisions. Analytical failure loads for each set of slabs are determined from the carried preliminary calculations. The construction procedures, steps and the test set up are presented in chapter four; then the calculations are repeated to have more accurate analytical failure loads for each system using the actual jacking forces and the actual concrete compressive strength. Chapter five includes the failure loads recorded during the flexural test under four-point loading for the six slab specimens and the behavior of each system is presented and discussed. The failure loads recorded during testing for the bonded system, unbonded system and the unbonded system with non-prestressing steel reinforcement are 45.6 kN, 63.3 kN and 102.7 kN. Through this research, the unbonded system had been proved to have better behavior and capacity than the bonded system. The following points summarize the conclusions reached upon

comparing the different aspects of the bonded and unbonded system's behavior, answering the previously raised questions.

6.2 Conclusions

Through this research the behavior and the flexural capacity of the bonded and the unbonded post-tension slabs are investigated deeply. The failure loads calculated analytically and recorded during the four-point flexural test for the three sets are compared to each other and the following points are concluded.

- The experimental program carried showed recorded failure loads for the unbonded slabs with non-prestressing steel reinforcement higher than the other two systems. The bonded slab's recorded failure load was not correct and was calculated from the strain determined from the tendon's profile at failure. The calculated failure load for the bonded slab was greater than the failure load recorded for the unbonded slabs with no non-prestressing steel reinforcement.
- The difference between the analytical and experimental loads for the two unbonded sets of slabs was less than 10%, confirming the analytical calculations and the carried experimental program accuracy.

The limitation governed by the ACI 318-19 on the unbonded tendon's ultimate stress is examined through this research by comparing set 2 (UBS1 and UBS2) specimen's analytical and experimental failure loads. The below points demonstrate the conclusions derived assessing the accuracy of the code empirical equation used to calculate the unbonded tendon's ultimate stress and its limitations.

- The unbonded slabs with no non-prestressing steel reinforcement recorded failure loads almost equal to the analytical failure loads calculated according to the ACI 318-19 provisions. This conveys the accuracy of the empirical equation governed by the ACI 318-19 to calculate the unbonded tendon's ultimate stress. Still, the used design analytical stress is less than the tendon's stresses recorded at failure which have surpassed the tendon's yielding stress.

- The limitations provided by the ACI 318-19 for the unbonded tendon's ultimate stress need more development. The equation for calculating the unbonded tendon's ultimate stress needs enhancement to estimate more accurate values.

In addition, the non-prestressing steel reinforcement contribution to the capacity and the behavior of the post-tension slabs is assessed through this thesis and it is concluded that the addition of the non-prestressing steel reinforcement increases the capacity of the unbonded members significantly, distributes the cracks and makes them finer.

Also, the ductility of the three systems, BS, UBS and UBSR is investigated. The deformation and the rebound of the slabs after failure are discussed and it is concluded that:

- The unbonded slabs with non-prestressing steel reinforcement show the highest ductility, followed by the unbonded slabs with no non-prestressing reinforcement. At the same time, the least ductile specimen is the bonded slab.
- The unbonded slabs with non-prestressing steel reinforcement recorded the highest deflection, followed by the unbonded slabs with no non-prestressing steel reinforcement, while the bonded slab recorded the least deformation.
- The unbonded system with no non-prestressing steel reinforcement showed a very high rebound percentage, 80%, upon removing the load and ending the test. The unbonded slabs with non-prestressing reinforcement also rebounded back after the end of the test and the removal of the load but with a lower percentage of 55%. The bonded slabs failed entirely to the ground and crushed after seconds from ending the test.
- The higher rebound percentage of the unbonded system with no non-prestressing steel reinforcement over the unbonded system with non-prestressing steel reinforcement is due to the presence of the non-prestressing steel reinforcement.

At last, the performance of the three systems under four-point flexural loading test is assed and compared reaching the following points.

- The bonded and the unbonded systems with no non-prestressing reinforcement have very close flexural capacities. Due to using the ACI 318-19 code equation to calculate the unbonded tendon's ultimate stress, the unbonded system has a slightly lower capacity than

the bonded slabs. Still, the behavior of the unbonded slabs during failure is better than the bonded system.

- The unbonded slabs with non-prestressing reinforcement provide better capacity and behavior at the failure stage than the bonded slabs. The addition of the minimum amount of reinforcement enhances the capacity of the post-tension unbonded slabs by almost 40% compared to the bonded slabs with no non-prestressing reinforcement.
- The unbonded slabs with non-prestressing steel reinforcement (UBSR) have a higher capacity by almost 60% than the unbonded slabs with no non-prestressing reinforcement (UBS). Also, UBSR system has better ductility, more uniformly distributed and finer cracks.
- The requirement for the addition of non-prestressing steel reinforcement upon using unbonded tendons could be removed as the unbonded slabs without non-prestressing steel reinforcement showed high ductility and good behavior at failure.

As discussed and presented through this research it can be generally concluded that the unbonded post-tension slab system provides better behavior and flexural capacity at the ultimate stage than the bonded post-tension slab system specially in the addition of non-prestressing steel reinforcement. This can persuade the designers and contractors to use the unbonded system more broadly to benefit from its various advantages.

6.3 Recommendations for future work

Although the carried experiment proved the adequacy of the empirical equation provided by the ACI 318-19 for the unbonded tendons ultimate stress, still more research and experimental work is recommended to collect more data and be able to have an accurate and detailed analysis for the behavior of the unbonded and the bonded system at the ultimate stage. Also, it is recommended to have more research focusing on verifying the code limitations on the maximum allowable design value of the unbonded tendon's ultimate stress and on developing the empirical equation used to calculate the unbonded tendon's ultimate stress. It is highly recommended to find a successful procedure for attaching strain gages to prestressed tendons through future research.

References

1. Aalami, B. (1994). Unbonded and Bonded Post-Tensioning Systems in Building Construction: A Design and Performance Review. PTI Technical Notes, 5th ser.
2. Abdelrahman, A. (2017). Applications of Sustainable Post-Tension Concrete Slabs. Innovative Infrastructure Solutions, Springer, (1). doi:10.1007/s41062-017-0075-6
3. ACI Committee 318. (2019) Building Code Requirements for Structural Concrete (ACI 318–2019) and Commentary (ACI 318–2019). American Concrete Institute.
4. Alqam, M., & Alkhairi, F. (2019). Numerical and Analytical Behavior of Beams Prestressed with Unbonded Internal or External Steel Tendons: A State-of-the-Art Review. Arabian Journal for Science and Engineering, Springer, (10), 8149-8170. doi:10.1007/s13369-019-03934-3
5. Au, F., J.S., & D. (2004). Prediction of Ultimate Stress in Unbonded Prestressed Tendons. Magazine of Concrete Research, 56(1), 1-11. doi:10.1680/macr.2004.56.1.1
6. Baker, A. (1949). A Plastic Theory of Design for Reinforced and Prestressed Concrete, Including Moment Redistribution in Continuous Members. Magazine of Concrete Research, 1(2), 57-66. doi:10.1680/macr.1949.1.2.57
7. Bondy, B.K., Gupta, P.R., Alkhairi, F., & Neff, T.L. (2006) Post-tensioning Manual (sixth edition). Phoenix, AZ.
8. Bondy, K. (2012). Two-Way Post-Tension Slabs with Bonded Tendons. PTI Journal.
9. Burns, N. H., & Pierce, D. M. (1967). Strength and Behavior of Prestressed Concrete Members with Unbonded tendons. PCI Journal.
10. Chouinard, K. L. (1989). Tendon Stress at Ultimate in Unbonded Partially Prestressed Concrete Beams. Master's thesis, Department of Civil Engineering, Queen's University, Kingston, Ontario.
11. Chung, K., Park, J., Kim, Y., & Kim, D. (2017). Application of Post-Tension Technology on Tall Buildings. International Journal of High-Rise Buildings, 6(3), 285-296. doi:10.21022/IJHRB.2017.6.3.285
12. Cooke, N., Park, R., & Yong, P. (1981). Flexural Strength of Prestressed Concrete Members with Unbonded Tendons. PCI Journal, 26, 52-81. doi:10.15554/pcij.11011981.52.81

13. Dsi monostrand system prevents loss of material. (n.d.). Retrieved 2021, from https://www.dywidag-systems.com/projects/2009-info-17/dsi-monostrand-system-prevents-loss-of-material/
14. Ellobody, E., & Bailey, C. (2008). Behavior of Unbonded Post-Tension One-way Concrete Slabs. Advances in Structural Engineering, 11(1), 107-120. doi:10.1260/136943308784069504
15. Elzanaty, A., and Nilson, A. H. (1982). Flexural Behavior of Unbonded Post-Tensioned Partially Prestressed Concrete Beams. Master's thesis, Department of Structural Engineering, School of Civil and Environmental Engineering, Cornell University.
16. GTI, https://gti-usa.net/, 2021
17. Harajli, M. (2006). On The Stress in Unbonded Tendons at Ultimate: Critical Assessment and Proposed Changes. ACI Structural Journal, 103, 803-812.
18. Harajli, M. H. (1990). Effect of Span-depth Ratio on the Ultimate Steel Stress in Unbonded Prestressed Concrete Members. ACI Structural Journal, 87(3), 305-312. doi:10.14359/2631
19. Harajli, M. H., and M. Y. Kanj. (1991). Experimental and Analytical Study of the Behavior of Concrete Beams Prestressed with Unbonded Tendons. Report No. CE/FSEL 90-02, Department of Civil Engineering and Environmental Science, University of Oklahoma, Norman.
20. Harajli, M. H., and S. A. Hijazi. (1991). Evaluation of the Ultimate Steel Stress in Partially Prestressed Concrete Members. PCI Journal 36 (1), 62-82.
21. He, Z., & Liu, Z. (2010). Stresses in External and Internal Unbonded Tendons: Unified Methodology and Design Equations. Journal of Structural Engineering, 136(9), 1055-1065. doi:10.1061/(asce)st.1943-541x.0000202
22. Janney, J. R., Hognestad, E., & McHenry, D. (1956). Ultimate Flexural Strength of Prestressed and Conventionally Reinforced Concrete beams. ACI Journal Proceedings, 52(2), 601-620. doi:10.14359/11618
23. Kang, T. H., Huang, Y., Shin, M., Lee, J. D., & Cho, A. S. (2015). Experimental and Numerical Assessment of Bonded and Unbonded Post-Tension Concrete Members. ACI Structural Journal, 112(6). doi:10.14359/51688194

24. Lee, D. H., & Kim, K. S. (2011). Flexural Strength of Prestressed Concrete Members with Unbonded Tendons. Structural Engineering and Mechanics, 38(5), 675-696. doi:10.12989/sem.2011.38.5.675
25. Lee, L. H., Moon, J. H., & Lim, J. H. (1999). Proposed Methodology for Computing of Unbonded Tendon Stress at Flexural Failure. ACI Structural Journal, 96(6), 1040-1048. doi:10.14359/781
26. Manisekar, R., & Senthil, R. (2006). Stress at Ultimate in Unbonded Post-Tensioning Tendons for Simply Supported Beams: A State-of-the-Art Review. Advances in Structural Engineering, 9(3), 321-335. doi:10.1260/136943306777641922
27. Mattock, A. H., Yamazaki, J., & Kattula, B. T. (1971). Comparative Study of Prestressed Concrete Beams, with and without Bond. ACI Journal Proceedings, 68(2), 116-125. doi:10.14359/11298
28. Modular Construction: The Future of the Construction Industry, Post Tension Slab – Working Principle, Comparison of Pre-Engineered with Conventional Steel Buildings, Foundations & Anchorage for Pre-Engineered Building, & Systems, A. (n.d.). Pre-Engineered building Archives. Retrieved 2021, from https://theconstructor.org/structural-engg/pre-engineered-building/
29. Mojtahedi, S., & Gamble, W. L. (1978). Ultimate Steel Stresses in Unbonded Prestressed Concrete. Journal of the Structural Division ASCE, 1159-1165.
30. Moon, J. H., & Burns, N. H. (1997). Flexural Behavior of Members with Unbonded Tendons. II: Applications. J. Struct. Eng, 123(8), 1095-1101.
31. Naaman, A. E., & Alkairi, F. (1991). Stress at Ultimate in Unbonded Post-Tensioning Tendons: PART 1-Evaluationof the State-of-the-Art. ACI Structural Journal, 88(5). doi:10.14359/2763
32. Naaman, A. E., & Alkhairi, F. M. (1991). Stress at Ultimate in Unbonded Post-Tensioning Tendons: Part 2-Proposed Methodology. ACI Structural Journal, 88(6), 683-692. doi:10.14359/1288
33. Naaman, A. E., Burns, N., French, C., Gamble, W. L., & Mattock, A. H. (2002). Stresses in Unbonded Prestressing Tendons at Ultimate: Recommendation. ACI Structural Journal, 99(4), 518-529. doi:10.14359/12121

34. Ocean heights. (2018, April 27). Retrieved 2021, from https://www.aedas.com/en/what-we-do/architecture/residential/ocean-heights
35. Ozkul, O., Nassif, H., Tanchan, P., & Harajli, M. (2008). Rational Approach for Predicting Stress in Beams with Unbonded Tendons. ACI Structural Journal, 105(3). doi:10.14359/19793
36. Pannell, F. N. (1969). The Ultimate Moment of Resistance of Unbonded Prestressed Concrete Beams. Magazine of Concrete Research, 21(66), 43-54. doi:10.1680/macr.1969.21.66.43
37. Post tension gi sheathing duct (gi corrugated duct). (n.d.). Retrieved 2021, from https://www.indiamart.com/proddetail/post-tension-gi-sheathing-duct-gi-corrugated-duct-21519115162.html
38. Post tensioned Slab Design, Supply, Install: Tensioned concrete. (2020, September 01). Retrieved 2021, from http://www.tensionedconcrete.com.au/post-tensioning-services/
39. Post tensioning. (n.d.). Retrieved 2021, from https://www.tmgglobals.com/post-tensioning
40. Retrieved 2021 https://www.researchgate.net/figure/Figure-5-stress-strain-curve-of-grade-270-low-relaxation-seven-wire-strands-at-127_fig1_338261560.
41. Sayed-Ahmed (2019), Design of PC members, Lecture notes, AUC
42. Sergio, P., &Dalmau Sr., PTE Unbonded Post-Tensioned Floor System. PTE SYSTEMS INT'L. LLC.
43. Sisi, W. (2013). The Effect of Bonded Reinforcement Steel On Increase in Stress in Unbonded Prestressing Steel at Ultimate Stage. Master of Applied Science, University of Toronto.
44. Süleymanoğlu, H., Uzel, A., & Arslan, G. (2017). Use of Post-Tension Concrete Slabs for Sustainable Design of Buildings. High Tech Concrete: Where Technology and Engineering Meet, 2390-2395. doi:10.1007/978-3-319-59471-2_272
45. Tam, A., & Pannell, F. N. (1976). The Ultimate Moment of Resistance of Unbonded Partially Prestressed Reinforced Concrete Beams. *Magazine of Concrete Research, 28*(97), 203-208. doi:10.1680/macr.1976.28.97.203
46. Tao, X., & Du, G. (1985). Ultimate Stress of Unbonded Tendons in Partially Prestressed Concrete Beams. PCI Journal, 30(6), 72-91. doi:10.15554/pcij.11011985.72.91

47. Török, I., Puskás, A., & Virág, J. (2019). Post-tension Flat Slabs with Unbonded Tendons for Public Buildings. Procedia Manufacturing, 32, 102-109. doi:10.1016/j.promfg.2019.02.189
48. Warwaruk, J., Sozen, M.A., & Siess, C. P. (1962). Investigation of Prestressed Reinforced Concrete for Highway Bridges, Part 3: Strength and Behavior in Flexure of Prestressed Concrete Beams. Bulletin No. 464, University of Illinois Engineering Experiment Station, Urbana.
49. Williamson, C. (2020, March 30). The Sydney Opera house has unveiled a massive free digital program of Concerts, talks and podcasts. Retrieved 2021, from https://concreteplayground.com/sydney/arts-entertainment/the-sydney-opera-house-has-unveiled-a-massive-free-digital-program-of-concerts-talks-and-podcasts
50. Yang, K., Mun, J., & Kim, G. (2013). Flexural Behavior of Post-Tension Normal-Strength Lightweight Concrete One-way Slabs. Engineering Structures, 56, 1295-1307. doi:10.1016/j.engstruct.2013.07.004
51. Zhang, N., & Fu, C. C. (2010). Experiment and Numerical Modeling of Prestressed Concrete Curved Slab with Spatial Unbonded Tendons. ELSEVIER, 33(3), 747-756. doi:10.1016/j.engstruct.2010.11.029
52. Zheng, W., & Wang, X. (2010). Ultimate Stress Increase in Unbonded Tendons in Prestressed Concrete Beams. Journal of Zhejiang University - Science A: Applied Physics & Engineering, 11, 998-1014. doi:10.1631/jzus.A0900618